Doc.-Nr.:	**FR.DLR.WindVal_III.V1.0**	
Doc.-Title:	**WindVal III** **Final Report (FR)**	
Contract Number	ESA 4000114053/15/NL/FF/gp	
Number of pages:	76 pages	
Prepared by:	Christian Lemmerz	Deutsches Zentrum für
	Oliver Lux	Luft- und Raumfahrt DLR e. V.
	Benjamin Witschas	Oberpfaffenhofen
	Oliver Reitebuch	Germany

0   Document Change Log

Issue.	Date	New pages	Modified pages (after introducing new pages)	Observations	Name
V0.9	12.07.2019	all	-	Draft prepared by Lux, Lemmerz and Witschas	Lemmerz, Lux, Witschas
V1.0	02.08.2019	54, 76	22, 27, 50, 66, 71	Editorials and changes according to request from T. Fehr	Lemmerz, Lux, Witschas

1   Table of Contents

2   Introduction and Purpose of Document

This Final Report (FR) discusses the results obtained during the wind validation campaign (WindVal III) which was the first airborne campaign aiming at the validation of Aeolus after its launch on 22 August 2018. It is also the only airborne campaign in the commissioning phase E1 of the Aeolus mission with flight laser FMA active after its first switch-on.

It covers tasks in response to the Statement of Work (SoW) from ESA (ESA-EOPSM-AEOL-SOW-3319 issue 1, revision 1, dated 17/05/2018) entitled "Technical Assistance for the Deployment of the ALADIN Airborne Demonstrator (A2D) lidar during WINDVAL III" (ESA 2018) and is a follow on to previous activities within WindVal II requested in (ESA 2016). The task details are covered in CCN 3 to contract no. 4000114053/15/NL/FF/gp (signed on 2 August 2018).

The WindVal III campaign was carried out from the airport at DLR Oberpfaffenhofen in the timeframe from 5 November to 5 December 2018. The objectives and implementation of the campaign are described in detail in the final version of the WindVal III CIP (V 1.1, 15 November 2018, DLR 2018b), while an overview of the obtained data is provided in the WindVal III DAR (V 1.0, 23 March 2019, DLR 2019). Flight reports and preliminary results (quick looks) of the six flights (including the test flight) were already sent to ESA by e-mail during the campaign and are attached to the appendix of this document.

This FR is output from WP300 of DLR´s proposal and Deliverable Item D5 in correspondence with Task 3 of ESA´s SoW. It was prepared by Christian Lemmerz, Oliver Lux, Benjamin Witschas and Oliver Reitebuch from the German Aerospace Centre (DLR) Oberpfaffenhofen, Germany. Preliminary results of the campaign have been presented at a Preliminary Data Meeting on 18 January 2019 at DLR.

3 Acronyms and Abbreviations

A2D	ALADIN Airborne Demonstrator
a/c, AC	aircraft
ACCD	Accumulation Charge-Coupled Device
ADM	Atmospheric Dynamics Mission
ALADIN	Atmospheric LAser Doppler Instrument
AMV	Atmospheric Motion Vector
AOCS	Attitude and Orbit Control System
AOM	Acousto-Optic Modulator
AOT	Aerosol Optical Thickness
ATM	Atmosphere
Cal	Calibration
CC	Cavity Control
CI	Confidence Interval
CIP	Campaign Implementation Plan
CLIMAT	Conveyable Low-Noise Infrared Radiometer for Measurements of Atmosphere and Ground Surface Targets
CoG	Centre of Gravity
CP	Crosspoint
DAR	Data Acquisition Report
DBS	Doppler Beam Swinging
DCO	Detection Chain Offset
DEM	Digital Elevation Model
DLR	Deutsches Zentrum für Luft- und Raumfahrt
DS	DropSonde
DSA	Downhill Simplex Algorithm
DWL	Doppler Wind Lidar
DCMZ	Dark Current in Memory Zone
EARLINET	European Aerosol Research Lidar Network
ECMWF	European Centre for Medium-Range Weather Forecasts
EMC	Electro-Magnetic Compatibility
EOM	Electro-Optic Modulator
E2S	End-to-End Simulator
ERA-I	ECMWF Re-Analysis - Interim
ERR	Nonlinearity Error of the Rayleigh response calibration curve
EMR	Nonlinearity Error of the Mie response calibration curve
FL	Flight Level

FM	Final Meeting
FOV	Field of View
FPI	Fabry-Pérot Interferometer
FR	Final Report
FWHM	Full Width Half Maximum
GCOS	Geodetic Coordinate System
GR	Ground Return
HALO	High Altitude and Long Range research aircraft
HHG	Higher Harmonic Generation
HLOS	Horizontal Line-of-Sight
HSR	High Spectral Resolution
HU	Heterodyne Unit
IATA	International Air Transport Association
INT	Internal reference
IOCV	In Orbit Commissioning and Verification
IR	Infrared
IRC	Instrument Response Calibration
IRS	Inertial Reference System
L1B	Level 1B
L0/1/2	Level 0 / 1 / 2
LNG	LEANDRE New Generation
LOS	Line-of-Sight
LSB	Least Significant Bit (digitizer counts)
LR	Lidar Ratio
MAD	Median Absolute Deviation
MO	Master Oscillator
MODIS	MODerate resolution Imaging Spectroradiometer
MOUSR	Mie Out of Useful Spectral Range
MSP	Mie Spectrometer
MZI	Mach–Zehnder Interferometer
NAWDEX	North Atlantic Waveguide and Downstream Impact Experiment
N. B.	Nota Bene
netCDF	Network Common Data Format
no.	number
NWP	Numerical Weather Prediction
OBA	Optical Bench Assembly
PBS	Polarizing Beam Splitter
PM	Progress Meeting

PPI	Plan Position Indicator
PRF	Pulse Repetition Frequency
QC	Quality Control
RALI	Radir-Lidar
RASTA	RAdar SysTem Airborne
RBS	Range Bin Setting
RH	Relative Humidity
RHI	Range Height Indicator
RL	Reference Laser
rms	root-mean-square
RSP	Rayleigh Spectrometer
SAFIRE	Service des Avions Français Instrumentés pour la Recherche en Environnement
SD	Standard Deviation
SHG	Second Harmonic Generation
SL	Seed Laser
SMART	Spectral Modular Airborne Radiation measurement sysTem
SNR	Signal to Noise Ratio
SO	Slave Oscillator
SoW	Statement of Work
STD	Standard Deviation
SWIR	Short-Wave InfraRed
THG	Third Harmonic Generation
TIm	Telescope Image
TOBS	Tripod Obscuration
UV	UltraViolet
UTC	Universal Time Coordinated
UV	Ultraviolet
VAD	Velocity Azimuth Display
Val	Validation
VNIR	Visible to Near-InfraRed
WM	Wavelength Meter
wrt.	with respect to
ZWC	Zero Wind Correction

4   Objectives of the WindVal III campaign in 2018

The objectives the WindVal III campaign were derived from results, experience and lessons learnt of the last airborne campaigns in 2009, 2015 and 2016, which also were presented and discussed at Mission Advisory Group Meetings in 2015-2018. The main objectives of the WindVal III campaign according to the SoW (ESA 2018, Chap. 4) are:

1. Early correlative observations between Aeolus and the airborne A2D and 2-µm DWL wind lidar systems

2. Rehearsal for Aeolus Cal/Val activities (satellite underpasses, ground-truth overflights, air traffic control limitations)

3. Test of airborne lidar response calibrations over land, Zero-Wind Calibration and ground returns strongly varying terrain

4. Verification of airborne instrument modifications

In addition, the more general objectives from WindVal I and II in 2015 and 2016 are also applicable to the recent campaign:

5. Provide feedback on measurement and comparison strategies and procedures of data collection for future campaigns

6. Extend lessons learnt from previous campaigns

Therefore, the WINDVAL III campaign extended the work and analyses to include first airborne measurements collocated with Aeolus over Europe during fall 2018. The objectives and achievements are summarized in Table 4-1.

Table 4-1: Objectives of the campaign and the respective achievements which are substantiated in the following chapters and in the summary of this report. All major objectives no. 1-6 were accomplished.

No.	Objective	Achievement
1	Early correlative observations	6 flights (24 flight hours, incl. test flight and A2D calibration flight; block time) performed under various and partly complex meteorological conditions including 4 satellite underflights
2	Rehearsal for Aeolus Cal/Val activities	• 4 satellite underflights with use of orbit prediction tools • 5 ground-truth overflights (Lindenberg, Leipzig, Bayreuth, Lecce and Lille) performed. • 20 flights planned under difficult weather and air traffic control conditions due to permit-to-fly certification status of Falcon
3	Response calibrations over land, Zero-Wind Calibration and ground returns from strongly varying terrain	4 response calibrations over land (29/11/2018) in Italy; ground-returns were obtained during flights over the Alps
4	Verification of airborne instrument modifications	Modifications tested successfully during campaign. Speckle influence on internal reference signal reduced to almost Poisson limit; influence of solar background light through a/c window verified.
5	Provide feedback for Cal/Val campaigns	The Aeolus commissioning phase recommendations for the upcoming Cal/Val campaigns were communicated at the Aeolus Cal/Val workshop in Frascati in March 2019, presented at the Final Meeting of the project and are listed in this Final Report.
6	Extend lessons learnt	Campaign experience and data analysis provided additional lessons learnt with respect to flight planning in European airspace as well as the A2D/Aeolus range-bin settings and comparison flight strategies which were provided during the PMs and in the present Final Report.

5 Airborne instrumentation and flights

5.1 Payload of the DLR Falcon aircraft

The payload of the DLR Falcon aircraft was identical to the payload of WindVal II 2016, consisting of the A2D (Reitebuch et al. 2009, Paffrath et al. 2009) and the 2-µm Doppler wind lidar system (DWL, Weissmann et al. 2005). Two seats were available on the aircraft and shared among the operators for the A2D and 2-µm DWL systems (Figure 5-1).
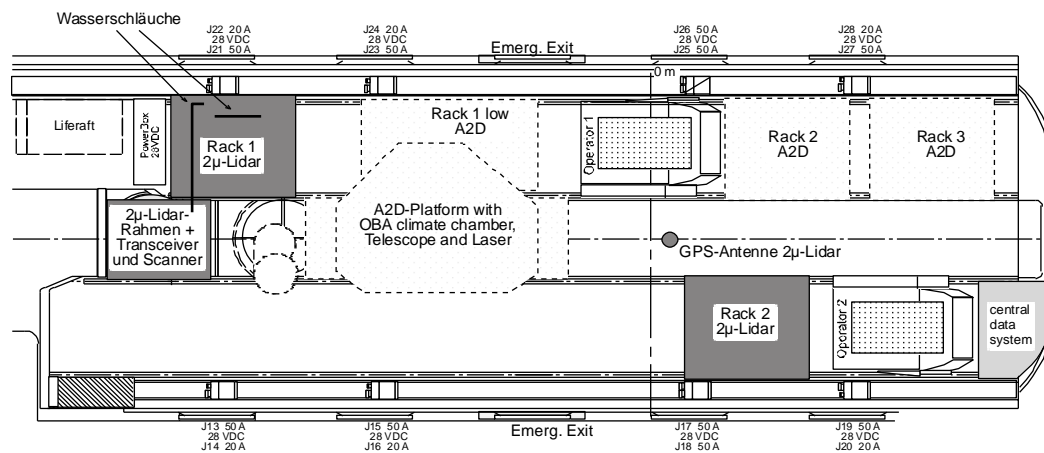
Figure 5-1: Cabin layout of the DLR Falcon aircraft with the A2D and the 2-µm lidar systems.

Due to minor modifications on the A2D, a new airworthiness certification by Enviscope/Gomolzig needed to be achieved. The cabin layout and mission certificate was not affected by these minor modifications, thus this task was handled by DLR Flight Experiment (FX).

The following modifications on the A2D have been performed since the airborne campaign in 2016:

- The A2D laser was re-aligned from Power Amplifiers to Higher-Harmonic Generation (HHG).
- The A2D reference laser was re-aligned and extensively tested.
- Several different scrambling strategies and fibre types have been tested for suitability to minimize the speckle variation influence, especially on the Fizeau/Mie internal reference signal. A fibre scrambler was finally procured and implemented into the A2D architecture (including certification).
- The Go-Pro camera mounted above the A2D output window to capture in-flight photographs of the atmospheric/ground scene below the aircraft had to be modified for being externally powered because of certification reasons.

The A2D and the 2-µm lidar were pointing in the same line-of-sight LOS direction to the right side of the aircraft (in flight direction) with a nadir angle of 20°. The instruments were mounted as follows:

- the A2D aircraft frame was mounted with a pitch angle of -6° (pointing to the back) along the aircraft axis; the telescope was mounted such that it pointed towards the right with a roll angle of 20° and pointing back by -4°; thus the A2D telescope pointed backwards by -2° and 20° to the right side.

- the 2-µm was mounted with a pitch angle of -2° (pointing to the back) along the aircraft axis. It was equipped with a double-wedge scanner, which allowed pointing towards -6° and a roll angle of 20°. Small offsets in the order of 0.1° of the 2-µm pointing direction were determined in-flight.

The nominal operation of the 2-µm DWL aimed at performing conical step-stare scans (21 LOS directions, 20° off-nadir angle) in order to determine the horizontal wind vector during flight.

The vertical sampling of the A2D was similar to those during the airborne campaigns in 2009, 2015 and 2016 (Figure 5-2). It was set such that the ground layers are sampled with highest vertical resolution (2.1 µs, 315 m range) and in case of strong jet-stream wind gradients also with high vertical resolution close to the aircraft. The higher resolution in the lower troposphere was the baseline for best fit to the active ALADIN range bin setting during the campaign (SURFA).The horizontal sampling was also set as during previous campaigns to 20 measurements per observation (N/P = 35/20).
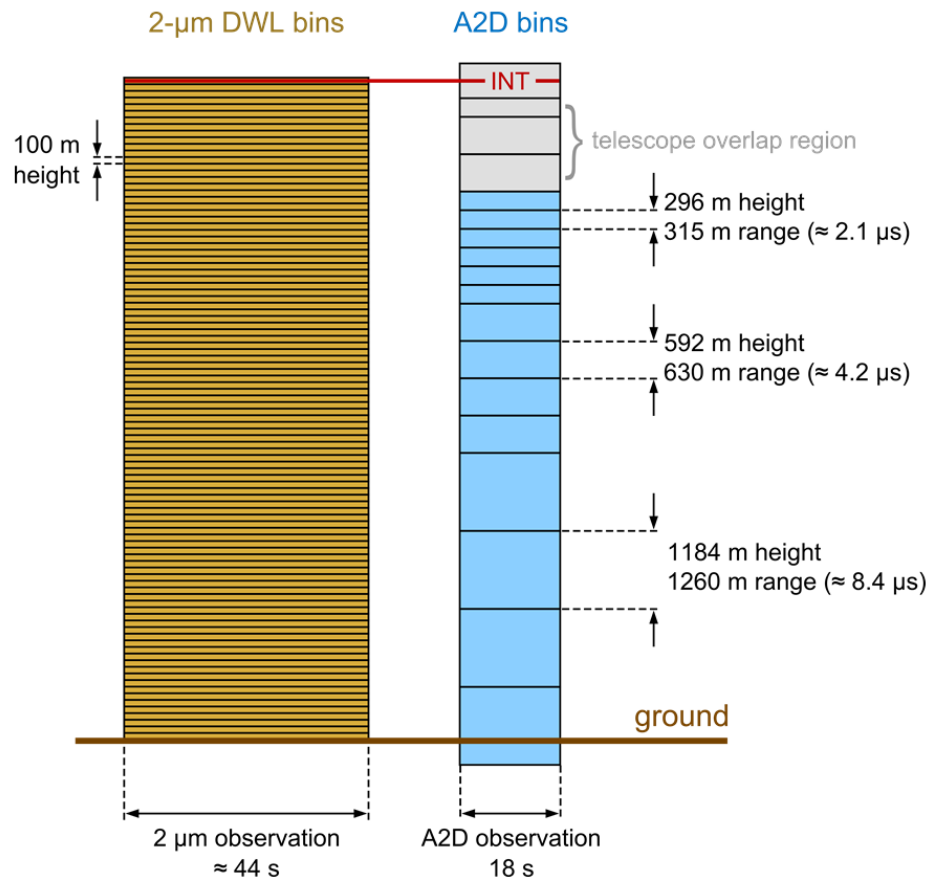
Figure 5-2: Principle of vertical and horizontal sampling of the 2-µm wind lidar with 100 m range gates and a duration of 44 s for 1 scan and A2D with vertical sampling optimized for high resolution in the jet stream area in this example, which was adapted for each flight. The horizontal distance of each A2D profile is 18 s and the averaging time is 14 s; 4 s are needed for data transfer.

The 2-µm DWL measured time series of raw signal with a sampling rate of 500 MHz, which corresponds to a range resolution of 0.3 m for each emitted laser shot with a repetition rate of 500 Hz. This amounts to rather high raw-data rates of up to 60 GByte/hour depending on maximum range. The data was processed on-ground to range-gates of 100 m resolution and temporal resolution of 1 s (500 shots). Furthermore, a new processing routine was developed, applying the accumulation algorithm (Witschas et al. 2017) with a vertical resolution of 500 m and a horizontal resolution of about 40 km. It is shown that this processing enhances the 2-µm data coverage. And as the Aeolus resolution (vertical and horizontal) is not larger, no information is lost for data comparison.

The system parameters of the A2D and 2-µm DWL systems are summarized in Table 5-1. An extensive and detailed description on the data analysis methods for deriving results from A2D calibrations and wind mode can be found in (DLR 2012a, DLR 2012b, DLR 2017, DLR 2018a) and Marksteiner (2013, Chap. 3). The methods for validation and comparison of A2D data with 2-µm DWL and other observations (e.g. ECMWF model) are discussed in DLR (2012 Chaps. 5.2., 6.2), Marksteiner (2013, Chap. 4), Marksteiner et al. (2018) and Lux et al. (2018).

The Falcon nose-boom was not mounted during the campaign due to fatigue investigations and airworthiness certification issues. Thus, no standard meteorological parameters (pressure, horizontal wind vector, vertical wind speed, temperature, humidity (relative humidity, mixing ratio) are available. However, wind information in flight altitude could be derived from GPS and aircraft attitude data of the Flight Management Computer. Because of the missing nose-boom the Falcon was operated on a permit-to-fly status which required asking overflight permissions from the planned target countries in the weeks ahead of the campaign.

Table 5-1: Main specifications and products of the two different wind lidar systems on-board the Falcon aircraft.

Parameter	DLR A2D	DLR 2-µm DWL
Wavelength	354.89 nm	2022.54 nm
Laser energy	48 to 55 mJ	1 to 2 mJ
Pulse repetition rate	50 Hz	500 Hz
Pulse length	20 ns (FWHM)	400 to 500 ns (FWHM)
Telescope diameter	20 cm	10.8 cm
Vertical resolution	300 m to 2.4 km	100 m
Temporal averaging raw data (horizontal)	20 laser shots = 400 ms	single shot = 2 ms
Temporal averaging product (horizontal)	14 s (+4 s data gap)	1 s LOS, 42 s scan (21 LOS)
Horizontal resolution @ 200 m/s=720 km/h = 12 km/min.	3.6 km (18 s)	0.2 km LOS, 8.4 km scan
Scanning capabilities	No, fixed 20° off nadir	Yes, double wedge, conical scan, fixed LOS (vertical)
Precision (random error)	1.5 m/s Mie wind 2.5 m/s Rayleigh wind	< 1 m/s wind speed

5.2 Flight Tracks

The flight tracks of the DLR Falcon performed in the framework of the airborne campaign WindVal III in 2018 are shown in Figure 5-4, while the date, time, route and objective of the respective flights are summarized in Table 5-2. These flights are the results of the flight planning strategy as described in the CIP (DLR 2018b) based on the lessons learned from previous campaigns, different weather forecast and the Aeolus track predictions combined in a flight planning tool. An example is shown in Figure 5-3.
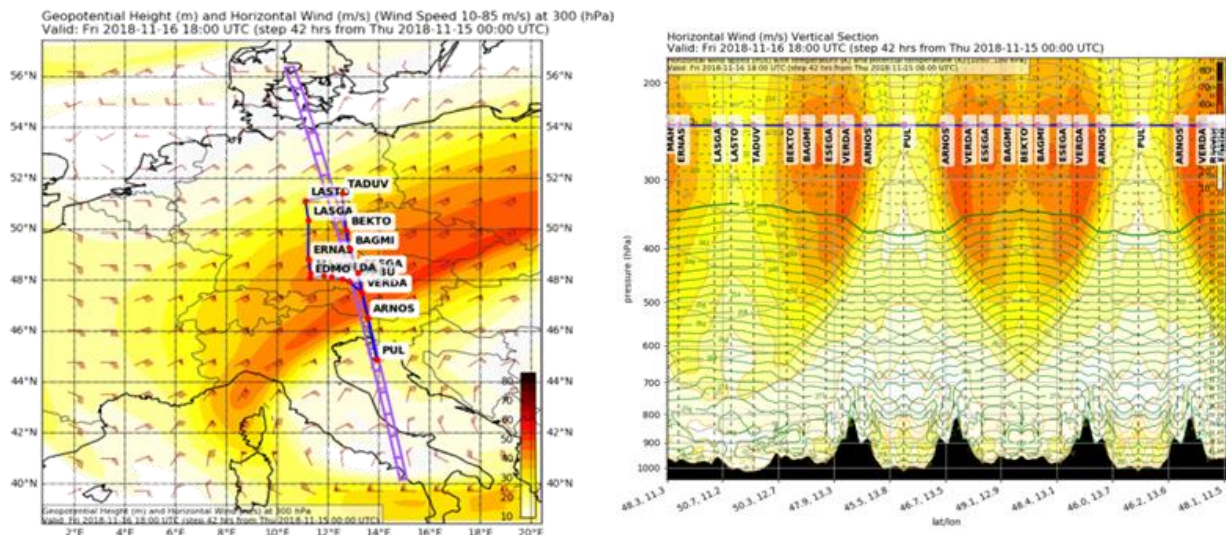
Figure 5-3: Example of the flight planning based on actual Aeolus track predictions and ECMWF weather forecast with extracted wind information in the target area (right) and along the planned flight track (left)

A total of 22 flight hours were conducted with the Falcon aircraft including the test flight. When taking into account the blocking time on-ground, which includes the pilots starting and shutting down procedures (and is relevant for flight hour costs), this amounts to 24.2 flight hours. Table 5-2 also provides information on the start and stop times and geolocations of the Aeolus underflights, which allows for an easier access to the relevant satellite wind data for comparison. Adding up the lengths of the satellite swaths covered by the DLR Falcon during the four underflights, the overall track length for which wind data is available for validation purposes is nearly 3000 km. The longest flight along the Aeolus measurement swath (1155 km) was performed on 17 November, yielding wind data from Northern Italy up to the North Frisian Islands.

Table 5-2: List of all flights performed during the airborne campaign WindVal III in 2018 with the following IATA codes: OBF: Oberpfaffenhofen, FMM: Memmingen. For the Aeolus underflights, the start and stop times and geolocations of the satellite are given.

Date	Time (UTC)	Route	Objective	Start/stop times and locations of the Aeolus underflight	
12/11	14:12 – 17:29	OBF-OBF	Test flight	-	
17/11	15:14 – 19:14	OBF-OBF	Aeolus Underflight #1	17:01:21 UTC 44.7°N, 10.6°E	17:03:56 UTC 54.9°N, 7.8°E
22/11	14:29 – 17:56	OBF-OBF	Aeolus Underflight #2	16:34:14 UTC 40.0°N, 18.3°E	16:36:02 UTC 47.2°N, 16.5°E
29/11	09:56 – 14:00	OBF-OBF	Calibration flight	-	
03/12	15:48 – 19:31	FMM-OBF	Aeolus Underflight #3	17:27:55 UTC 47.1°N, 3.6°E	17:28:51 UTC 50.8°N, 2.6°E
05/12	14:56 – 18:22	OBF-OBF	Aeolus Underflight #4	16:23:50 UTC 50.2°N, 19.0°E	16:25:02 UTC 54.9°N, 17.5°E
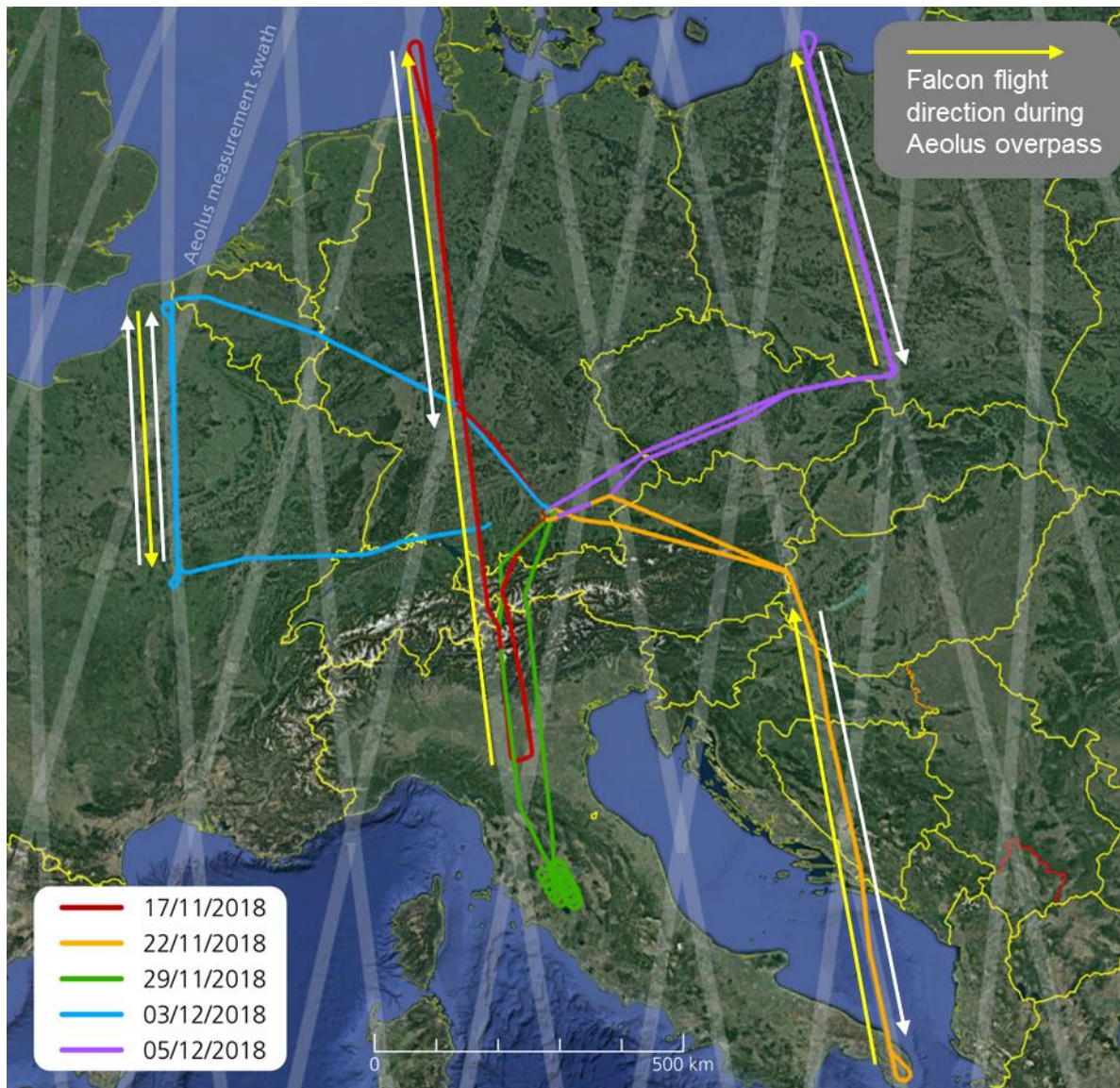
Figure 5-4: Flight tracks of the Falcon aircraft during the WindVal III campaign from 17 November to 5 December 2018 (excluding the test flight on 12 November). Each colour represents a single flight. The Aeolus measurement swath is shown in grey colour. The yellow arrow shows the Falcon flight direction during the Aeolus overpass which was always from south to north during the probed evening satellite tracks.

5.3 Data processing and availability

The data processing of the WindVal III A2D data was similar to what is described in more detail in the Data Acquisition report (DLR 2019) and the Final Report for WindVal II (DLR 2018a).

6 The 2-µm Doppler wind lidar

In this chapter, the performance of DLR's 2-µm Doppler wind lidar (DWL) during the WindVal III campaign in 2018, conducted from Oberpfaffenhofen, Germany, is revealed and corresponding measurement results from several flights are shown and discussed.

Besides the A2D, the 2-µm DWL is the second wind lidar on board the Falcon aircraft serving as reference system by providing accurate measurements of the three-dimensional wind vector. Thus, 2-µm DWL measurements are useful for both validating the A2D and the results from ALADIN on-board Aeolus which was successfully launched on August 22nd 2018 and which is now available for calibration and validation procedures.

First, the instrumental setup of the 2-µm DWL is briefly presented (section 6.1), followed by a description of the data retrieval procedure (section 6.2). For further details about these topics, it is referred to a publication by Witschas et al. (2017). After that, the performance of the 2-µm DWL during the WindVal III campaign is discussed (section 6.3) and a few measurement examples are given in section 6.4.

6.1 Instrument description

Compared to the A2D, the 2-µm DWL is based on coherent and heterodyne detection and delivers accurate wind speeds with negligible bias even without performing any receiver calibration procedures. However, as the backscattered light has to have a small spectral bandwidth in order to reach sufficient SNR, only light backscattered on aerosols and clouds or ground can be used for the wind retrieval.

A photograph of the 2-µm DWL system as setup in the Falcon aircraft is shown in Figure 6-1. In particular, the downward looking transceiver unit, developed by CLR Photonics (today Lockheed Martin Coherent Technologies) including the scanner unit, developed by DLR, and the corresponding racks including the laser power supply, cooling unit, data acquisition and the GPS module is shown.
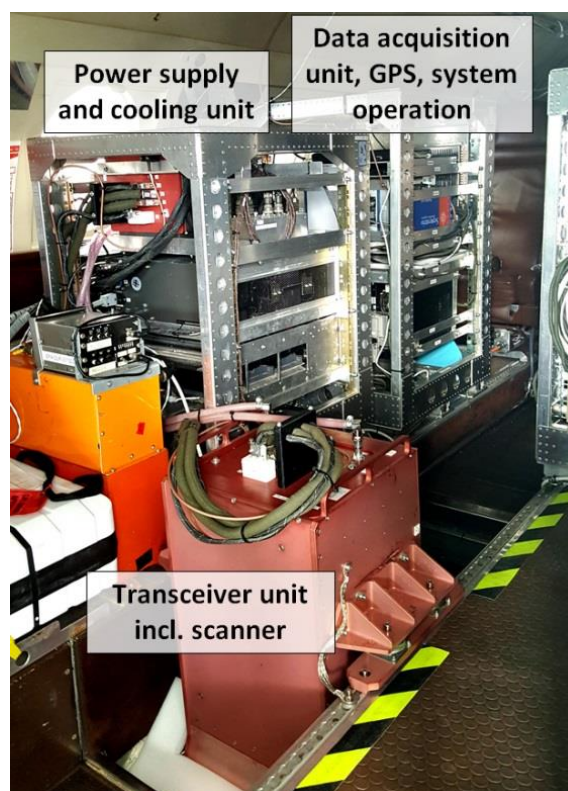
Figure 6-1: Photograph of the 2-µm DWL setup in the Falcon aircraft during a campaign without A2D.

The transceiver unit comprises a continuous-wave, single frequency, narrow bandwidth master oscillator (MO) which is used as an injection seeder for the slave oscillator (SO) and additionally as local oscillator for the coherent heterodyne detection. A part of the MO radiation is coupled into the SO via an acousto-optic modulator (AOM) which is shifting the original MO-frequency by 100 MHz, and thus, permitting determination of the magnitude and sign of the frequency difference between MO and SO which is later needed for wind measurements. The SO produces laser pulses with a wavelength of 2022.54 nm (vacuum), a pulse energy of 1-2 mJ, a pulse length of 400 ns (~120 m FWHM) at a pulse repetition rate of 500 Hz, leading to an average transmitted laser power of 0.5-1.0 W. The laser wavelength of 2022.54 nm allows for an eye-safe operation in an atmospheric window with low absorption of water vapour enabling wind measurements up to a range of 12 km. To ensure resonance between the SO cavity length and the MO radiation, the SO-cavity length is controlled by the ramp and fire technique, where the resonance signal is monitored by the reference detector (REF).

After the SO, the laser beam is expanded to a diameter of about 11 cm by means of a telescope after it is passing a polarizing beam splitter (PBS). The expanded laser beam then enters an optical double-wedge scanner which enables to steer the laser beam to any position within a cone angle of 30° off nadir. The actual wedge positions for the desired beam direction are set by two stepper motors working with a micro-stepping driver that is controlled by the housekeeping computer (HK).

Once traveling through the atmosphere, a small portion of the emitted laser pulse partly scatters on aerosols and cloud particles back to the lidar system, where it is received with the same telescope that was used for emission. The backscattered light is reflected on the PBS and directed to the optical signal detector (DET), where it is mixed with a portion of the MO laser. Now, the time-resolved detector signal resulting from each single laser shot is sampled with 500 MHz and 8 bit resolution before it is stored to a solid-state drive. This procedure leads to a data rate of 15 MByte/s (54 GByte/h) and gives maximum flexibility for post-processing. In order to achieve a high timing accuracy for the data processing, all measured quantities are stored with an accurate time stamp generated by a custom made GPS controlled oscillator. Additionally, the aircraft speed and the aircraft attitude is measured and considered for the wind retrieval. For that reason, roll, pitch and yaw angles are measured with an inertial reference system from the Falcon aircraft whose data including time stamp is also stored on the HK-computer. The velocity and the actual position of the aircraft are obtained by GPS. The accuracy of the horizontal velocity measured with the GPS receiver is specified to be 1.5 mm·s^{-1}. The main parameters of the DWL are summarized in Table 6-1.

Table 6-1: Overview of the 2-µm wind lidar system parameter.

Laser		
	Laser active medium	Tm:LuAG
	Wavelength (vacuum)	2022.54 nm
	Repetition rate	500 Hz
	Energy/pulse	1-2 mJ
	Output power	0.5-1 W
	Pulse length (FWHM)	~400 ns (~120 m)
	Frequency offset	100 ± 2 MHz
Transceiver		
	Telescope type	Off-axis
	Telescope diameter	0.11 m
Scanner		
	Type	Double wedge
	Wedge angle	6°
	Maximum displacement	30°
Detector		
	Type	InGaAs PIN photo diode
Data acquisition		
	Type	Single shot
	Sample frequency	500 MHz
	Digitizer resolution	8 bit

6.2 Measurement procedure and wind retrieval

During the WindVAL III campaign, the 2-µm DWL was mainly operated in scanning mode aiming at the measurement of vertical profiles of the three-dimensional wind vector. Alternatively, the system can measure with a fixed line-of-sight (LOS) e.g. in order to measure vertical wind speed by pointing the laser in nadir direction or measuring with the same geometry as the A2D instrument i.e. 20° off-nadir. While operating in scanning mode, a conical step-and-stare scan (Velocity Azimuth Display (VAD)-technique) around the vertical axes with a nadir angle of 20° is performed. 21 LOS wind velocities are measured per one scanner revolution and used to retrieve the three-dimensional wind vector as described in section 6.2.2. Considering 1 s averaging time for each LOS measurement (21 s), 21 s for the scanner motion between each measurement position, and an aircraft speed of about 200 m·s^{-1}, the spatial resolution along flight track of the horizontal wind speed data is about 8.4 km. Operating in fixed LOS mode, the laser beam is intentionally pointed to a user-defined direction. Considering 1 s averaging time, the horizontal resolution for the retrieved LOS wind profiles is about 200 m.

6.2.1 Line-of-sight wind speed

LOS winds are retrieved from the detector raw signal, which itself is stored for each single laser pulse with a sampling rate of 500 MHz, 8 bit resolution and a duration of $t = 97.8$ µs. This leads to an overall sampling range of $r = c·t/2 = 14.659$ km which is sufficient as the distance to ground is always lower considering a maximum flight altitude of 12 km and maximum off-nadir angles of 30°. A schematic overview of the LOS wind processing steps is given in Figure 6-2.
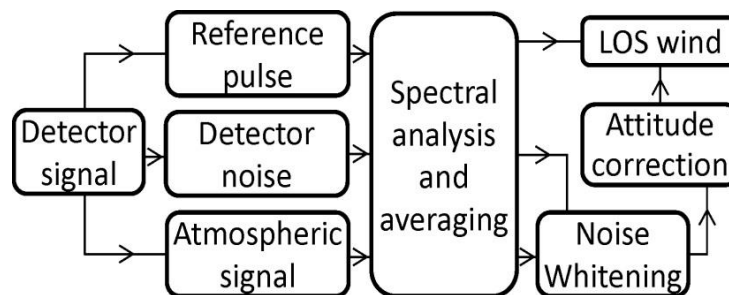
Figure 6-2: Schematic overview of the LOS wind processing procedure.

The power spectrum of the reference pulse signal, which is the beat signal of the local oscillator (MO) and the emitted laser pulse, is calculated and analysed regarding its frequency. If the beat frequency differs by more than 10% of the nominal AOM-frequency of 100 MHz, or if the laser pulse built-up time is larger than 3.5 µs (about 2.6 µs is the baseline), the laser pulse is not considered for accumulation. Moreover, before accumulating respective reference pulse spectra, they are frequency shifted to a defined reference value of e.g. 100 MHz in order to correct for pulse-to-pulse frequency variations and thus to avoid spectral broadening in the accumulation process. The applied frequency shift is afterwards equally applied to the atmospheric signal power spectra.

The part of the detector raw signal containing the atmospheric return is divided in segments that lead to 100 m range gates in the vertical by considering the actual laser beam pointing angle, the aircraft altitude and attitude. After that, the power spectrum is calculated for each range gate and laser pulse, and is frequency shifted according to the reference pulse frequency shift and subsequently accumulated.

The ground and cloud returns are identified and processed separately. On the one hand, this gives the possibility of determining ground and cloud-top altitudes with a much better accuracy. Considering the sampling frequency of 500 MHz, and the velocity of light ($3·10^8$ m·s^{-1}), and the back and forth travelling of the beam, the range resolution of the sampled atmospheric time signal is 0.3 m. On the other hand, this enables to exclude areas with hard-target returns from the actual wind analysis as they can contaminate the wind retrieval (e.g. zero wind from ground will contaminate the wind retrieved for the first atmospheric range gate).

The detector signal at the end of the record (after ground return) is used to analyse the detector noise characteristics which is especially important in the weak signal regime. Consequently, each power spectrum for each single range gate is divided by the respective noise spectrum for correction purposes (Figure 6-2, Noise Whitening).

In a next step, the resulting power spectra are corrected for the actual LOS direction which is derived as explicitly described by Chouza et al. (2016a), and for the aircraft speed projected onto LOS direction which is derived from the ground speed measured by the GPS module and the actual laser pointing direction (Figure 6-2, Attitude correction).

The remaining frequency shift Δf between reference pulse and atmospheric signal is proportional to the wind speed v according to $\Delta f = (2f_0 \cdot v)/c$, where f_0 is the laser frequency, c is the velocity of light and $\lambda_0 = c/f_0 = 2022.54$ nm the laser wavelength. Using this relation, the actual LOS wind speed v is calculated. For instance a wind velocity of $v = 1$ m·s^{-1} leads to a frequency shift of $\Delta f = 2/\lambda_0 = 0.9889$ MHz. The backscattered signal close to "hard targets" as for example ground or clouds is usually not considered for wind retrieval as the backscattered laser pulse and its frequency chirp may distort the wind retrieval. As shown in recent publications by Witschas et al., (2017) and Chouza et al. (2016a), the mean bias of LOS winds is less than **0.05 m·s^{-1}** and the statistical uncertainty is about **0.2 m·s^{-1}**. In order to get the actual vertical wind speed or rather the three-dimensional wind vector from respective LOS wind measurements, further processing steps are needed as discussed in the following.

6.2.2 Horizontal wind speed and direction

In order to measure the horizontal wind speed and direction with the 2-µm DWL, a conical step-and-stare scan of the laser beam around the vertical axes with an off-nadir angle of 20° is performed with 21 LOS measurements per one scanner revolution of 360°. Various LOS or rather radial velocities at different azimuth angles are derived and analysed, leading to the mean wind vector in the measurement volume. As summarized by Smalikho (2003), there are several techniques of wind vector estimation from DWL data. For the 2-µm DWL, two different retrieval algorithms are applied.

The commonly used inversion algorithm for 2-µm DWL data processing derives the LOS velocity for each of the 21 scanner positions during one scan (Weissmann et al. (2005)). Afterwards, the 21 LOS velocities are grouped in three 120° sectors. Thus, seven different wind vectors (21/3) are calculated for each scan and averaged afterwards. LOS values that do not agree with the resulting wind vector (e.g. deviation larger than 1 m·s^{-1}) are eliminated and a new wind vector is calculated by using the remaining LOS velocities. Finally, an averaged wind vector is reported as valid, if a minimum number of wind vectors (default 4) were obtained from the inversion results of one scan. Hence, the inversion algorithm gives a good possibility for quality controlling, as "bad" estimates of single LOS measurements with e.g. low SNR, or with partial data coverage due to inhomogeneous cloud coverage, can be excluded.

On the other hand, an alternative algorithm based on the maximum function of accumulated spectra (Witschas et al. (2017)) is used in regions of low SNR. All spectra of one conical scan are accumulated after they were shifted to different hypothetical winds. If the hypothetical wind matches the real wind, the accumulated spectra show an intensity maximum. Using this approach, no estimates of single LOS winds are needed and reliable winds can be retrieved for lower SNR levels compared to the inversion algorithm. However, as the inversion algorithm provides the better quality control, it is decided to use wind estimates of the accumulation algorithm only in cases where the inversion algorithm provides no wind data. As a final step a median filter is applied to each range bin. The neighbouring range bins in a box of N by N (default $N = 5$) are investigated. The range bin is considered as valid, if a fraction (default value is 20 %) of all horizontal wind speed values surrounding this range bin is within a certain range of wind speeds (default is ±4 m·s^{-1}). In order to additionally increase the accuracy of 2-µm DWL winds, the ground return is used to determine the exact installation position (e.g. mounting angles) of the lidar with respect to the aircraft (see also Chouza et al. (2016a)). As the installation position is shown to stay constant during one campaign, a flight scene of about 15 minutes with ground visibility in flat terrain is enough (and needed) to correct all measurements acquired during on campaign. Based on dropsonde comparisons performed during the A-TREC campaign in 2003 (Weissmann et al. (2005)), the systematic (bias) and statistical (standard deviation) uncertainty of horizontal wind speeds derived from the 2-µm DWL have been estimated to be **(0.0 ± 1.2) m·s^{-1}** (by applying the inversion algorithm).

The 2-µm DWL data are provided for wind vector profiles (Level 2; filename *_L2.txt) from conical scans and as LOS wind profiles from conical scans and in case of fixed LOS mode (Level 1, filename *_L1.txt). For the Level 2 wind vector profiles only altitude levels from aerosol backscatter are reported. No level 2 wind vector profiles are derived from high SNR targets as clouds or ground. Cloud backscatter is not reported in the Level 2 product, because the cloud backscatter is often not uniform within 1 scan, e.g. clouds are present only for some LOS pointing directions. In contrast the information for aerosol, clouds and ground LOS winds is obtained in the Level 1 product.

It is also worth mentioning that the times provided in the Level 1 and Level 2 files are based on GPS time, which is not corrected for leap seconds. Thus, the following correction needs to be applied to obtain time in UTC (from 1 July 2015 to 1 January 2017): UTC = GPS -17 s. Further information about the 2-µm Wind Lidar data product can be found in the data acquisition report (DLR 2018) and in Witschas et al. (2017).

6.3   2-µm Wind Lidar performance during WindVal III

An overview of all flights performed in the framework of the WindVal III campaign and the corresponding 2-µm DWL wind measurements are given in Table 6-2.

During the test flight on November 12, the instrumental performance was tested and several VAD scans with different off-nadir angles were performed in order to calibrate the 2-µm DWL and to determine its installation position within the aircraft. For that reason, no wind data are available from the test flight. The test flight already confirmed that the 2-µm DWL laser performance was decreased compared to previous campaigns. Anyway, four successful satellite underflights could be performed in the framework of the WindVal III campaign. Reasons for the decreased 2-µm DWL performance are discussed later in this chapter.

The first Aeolus underflight was performed on November 17 from Oberpfaffenhofen (15:14 to 19:14 UTC). First, the Falcon was heading south in order to be below the satellite track in the north of Italy. After that, it turned north and flew a long leg of about 1200 km until Denmark below the satellite. As can be seen from the wind lidar curtain shown in Table 6-2, the 2-µm DWL was working without any failures, however, continuous laser parameter optimization was needed to maintain proper laser performance. The data coverage above the Alps and southern Germany was good (~ 50 %), while it was less than 10 % in the northern part of the flight, due to aerosol-poor conditions in the atmosphere. Because of a broken fuse that could not easily be replaced, the A2D was not operational during this flight. For further details about the flight path, the weather situation and wind measurement results, it is referred to section 6.4.1.

The second Aeolus underflight was performed on November 22 from Oberpfaffenhofen (14:29 to 17:56 UTC). Also during this flight, the 2-µm DWL was working properly when continuous laser parameter optimization was applied. Due to aerosol-poor conditions, the measurement coverage was low. For further details about the flight path, the weather situation and wind measurement results, it is referred to section 6.4.2.

The third Aeolus underflight was performed on December 3 (15:48 to 19:31 UTC) from the airport of Memmingen which was used for refuelling as it was not possible to take off from Oberpfaffenhofen with the needed amount of fuel due to weather and aircraft limitations. With constant laser parameter optimization, the lidar worked accordingly throughout the entire flight. Due to aerosol-poor conditions and also the slightly decreased 2-µm laser performance, the data coverage is comparably low. For that reason, it was decided to fly one leg at FL350 and the other one at FL300. This gives the possibility to increase the number of data points that can be used for comparison to Aeolus data.

The fourth Aeolus underflight which was also the last flight of the campaign was performed on December 5 (14:56 to 18:22 UTC) from Oberpfaffenhofen. With constant laser parameter optimization, the lidar worked accordingly throughout the entire flight. Due to aerosol-poor conditions, the data coverage is low. For that reason, it was decided to fly the second leg below the satellite track at a lower flight level. This gives the possibility to slightly increase the number of measurement points that can be used for comparison to Aeolus data.

From the above given short summary about the 2-µm DWL performance during the WindVal III campaign it gets clear that the system was working properly throughout all the flights. However, it also can be seen that a lot of laser parameter optimization and tweaking was needed, which is unusual for the 2-µm DWL. Further-

more, it is shown that the data coverage was poor for all of the flights. On the one hand this is caused by aerosol-poor conditions during these flights. On the other hand, this is also a hint for decreased laser pulse energy.

For that reason, it was decided to send the 2-µm DWL to the former manufacturer Beyond Photonics for maintenance directly after the campaign. It turned out that this was a good decision. Even the experts at Beyond Photonics needed several weeks and a lot of spare parts from an old lidar system to bring back the 2-µm DWL to life. This is also confirmed by a statement of a lidar expert at Beyond photonics who wrote the following after he spend several weeks in the lab: *"Even for the laser veteran being trained for this, alignment is extremely tedious and difficult. Most of the optics in the system are over 19 years old and performance is degrading causing us to replace many of the optics with optics we had available from another MAG1 we own at Beyond Photonics – which is now seriously cannibalized to support continued operation of the DLR MAG1".*

In particular, the following modifications were performed on the 2-µm DWL:

- Replaced the output coupler and mount assembly with one from a different MAG-1. Modified mounting holes and moved its mount slightly to get away from damage on coating.
- Replaced the end mirror with one we had available from a different MAG1.
- Replaced one of the quarter wave plates on the rod housing with one we had available from a different MAG1.
- Replaced the SO 45° output turn mirror with one we had available from a different MAG1.
- Replaced the SO up-collimator with one we had available from a different MAG1.
- To aid in quicker realignment, it was finally decided to replace the second OC with a third OC out of a modified MAG1 in our possession that was on an adjustable mount.
- Found the resonant signal threshold potentiometer to be turned a few revolutions beyond what it should have been set at, causing unstable triggering of the Q-switch.
- A complete realignment including OC, Q-switch, 45deg dichroic, and end mirror shifted the output beam position so much that most of the external optics needed a large re-alignment.
- The master oscillator needed to be removed to remove the rod housing for access to the end HR mirror. This along with the output beam shift required a significant and complete realignment of the seed beam and all associated BPLO optics.
- Adjusted alignment to the telescope.
- Staked all mounts.
- Buttoned up the transceiver.
- Measured system performance off aerosol targets.
- Packed the system for shipment

The performance after maintenance was verified during the AVATARE campaign which was performed in May and June 2019 from Oberpfaffenhofen. The coverage but mainly the stability of the 2-µm DWL increased remarkably, confirming the success of the maintenance.

As can be seen from the wind data shown in Table 6-2, the 2-µm DWL was usually switched-on immediately after take-off and was operational after about 10 to 15 minutes. Considering the common climbing rate of the Falcon aircraft, reliable lidar data were available from an altitude of about 5 km. As the lidar has to be completely shut-down before landing in order to prevent any damages on the system at touchdown, and as the shut-down time is approximately 10 minutes, lidar data was available down to altitudes of about 5 km to 3 km.

The 2-µm DWL is based on coherent heterodyning detection, and thus, the data coverage of the measurements depends on the aerosol load and cloud coverage, as thick clouds cannot be penetrated by the laser beam. Usually, the flight planning is performed such that the aircraft flies in areas with high relative humidity (~60% to 80%) but without opaque clouds, as measurements during previous campaigns demonstrated that these conditions lead to maximum data coverage. However, being restricted to actual Aeolus orbits during Cal/Val activities, this cannot be considered for the flight planning.
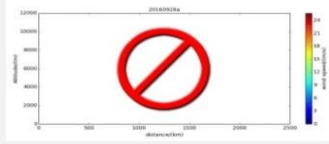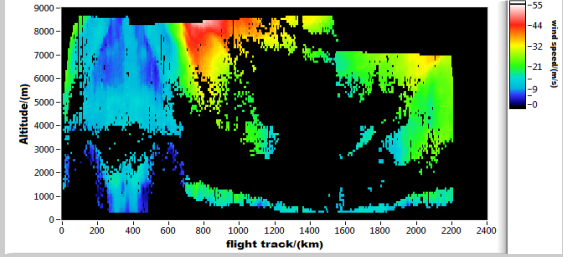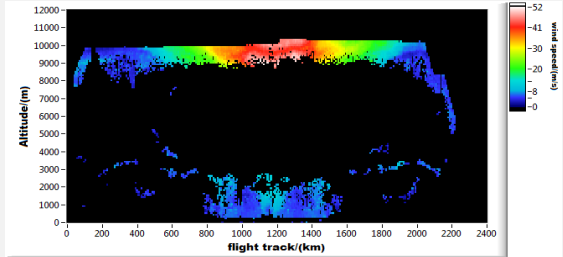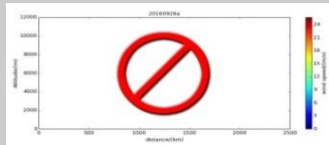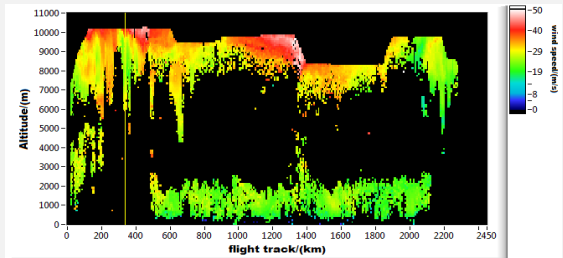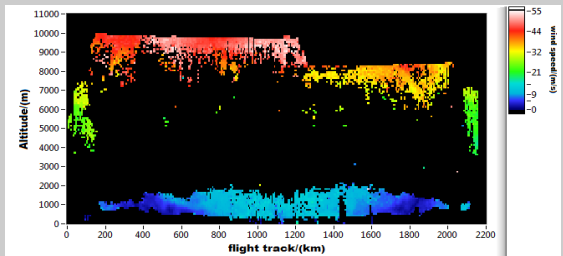
Table 6-2: Overview of flights and the corresponding 2-µm DWL wind vector measurements performed in the framework of the WindVal III campaign (TO: Take-off, Ldg. Landing).

Date in 2018	Time TO/Ldg. (UTC)	Route	Objective	2-µm DWL wind speed
12/11	14:12 – 17:29	OBF-OBF	Test flight	
17/11	15:14 – 19:14	OBF-OBF	Satellite underflight #1	
22/11	14:29 – 17:56	OBF-OBF	Satellite underflight #2	
29/11	09:56 – 14:00	OBF-OBF	A2D calibration flight	
03/12	15:48 – 19:31	FMM-OBF	Satellite underflight #3	
05/12	14:56 – 18:22	OBF-OBF	Satellite underflight #4	

6.4   Discussion of results

In this section, 2-µm wind measurements of the four Aeolus underflights are shown and comparisons to Aeolus data are given for the first two flights. A final statistical comparison is given in Section 6.5.

The flight tracks of the DLR Falcon performed in the framework of the airborne campaign WindVal III in 2018 are shown in Figure 5-4. Additionally, data, time, route and objective of the respective flights are summarized in Table 5-2. A total of 22 flight hours were conducted with the Falcon aircraft including the test flight. When taking into account the blocking time on-ground, which includes the pilots starting and shutting down procedures (and is relevant for flight hour costs), this amounts to 24.2 flight hours. Table 5-2 also provides information on the start and stop times and geolocations of the Aeolus underflights, which allows for an easier access to the relevant satellite wind data for comparison. Adding up the lengths of the satellite swaths covered by the DLR Falcon during the four underflights, the overall track length for which wind data is available for validation purposes is nearly 3000 km. The longest flight along the Aeolus measurement swath (1155 km) was performed on 17 November, yielding wind data from Northern Italy up to the North Frisian Islands. In the following, the first two underflights are discussed in detail also to explain the comparison procedure to Aeolus data. Details of the other two underflights can be found in the respective flight reports.

6.4.1   First Aeolus underflight performed on 17 November 2018

The first ever Aeolus underflight in the framework of DLR's Aeolus Cal/Val activities was performed on November 17, 2018 (see also Table 6-2). The flight was planned such that the Falcon flew a 1200 km long leg below the satellite from Northern Italy up to Denmark (15:57 UTC to 17:45 UTC). The satellite overpass was between 17:00 UTC to 17:05 UTC, flying from South to North. The Falcon flight track (yellow), the satellite swath (magenta) and the ground stations of Oberpfaffenhofen and Nordholz (red circles) are displayed in Figure 6-3 (left).

On the right side in Figure 6-3, the corresponding ECMWF horizontal wind forecast at 250 hPa pressure level for November 18, 00:00 UTC is shown. The wind is expected to blow from Easterly directions with speeds up to 50 m/s. Considering the viewing direction of ALADIN, a large range of measured wind speed is expected, providing an excellent possibility for validation the Aeolus wind product over a larger wind speed range.

Figure 6-3: (left): Aeolus swath (magenta) and the flown Falcon flight track (yellow) on 17 November 2018 are indicated. The ground stations of Oberpfaffenhofen and Nordholz are marked by red circles. (right): ECMWF forecast of the horizontal wind speed at 250 hPa for November 18, 2019, 00:00 UTC.

In Figure 6-4, the 2-µm DWL wind speed data (top) and wind direction (middle) is shown. Indeed, between 47.5° N and 50.5° N, enhanced wind speeds of up to 50 m/s were measured. Further south, above the Alps, only wind speeds lower than 10 m/s were measured. Further north, the wind speeds reached values of 20 m/s to 30 m/s. The wind direction was determined to be between 80° and 100°, thus verifying the ECMWF forecast.
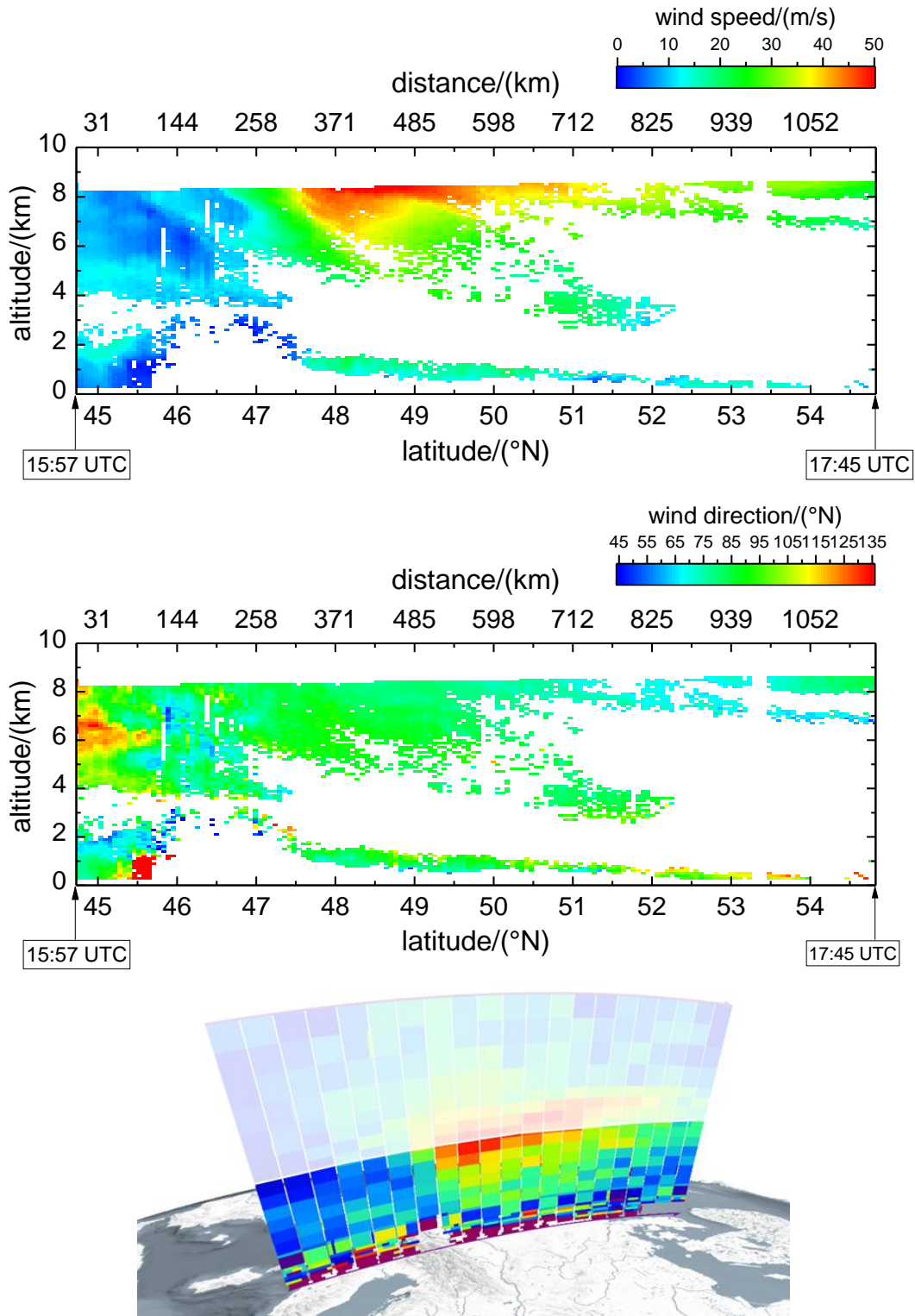
Figure 6-4: Wind speed (top) and wind direction (middle) measured with the 2-µm DWL along a 1200 km flight leg flown northern Italy up to Denmark (see also Figure 5-4). The bottom panel shows the corresponding Aeolus Rayleigh winds extracted by using the Virus-Software (https://aeolus.services/).

Additionally, it can be seen that the data coverage is remarkably good at the southern part of the flight leg, whereas it is quite low at the northern one. This is due to the dry and aerosol poor conditions in that region. Due to the temporal and spatial restrictions for flight planning due to the orbit, humidity and aerosol load cannot be considered or rather optimized for the flight planning.

For a first, qualitative comparison, the corresponding Aeolus Rayleigh winds are shown in the bottom panel of Figure 6-4. Aeolus data above Falcon flight level is indicated by the white shaded area. It is worth mentioning that these are horizontal line-of-sight (HLOS) wind speeds, whereas the 2-µm DWL data above shows the horizontal wind speed. However, as the wind direction of about 90° is very similar to the viewing direction of ALADIN, both measurements should correspond quite well.

This is actually what can be seen by visually comparing both curtain plots. Both, the low wind speeds above the Alps, as well as the high wind speeds above Germany are nicely represented by the Aeolus Rayleigh winds. In order to perform this comparison quantitatively, further processing steps are needed as described in the following.

The procedure of averaging 2-µm DWL in order to be ready to be using for Aeolus wind comparison is sketched in Figure 6-5.

- In a first step, 2-µm DWL wind speed and direction is averaged on the Aeolus grid which has a re-markably lower resolution. In order to do so, Aeolus top and bottom altitudes, as well as start and stop latitudes are used. After that, all valid 2-µm DWL measurements within these boundaries are averaged (mean). As the 2-µm data does not provide full coverage, a coverage threshold has to be introduced. In particular, if a certain Aeolus pixel contains at least 10% of valid 2-µm DWL data, it is used for further quantitative analysis. First investigations show that even the low value of 10% is a reasonable number. Increasing this threshold to larger values is mainly reducing the number of measurement points that can be used for comparison, but only has a marginal impact on the re-trieved systematic and random errors.
- After averaging, 2-µm DWL wind speed and direction is used to be projected on the horizontal LOS of Aeolus by considering the Aeolus azimuth that is given in the data product.
- Finally, Aeolus data is filtered by means of the estimated error that is written in the data product. In particular, all winds with an estimated error smaller than 8 m/s are used for further comparison.

The remaining wind measurements from a 1200 km flight leg that can be used for quantitative comparison are shown in the bottom panel of Figure 6-5. For this particular flight leg, 67 Rayleigh wind measurements and 8 Mie wind measurements are available. A statistical comparison of the entire campaigns data is given in section 6.5.
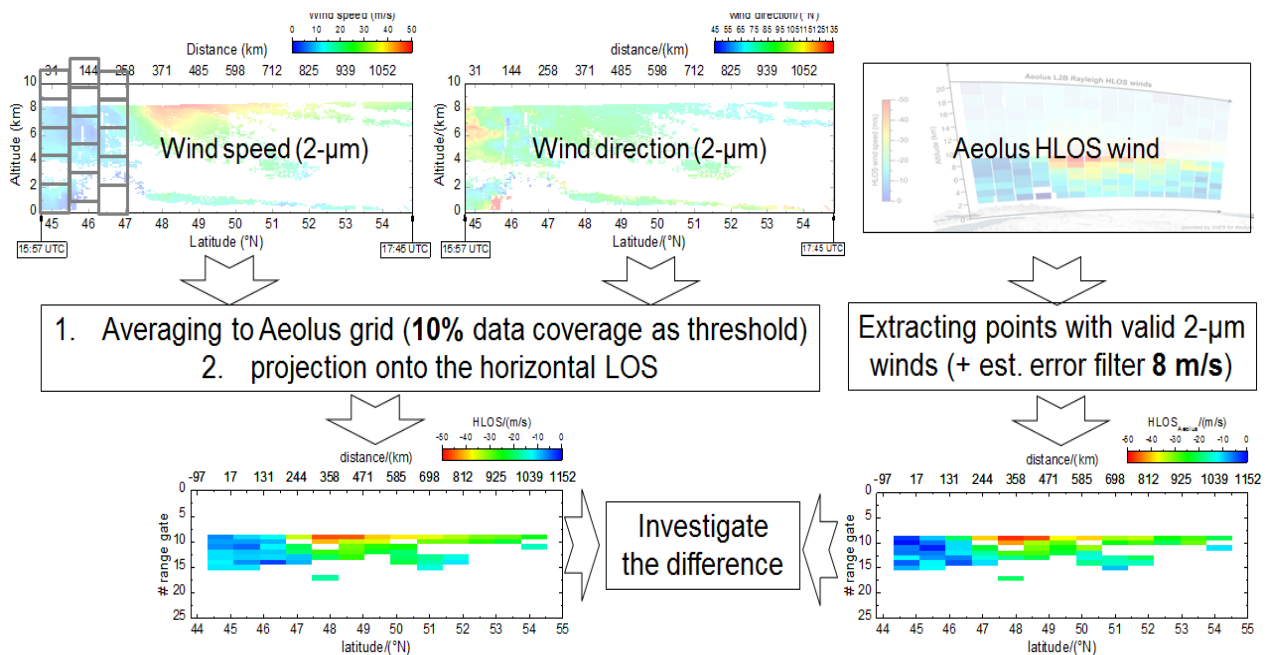
Figure 6-5: Sketch of the processing steps used to compared 2-µm DWL data and Aeolus data.

6.4.2 Second Aeolus underflight performed on 22 November 2018

The second Aeolus underflight was performed on November 22, 2018 (see also Table 6-2). This flight was planned such that the Falcon flew a 1200 km long flight leg below the satellite track from southern Italy up to Austria (16:07 UTC to 17:05 UTC). The satellite overpass was between 16:34 UTC and 16:36 UTC. The Falcon flight track (yellow), the satellite swath (magenta) and the ground stations of Oberpfaffenhofen and Lecce (red circles) are displayed in Figure 6-6 (left). On the right side in Figure 6-6, the corresponding ECMWF horizontal wind forecast at 250 hPa pressure level for November 22, 15:00 UTC is shown. The wind is expected to blow from north-westerly directions with speeds up to 50 m/s in the south of Italy. In order to get a larger range for wind speed comparison, the flight track was extended to go as far south as possible for the Falcon aircraft.
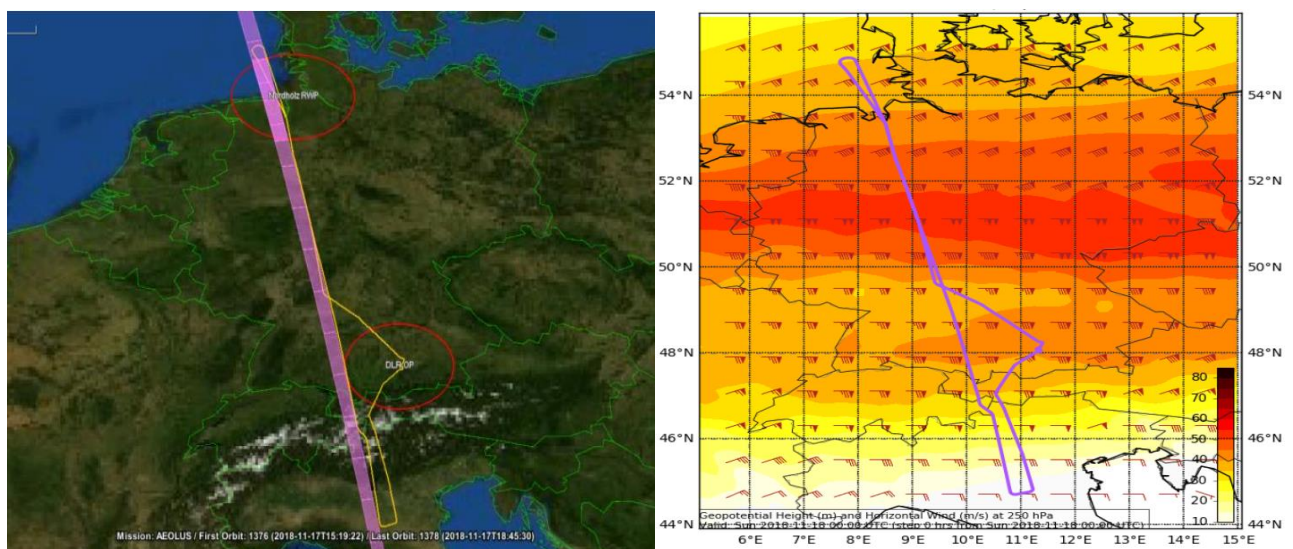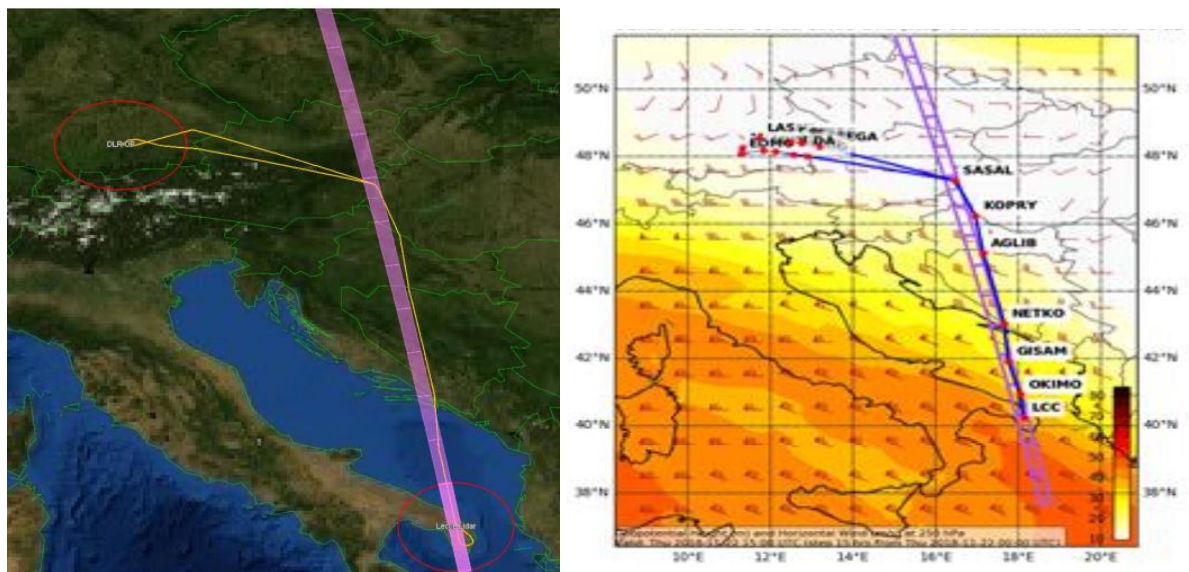

Figure 6-6: (left): Aeolus swath (magenta) and the flown Falcon flight track (yellow) on 22 November 2018 are indicated. The ground stations of Oberpfaffenhofen and Lecce are marked by red circles. (right): ECMWF forecast of the horizontal wind speed at 250 hPa for November 22, 2019, 15:00 UTC.

In Figure 6-7, the 2-µm DWL wind speed data (top) and wind direction (middle) is shown. As forecasted, the higher wind speeds of up to 50 m/s were measured in the south of Italy (40° N to 41° N). Flying north, the wind speed gradually decreased down to 0 m/s.
The determined wind speed ranged from 270° to 315° and thus also confirms the wind direction as forecast-ed by ECMWF. Considering the viewing direction of ALADIN, a remarkable Doppler shift is also expected to be prominent in the Aeolus data.
Additionally it is obvious, that the data coverage is poor during the entire flight. On the one hand, this is owed to the aerosol-poor and dry conditions during the flight. On the other hand, the decreasing 2-µm DWL laser performance may also negatively contribute to the data coverage. Because of the temporal and spatial restrictions for flight planning due to the orbit, humidity and aerosol load cannot be considered or rather optimized for the flight planning. Still the data coverage was low during this flight, 69 Rayleigh winds and 22 Mie winds are available from both flight legs and can be used for comparison.

As for the first underflight performed on November 17, a first qualitative comparison can be made to Aeolus Rayleigh winds as shown in Figure 6-7 (bottom). It is worth mentioning that these are horizontal line-of-sight (HLOS) wind speeds, whereas the 2-µm DWL data above shows the horizontal wind speed. However, as the wind direction of about 270° is very similar to the viewing direction of ALADIN, both measurements should correspond quite well (with different signs).
This is actually what can be seen by visually comparing both curtain plots. Both, the high winds speeds in the south of the flight leg and the low wind speeds in the north are nicely represented by Aeolus.

A statistical comparison of the entire campaigns data is given in section 6.5.
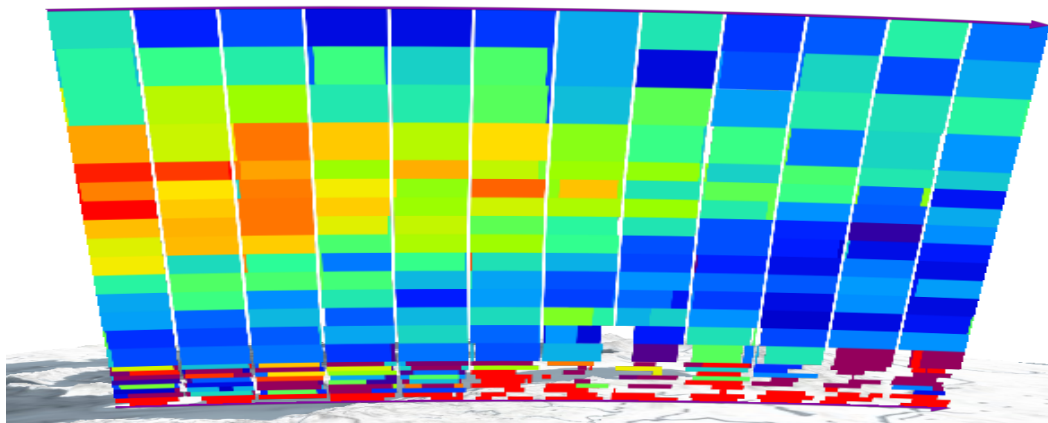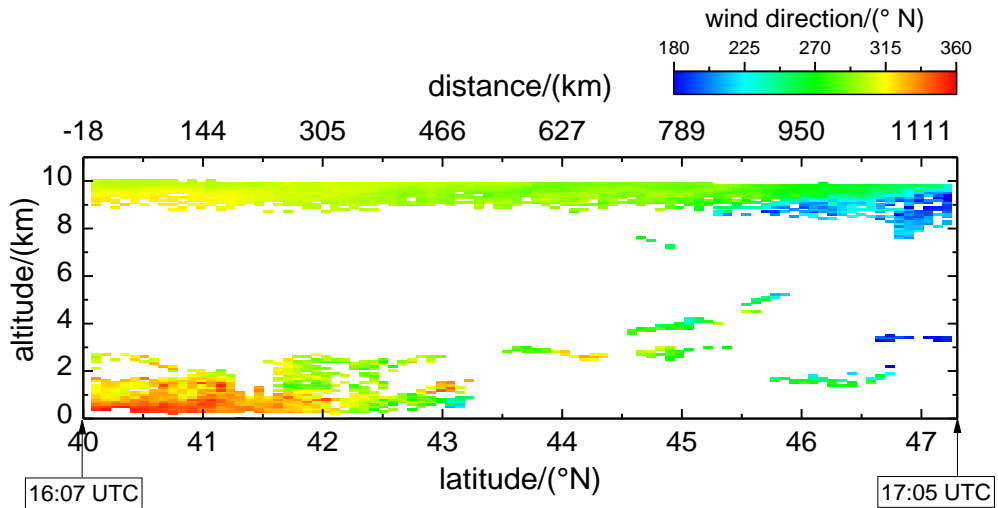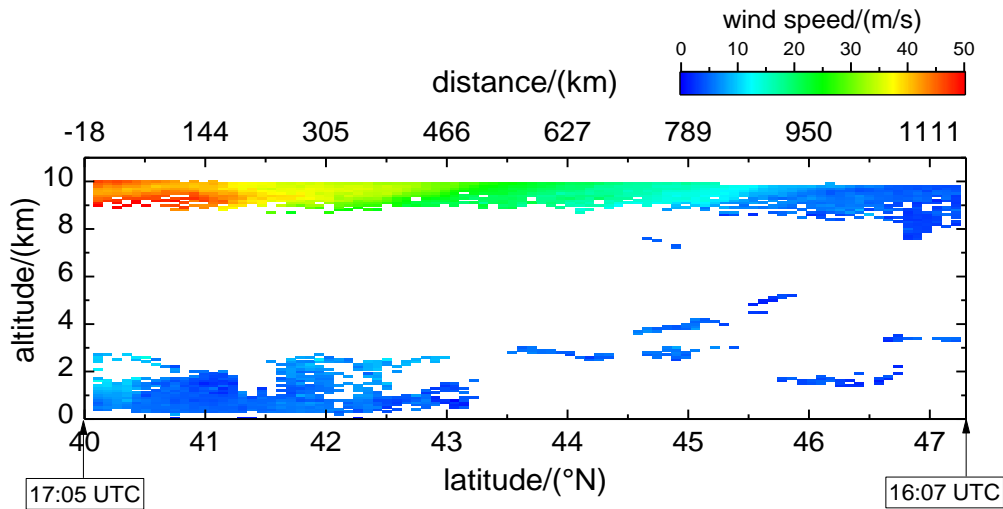
Figure 6-7: Wind speed (top) and wind direction (middle) measured with the 2-µm DWL along the underflight performed on November 22. (see also Figure 5-4). The bottom panel shows the corresponding Aeolus Rayleigh winds (L2B) extracted by using the Virus-Software (*https://aeolus.services/*) in November 2018.

6.5 Statistical comparison of Aeolus data to 2-µm DWL measurements

The overarching goal of the Cal/Val activities is to investigate or rather quantify the performance of Aeolus winds and to suggest further improvements for the wind processor. Thus, the L2B horizontal line-of-site winds are used and statistically compared to 2-µm DWL, considering the 2-µm winds as reference. That this is a justifiable assumption is demonstrated by several comparisons of 2-µm DWL data to dropsonde measurements as it was performed for several campaigns. The outcome of these comparisons was that the 2-µm DWL wind speeds are bias free (< 10 cm/s) and have a random error of 1.0 m /s to 1.3 m /s, where this random error contains the contribution of both, the lidar and the dropsonde.

During the WindVal III campaign, 4 satellite underflights were performed. For all of these flights, the satellite track was underflown in back and forth direction, leading to 8 flight legs that are available for comparison. All in all, this leads to 288 Rayleigh wind observations and 98 Mie wind observations that can be compared to 2-µm DWL data. The scatter plot of this comparison is shown in Figure 6-8.

The y-axes covers the Aeolus HLOS winds, whereas the x-axes covers the 2-µm data projected onto the Aeolus HLOS direction. The black circles indicate Rayleigh winds, and the orange circles indicate Mie winds. The red and green line represent line fits to the respective data set, and the grey dashed line is the x=y line. Furthermore, the corresponding fit results are indicated by the insets, whereas the scaled MAD is the median absolute deviation multiplied by 1.4826 in order to be comparable with the random error of a normal-distributed data set.
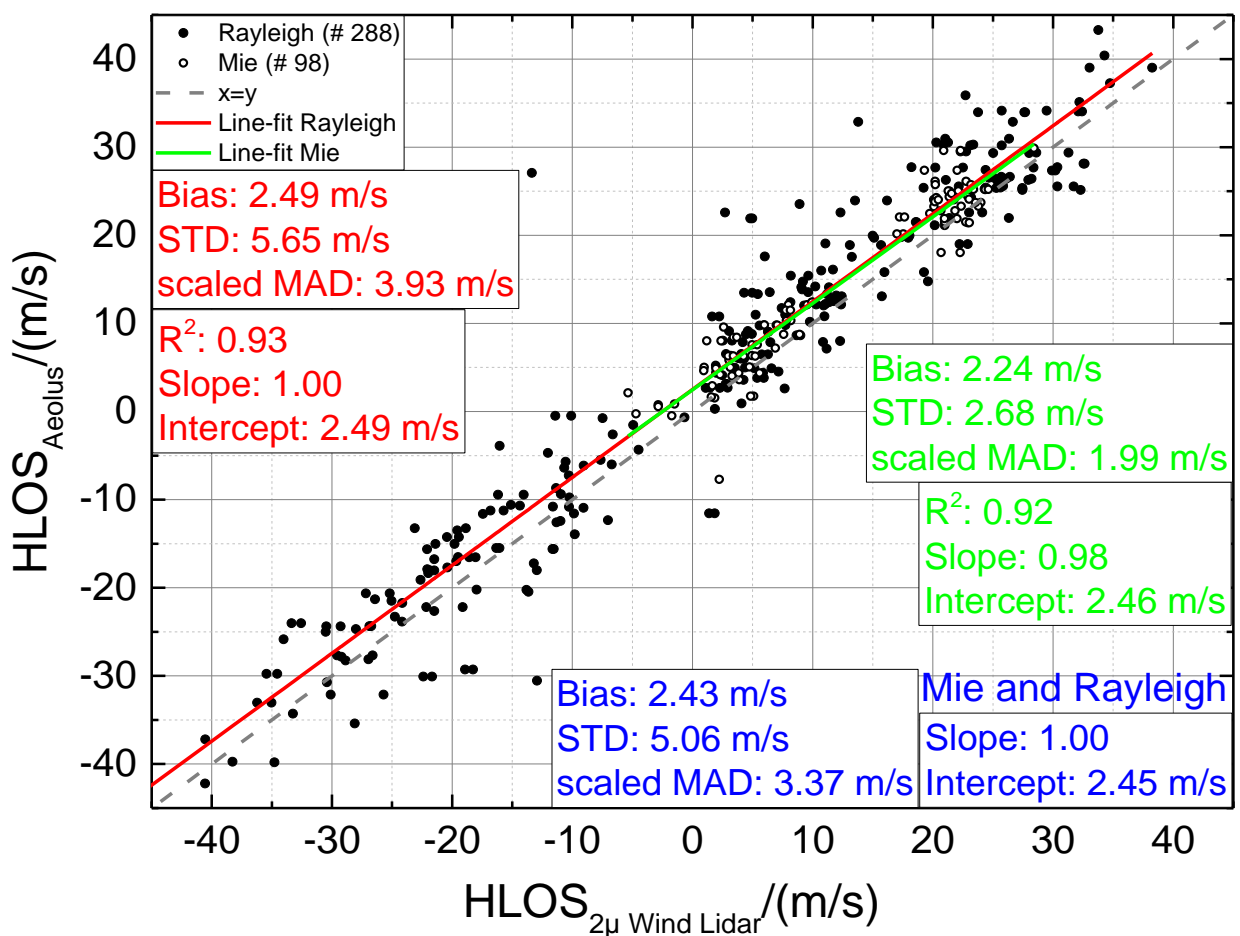
Figure 6-8: Statistical comparison of HLOS wind speeds of Aeolus and HLOS winds derived from 2-µm DWL data. Mie and Rayleigh data are indicated in different colours. A line-fit to all measurement points is indicated by the red line and corresponding fit results are shown by the inset. The x=y line is shown by the grey dashed line.

	Document Nr. **FR.DLR.WindVal_III. V1.0**	Issue: **V 1.0**	Date: **02.08.2019**	Page: 28/76	
	Doc. Title: **WindVal III Final Report (FR)**				**DLR**

aeolus

What can be seen from Figure 6-8 is that the overall accordance between Aeolus and 2-µm DWL data is good. All of the data points yield a slope which is close to 1.0. In particular, it is **1.00** for the Rayleigh winds and **0.98** for the Mie winds. On the other hand it can be seen that the systematic error (bias) is remarkably larger than specified for the Aeolus mission. It is **2.49 m/s** for the Rayleigh winds and **2.24 m/s** for the Mie winds. The enhanced systematic error at the current state can be explained by a not-updated instrument calibration file that is currently used for Aeolus data processing, together with continuous Aeolus instrumental drifts that were observed from the beginning of the mission. These instrumental drifts would actually require a calibration update on a weekly basis that is currently not possible. Still, investigations regarding that topic are ongoing. Additionally, since start of the mission, the ACCD-detectors suffer from hot-pixels with a slightly enhanced dark current signal which completely distort the accuracy of the wind retrieval. In the meantime (July 12, 2019) a correction of these hot pixel is operational implemented in the processor. However, for older data, such a correction is not available.

The random bias is described by two quantities. On the one hand, the ordinary standard deviation is calculated, on the other hand, the scaled median absolute deviation (MAD) is used. The MAD has the advantage that it is less sensitive to outliers as it is based on the median of the deviation instead of the mean. The scaled median, which is 1.4826 times the MAD is exactly the standard deviation in case of applying it to a normally distributed data set. For the comparison here, the standard deviation and the scaled MAD for Rayleigh winds are **5.65 m/s** and **3.93 m/s**, respectively. For the Mie winds it is **2.68 m/s** and **1.99 m/s**. The discrepancy between standard deviation and MAD already indicates that the data set is not normally distributed but contains a few outliers as it can also be seen in Figure 6-8. Furthermore, a random error of **3.93 m/s** for the Rayleigh winds is larger than specified and also larger than expected. One of the drivers is the laser energy which is lower than originally specified. This leads to a larger signal noise that finally translates into an enhanced random error. On the other hand, it is shown that there is a signal loss in the receiver that might originate from clipping of the return-light at the 18-µm field stop. Whereas it can be hoped that the second laser on the satellite (FMB) provides more laser pulse energy reducing the random error, the clipping problem on the field stop could still be present.

The scaled MAD for the Mie winds is **1.99 m/s** and thus, a factor of two smaller than the one of Rayleigh winds. This might be explained by the larger signal levels of Mie returns. Thus, in the future it is recommended to process Mie winds on measurement level in order to increase the number of Mie measurements.

All in all, the statistical comparison shows, that Aeolus is measuring real winds. Both, systematic and random biases are larger than specified and expected. For the systematic errors, several activities are ongoing in order to reduce them.

6.6   Summary of 2-µm performance and results

In the previous sections of this chapter, it was demonstrated that the 2-µm DWL is a valuable reference instrument for calibrating and validation Aeolus. The 2-µm DWL measured without any failures throughout all flights performed during WindVal III and provided accurate and valuable wind measurements that were used to quantitatively compare to Aeolus wind measurements. Still, the performance of the 2-µm DWL was degrading during the campaign, making the lidar operation during flights quite alignment intensive. For that reason, it was decided to send the lidar system back to the manufacturer Beyond Photonics in order to investigate the root cause of the performance degradation. In turned out that several optical components had to be changed, requiring an entire laser re-alignment. Even for the experts at Beyond Photonics, it was a delicate task to bring the 2-µm DWL back to lift. During the recently performed AVATARE campaign the success of the maintenance was demonstrated by a very stable laser operation and remarkably good data coverage.

During WindVal III, 4 satellite underflights were performed. The obtained 2-µm DWL wind data was used for a quantitative comparison to Aeolus data, enabling to estimate the accuracy of Aeolus winds, but also improve the Aeolus data product in the future. In particular, 288 Rayleigh wind measurements and 98 Mie wind measurements were statistically compared to 2-µm DWL measurements as discussed in section 6.5. The statistical comparison yields a bias for Rayleigh and Mie winds of **2.5 m/s** and **2.2 m/s**, respectively. Though, the bias is remarkably larger than specified (0.7 m/s) for the Aeolus mission, it is likely that it can be decreased in the future. Root-cause of the enhance bias is a not-update calibration file that was intentionally used for data processing, together with instrumental alignment drifts, actually requiring regular calibrations. Thus, it is expected to get rid of these large biases in near future.

Furthermore, the random error represented by the scaled median absolute deviation (MAD) for Rayleigh and Mie winds was determined to be **3.9 m/s** and **2.0 m/s**, respectively. Also here, the determined values are larger than specified and expected. Two main issues cause these enhanced deviations. On the one hand, the mean laser pulse energy of 45 mJ to 55 mJ during the campaign is much lower than originally specified. Furthermore, there is an additional signal loss in the receiver, leading to a further reduction of the signal levels. For operation with FMA, there seem to be no further possibility to optimize this situation. However, as FMB is expected to be operated at higher laser energy, this situation may improve once FMB is operational.

It is worth mentioning that the available data is very valuable for calibrating and validation Aeolus. However, it can also be shown that the performed four underflights only yield 288 Rayleigh and 98 Mie measurements. This is enough to do an overall Aeolus performance estimation, but is too little to analyse particular situations were Aeolus may have errors e.g. in broken cloud conditions. Thus, more measurements as foreseen to be performed during the AVATARE campaign in May/June 2019 are needed to perform such kind of topic related studies.

7 A2D operation and performance

This chapter summarizes the A2D technical and operational issues during the WindVal III campaign in 2018. An overview of applied modifications and system performance results before the campaign will be given, followed by a description of the operational procedures and constraints during the campaign. The performance will be discussed for all the flights.

7.1 A2D modifications and performance assessment before the campaign

Slow variations of the opto-mechanical components over time (temperature cycles) in the laser require a re-alignment of the laser oscillator and the following amplifier and HHG chain. The goal is to have the laser in an optimum alignment state to leave margins for drifts happening during the harsh airborne campaign deployment. After WindVal II the laser had 2.7 W and the beam parameters were $M^2(x/y)$ = 1.3 and a divergence of 110 µrad (x/y, +/-3σ). Also the reference laser system had been degrading in terms of frequency locking performance and required maintenance. The integration of a fiber scrambler for the internal reference signal required extensive tests of different technologies and fibres both with additional ground support UV lasers and a camera as well as with the A2D laser and also with the opened receiver climate chamber to get access to the fiber exit port. During this activity it was also observed that the illumination at fiber exit when the fiber attenuator is used at the required setting for receiver calibration changed significantly (only cladding modes left). The following preparations activities were performed prior to the campaign:

- Realignment and characterization of A2D power laser
- Realignment and optimization of A2D reference laser
- Maintenance and reintegration of A2D2G laser cooler
- Inspection of A2D receiver optics (Optical Climate Chamber, OCC, opened)
- Repair of thermal control unit switch for OCC
- Test of different speckle scrambling technologies with various fiber types to improve the A2D internal reference accuracy
- Procurement, system integration and performance verification of fiber scrambler
- Procurement, system integration and performance verification of a second fiber attenuator to be placed in the internal reference path to avoid saturation during Rayleigh Instrument Spectral Registration (ISR) calibrations without changing the illumination at fiber exit.
- Airworthiness certification preparation for A2D (addition of new scrambler and GoPro camera power supply)

The laser alignment activities were successful in restoring a stable and centrally aligned UV laser output, however, the obtained parameters couldn't be improved and resulted in a measured laser divergence of 115 µrad (+/-3σ), M^2 = 1.3 and an output power of 2.7 W.

7.2 Operational procedures and constraints

Additional to the preparatory work described above, there are system specific tasks to accomplish before and during both the campaign and every measurement flight. This section describes the procedures as well as the associated operational constraints of A2D.

The weather situation in November 2018 provided no good conditions for the alignment check of A2D on ground. For this the Falcon in on the apron outside of the hangar and a mirror on the ground redirects the A2D LOS into the atmosphere as shown in Figure 7-1. Fog and low clouds during the available days before the test flight just allowed a basic alignment check. However, during the performed test flight, the alignment check and refinement could be performed. Ground measurements were tried but finally aborted due to fog or low clouds during November 9, 13. and 14. but could successfully be performed on November 20.

Technical issues with the Falcon delayed the first flights and lead to a few flight cancellations during the campaign. With the obligation to file a flight plan to ATC 2 – 3 days in advance combined with the variable weather conditions in Europe in November, it was tried to find a flight possibility on every available flight day. Limitations due to fog during take-off or landing required cancelling 5 flights. Overall there were 20 flights planned out of 14 had to be cancelled and 6 could be performed. 2 out of the 3 performed underflights with A2D activated were only possible because of the extension of the campaign time by one week into December on short notice. This recommends planning a longer time frame for campaigns during this season with potential operational limitations due to weather on the track, but also at the airport.

For more information on the preparatory work prior to the first flight and before every flight as well as the operation of A2D in-flight please refer to the WindVal II Final Report (DLR 2018a), and the WindVal III CIP (DLR 2018b).

Figure 7-1: DLR Falcon on the DLR apron during alignment and ground measurements before the test flight and start of the WindVal I campaign.

7.3 A2D performance overview

During the WindVal III airborne campaign the A2D was operating without major technical problems and delivered a large amount of high-quality wind and calibration measurements. One exception is the first Aeolus underflight conducted on 12 November when the malfunction of a power supply modules prevented the switch-on of essential modules of the instrument. Additionally, two short data gaps (< 5 minutes) during the flights on 22 November and 3 December were caused by software issues or failure of the transmit-receive co-alignment loop. A limitation of the data quality may result from the failure of the electro-optic modulator (EOM) which blocks the atmospheric path for several µs after transmission of the laser pulse, thus preventing strong backscattered light produced close to the instrument (up to about 1 km) from being incident on the detectors. In this way, the EOM temporally separates the atmospheric signal from the internal reference signal. However, preliminary data analysis indicates that, despite the malfunction of the EOM, the internal reference signal is not significantly affected by the atmospheric signal. The limitations of the A2D data quality and their causes are summarized in Table 7-1 together with the set operation modes and additional comments for each flight.

Table 7-1: Mission objectives, A2D operation modes and quality limitations for all flights along with related information about the laser performance and causes for data gaps. Nominal operation refers to wind measurements as opposed to other instrument modes, e.g. MOUSR (Mie out of Useful Spectral Range), response calibrations, imaging mode.

Flight Date	Mission	A2D operation modes	Limitations / disturbances	Comments
12/11	Test flight	Nominal, 3 MOUSR in Imaging Mode	A2D alignment optimization was limited by cirrus cloud influence. EOM was not operable. Reference laser frequency stabilization had to be relocked after a sudden frequency jump.	Optimization of the transmit-receive path alignment using imaging mode. Laser power: 2.4 W at start, 2.55 W before landing.
17/11	Aeolus Underflight #1	-	The A2D was not operational due to malfunction of a power supply module supplying several essential devices of the instrument.	-
22/11	Aeolus Underflight #2	Nominal, 2 MOUSR in Lidar Mode	EOM was not operable, 3 min. data gap due to failure of transmit-receive co-alignment loop	The Falcon cabin pressure changed by 10 hPa when changing the flight level for the way back in southern Italy. Laser power: 2.4 W at start, 2.56 W before landing.
29/11	Calibration flight	4 IRCs	EOM was not operable, the wavemeter had to be connected to another laptop due to a broken USB connector. This required post-processing of the laser frequency data.	Laser power: 2.4 W at start, 2.55 W before landing.
03/12	Aeolus Underflight #3	Nominal, 2 MOUSR in Lidar Mode 1 MOUSR in Imaging Mode	EOM was not operable, 5 min. data gap due to failure of the transmit-receive co-alignment loop and LabVIEW software crash.	Due to tail wind on the runway for full-fuel take-off in Oberpfaffenhofen, a short flight with low fuel to Memmingen was the initial step. Laser power: 2.35 W at start, 2.45 W before landing.
05/12	Aeolus Underflight #4	Nominal, 2 MOUSR in Lidar Mode	EOM was not operable.	Laser power: 2.3 W at start, 2.3 W before landing

7.4   Fiber scrambling for speckle noise reduction

Speckle noise was identified as one of the major causes for the increased random error of the A2D Rayleigh and Mie channel internal reference. As already discussed in (DLR 2016) and (DLR 2018a), the noise is introduced by the use of a fibre to transmit the internal reference signal from the laser to the front optics where it is injected into the receiver reception path and co-aligned with the atmospheric signal. This is different compared to the free optical path set-up in the transceiver of the satellite instrument which does not suffer this difficulty. The speckle pattern which was estimated to consist of about only 2000 speckles is the input for the Fizeau spectrometer and, after modification by reflection, also for the Fabry-Pérot spectrometers (DLR 2016) (Figure 7-2).
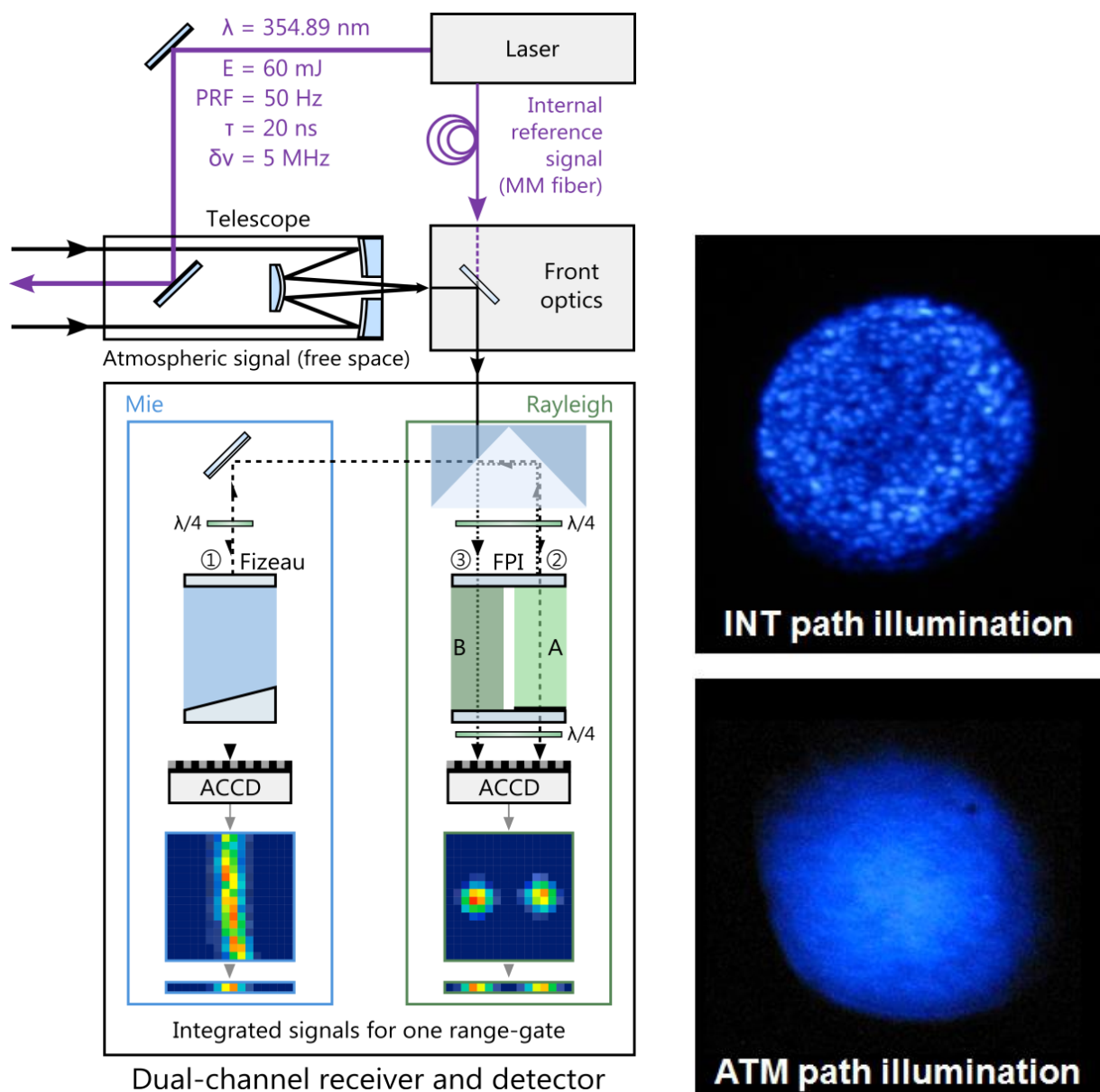
Figure 7-2: Schematic of the A2D consisting of a UV laser transmitter, a Cassegrain telescope, front optics and a dual-channel receiver. As opposed to the satellite instrument, the internal reference (INT) signal is guided to the front optics via a multimode fiber. This results in a speckle pattern of the INT intensity distribution incident on the Rayleigh and Mie channel. The images on the right show the INT and atmospheric (ATM) path illumination of the spectrometers measured with a continuous-wave UV laser (Zouk Cobolt) whose output was coupled into the respective optical paths of the A2D.

Although the speckle pattern is static over short time scales of a few seconds to minutes, slow changes in the intensity distribution of the internal reference signal are introduced by variations in laser frequency, polarization or (ambient) fibre temperature, which in turn modify the response of the Mie and Rayleigh spectrometers. Since the response measured for the internal reference forms the basis for the determination of the Doppler frequency shift, and thus, the wind speed in each atmospheric range gate, the speckle-induced fluctuations increase the random error over the entire wind profile.

Comparison of the internal reference frequencies derived from the Rayleigh and Mie channel responses against the frequencies measured using a wavemeter showed random variations on the order of 5.2 MHz (Mie) and 9.0 MHz (Rayleigh) on observation level (14s integration time, 700 laser pulses), corresponding to wind errors of 0.9 m/s and 1.6 m/s, respectively (top panel of Figure 7-3).
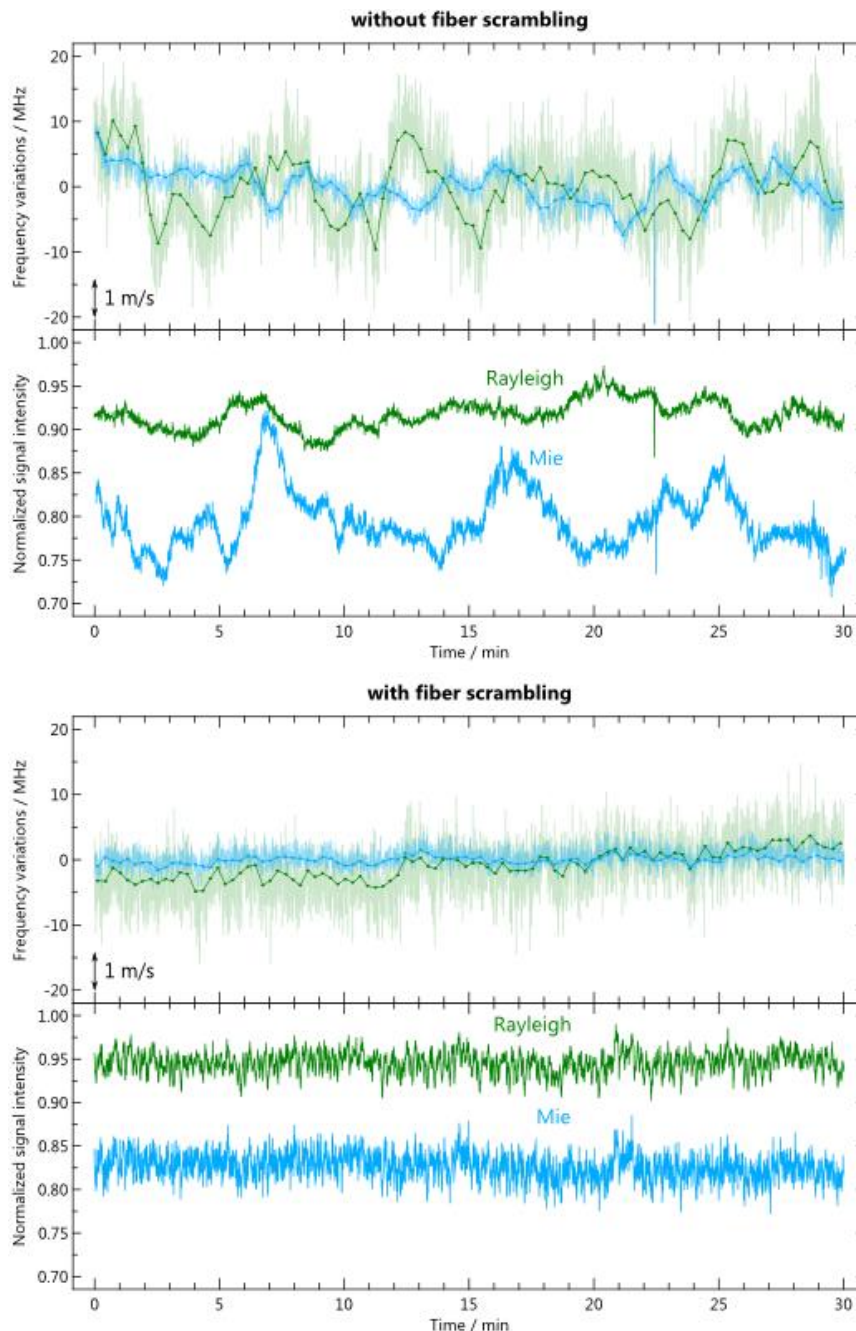
Figure 7-3: Rayleigh (green) and Mie (blue) internal reference frequency and intensity variations of the A2D internal reference without (top) and with (bottom) implementation of a fiber scrambler over a period on 30 minutes. The frequency data is given on measurement level (mean over 20 laser pulses, solid lines) and on observation level (700 pulses, dots). The intensity data is given on measurement level.
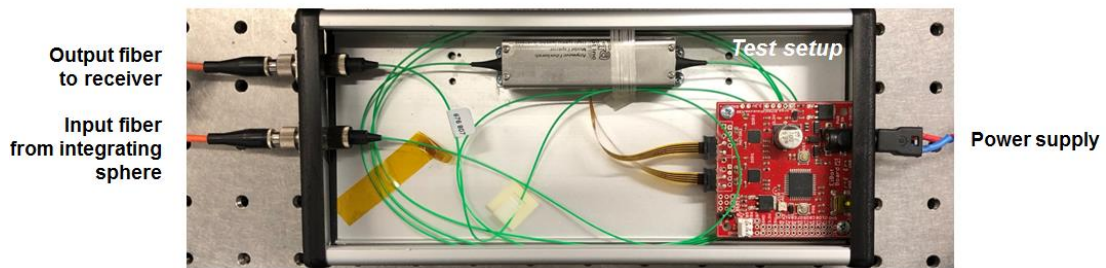
Figure 7-4: Setup for testing the fiber scrambler integrated in a compact box together with the driver.

Significant reduction of the internal reference response fluctuations has been accomplished by integrating a fiber scrambler in front of the multimode fiber. The mode scrambler (GiGa Concept Inc., Figure 7-4) is based on two counter-rotating step motors which squeeze a portion of a fiber at a time constant of a few milliseconds. Compressional and torsional stress of the fiber gives rise to local and stress-induced birefringence during these motions. This leads to a decorrelation of the modes supported by the fiber, thus homogenizing the intensity distribution at the fiber output and diminishing speckle noise.

As a result, the response variations of the internal reference signal are lowered to 1.1 MHz (Mie) and 4.2 MHz (Rayleigh), which corresponds to a reduction in random wind error by a factor of about five (0.2 m/s) and two (0.8 m/s), respectively (bottom panel of Figure 7-3). In addition, the intensity fluctuations are decreased by 55% (Mie) and 22% (Rayleigh). Smoothing of the speckle pattern hence has a large impact on the precision of the A2D.

Finally, the Rayleigh filter transmissions measured by means of an instrument spectral registration (ISR) showed significantly smaller deviations from the theoretical filter functions (smaller high-frequency residuals) after implementation of the fiber scrambler, thus allowing for a better characterization of the Rayleigh channel (Figure 7-5). Accurate knowledge of the filter parameters is crucial for simulating the behaviour of the A2D, especially the impact of pressure and temperature changes on response calibration results.
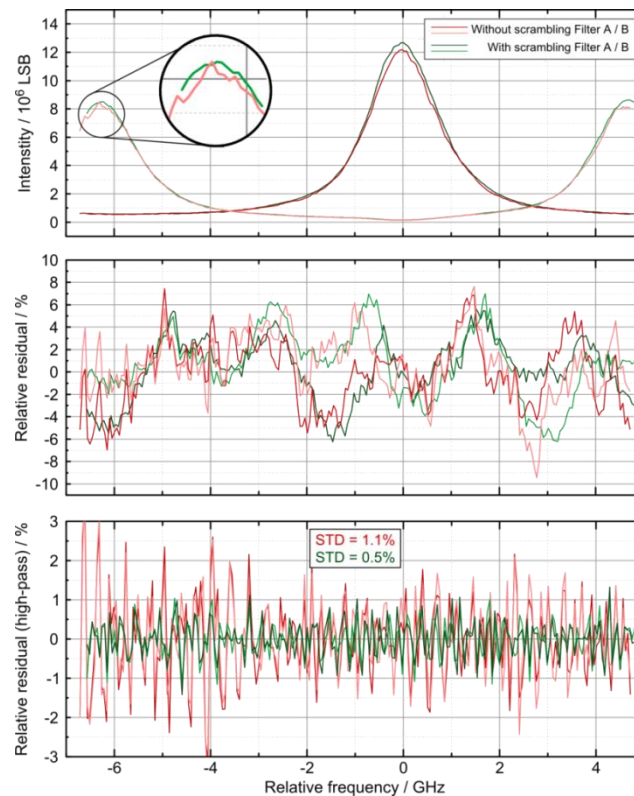
Figure 7-5: Top: A2D Rayleigh filter transmission curves measured without (red) and with (green) fiber scrambling of the internal reference. Middle: Relative residual of the measured transmission after subtraction of the theoretical filter transmission function. Bottom: Relative residual of the middle panel after application of a high-pass filter.

7.5 Summary of A2D performance during WindVal II

A2D was performing as expected and similar to good performances achieved during previous campaigns. Improved results for the stability of the internal reference could be demonstrated after successful integration of a fiber scrambler. The laser UV frequency stability was again in the range of 2 MHz – 3 MHz throughout the campaign and the laser power between 2.3 W and 2.6 W. All performance degradations during the campaign were of minor or negligible influence as for example the EOM non-operability. One flight had to be cancelled and A2D was off during one underflight due to a broken fuse which was poorly accessible and took time to replace. In addition to the detailed performance description in the previous chapters during the Preliminary Data Meeting (PDM) for WindVal III on 8 January 2019 at DLR Oberpfaffenhofen the explanation for the occasionally observed enhanced background ratio for Rayleigh and Mie signals was found to be originating from sunlight through the window next to the mirror in front of the A2D receiver. Although this enhanced asymmetric background on the two channels doesn't detriment the A2D performance, the window shutter will remain closed for future campaigns. Additionally and as a quick support to the Aeolus commissioning, two Dark Current in Memory Zone (DCMZ) measurements were recorded with the A2D and delivered to ESA as support to the hot-pixel issue found on the ALADIN ACCD signals. Although the A2D ACCDs are as old as the ones in orbit on ALADIN, no hot pixels were detected. Only a slightly warm pixel on the Mie ACCD with negligible influence on A2D performance was found as shown in Figure 7-6. This confirms the space environment driven hot pixel origin for the ALADIN ACCDs.
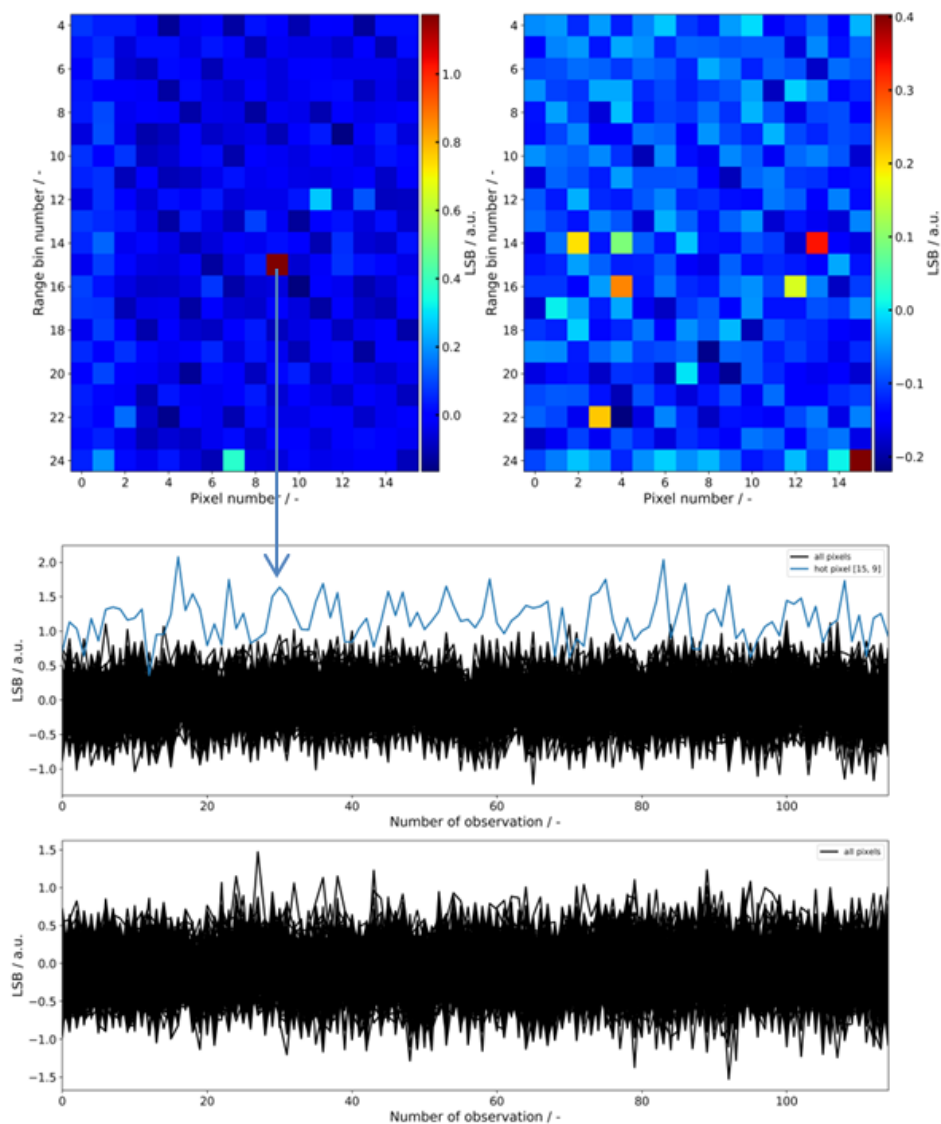
Figure 7-6: DCMZ measurements for Mie (left and upper timeline) and Rayleigh ACCD signals showing only one slightly warm pixel on the Mie ACCD.

8 Airborne response calibrations

In this chapter, the four airborne response calibrations (also named Instrument Response Calibration, IRC) performed by the A2D during the WindVal III campaign in 2018 are presented. For a more detailed discussion of A2D response calibrations in general and airborne response calibrations performed during campaigns in the past years please, refer to chapters 3 and 4 in (DLR 2012b), chapter 8 in (DLR 2017) and chapter 9 in (DLR 2018a).

8.5 Calibration flight in Italy on 29 November 2018

Spectral response calibration of the A2D is a prerequisite for the wind retrieval, since the relationship between the Doppler frequency shift of the backscattered light, i.e. the wind speed, and the response of the two spectrometers has to be known for the wind retrieval. In particular, proper knowledge of the Rayleigh response for different altitudes is necessary, as the spectral shape of the Rayleigh-Brillouin backscatter signal significantly depends on temperature and pressure of the sampled atmospheric volume and thus varies along the laser beam path.

For deriving the frequency-dependence of the Rayleigh and Mie channel spectral response, a frequency scan of the laser transmitter is carried out, thus simulating well-defined Doppler shifts of the radiation backscattered from the atmosphere within the limits of the laser frequency stability. During the calibration, the contribution of (real) wind related to molecular or particular motion along the instruments' LOS has to be eliminated, i.e. the LOS wind speed v_{LOS} needs to be zero. In practice, this is accomplished by flying curves at a roll angle of the Falcon aircraft of 20°, resulting in approximate nadir pointing of the instrument and hence $v_{LOS} \approx 0$, while assuming that the vertical wind is negligible. Consequently, regions with expectable non-zero vertical winds, e.g. introduced by gravity waves or convection are avoided in this procedure. Nadir pointing leads to a circular flight pattern of the aircraft which is preferably located over areas with high surface albedo in the UV spectral region (e.g. over ice), hence enabling strong ground return intensities and, in turn, high SNR. In the course of one calibration procedure which takes about 24 minutes, highest attention has to be paid to the minimization of all unknown contributions to the Rayleigh and Mie response such as biases resulting from inaccurate co-alignment of the transmit and receive path, temperature variations of the spectrometers or frequency fluctuations of the laser transmitter.
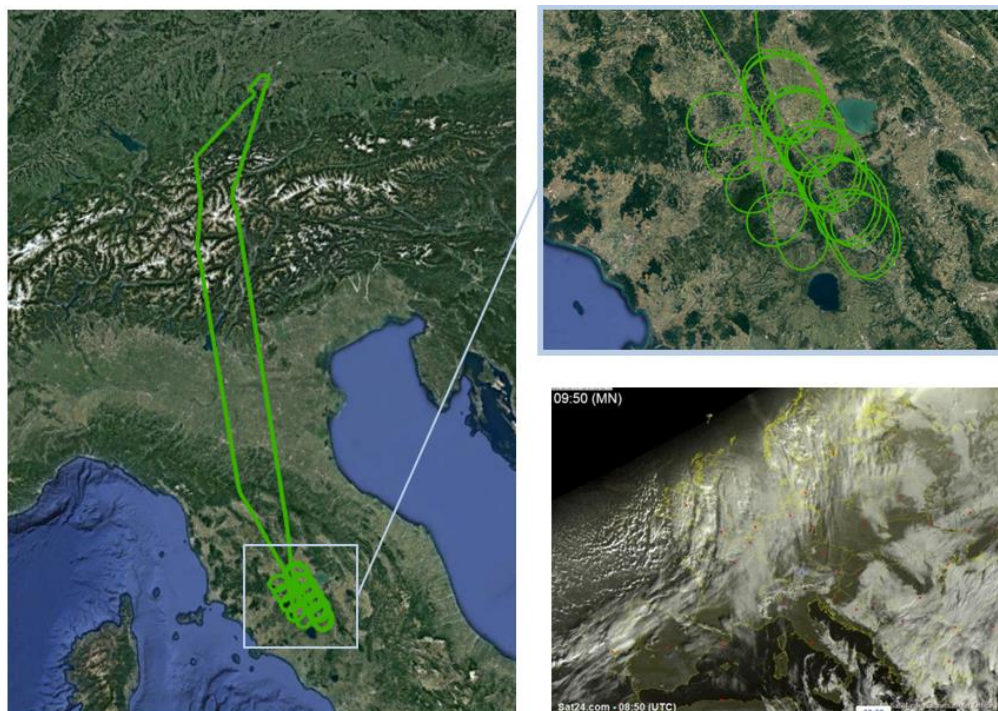
Figure 8-1: Flight tracks of the calibration flight carried out on 29/11/2018 (left and top right) and satellite image indicating cloud-free conditions in the target area between Rome and Florence.

In the frame of WindVal III one flight was dedicated to the calibration of the A2D. The flight was conducted on 29 November 2018 when cloud-free conditions were present in the region between Rome and Florence in Italy. Figure 8-1 shows the flight track of the calibration flight together with a satellite image of Europe showing the good conditions in Northern Italy on that day.

In the period from 10:48 UTC to 12:51 UTC, four response calibrations were performed without any interruption or limitation of the instrument. The start and stop times are given in Table 8-1 below.

Table 8-1: Overview of WindVal III calibration flights.

Flight number	Date	Flight time (UTC)
1	29/11/18	10:48 - 11:10
2	29/11/18	11:23 – 11:41
3	29/11/18	12:00 – 12:21
4	29/11/18	12:30 – 12:51

For assessing the overall quality of a response calibration, a number of recordings of parameters have to be checked for plausibility and whether or not these parameters moved within the given thresholds. Such parameters are for instance temperatures related to the RSP and the OBA, the cabin pressure and the laser beam pointing information. The temperature regulation of the Rayleigh spectrometer performed well with a peak-to-peak amplitude of only 8 to 10 mK, as depicted in Figure 8-2 (left panel). However, the OBA temperature showed relatively large variations, especially during calibration #3 (70 mK peak-to-peak) which can lead to systematic errors of the calibration data due to changes of the Fizeau interferometer spacing.

The pressure within the Falcon cabin showed a peak-to-peak range of 0.7 hPa which corresponds to a response range of 3 MHz (0.53 m/s) in the Mie channel and 7 MHz (1.24 m/s) in the Rayleigh channel if applying the results of a pressure campaign in April 2008 (DLR 2010). Moreover, the cabin temperature and humidity were in the normal range.
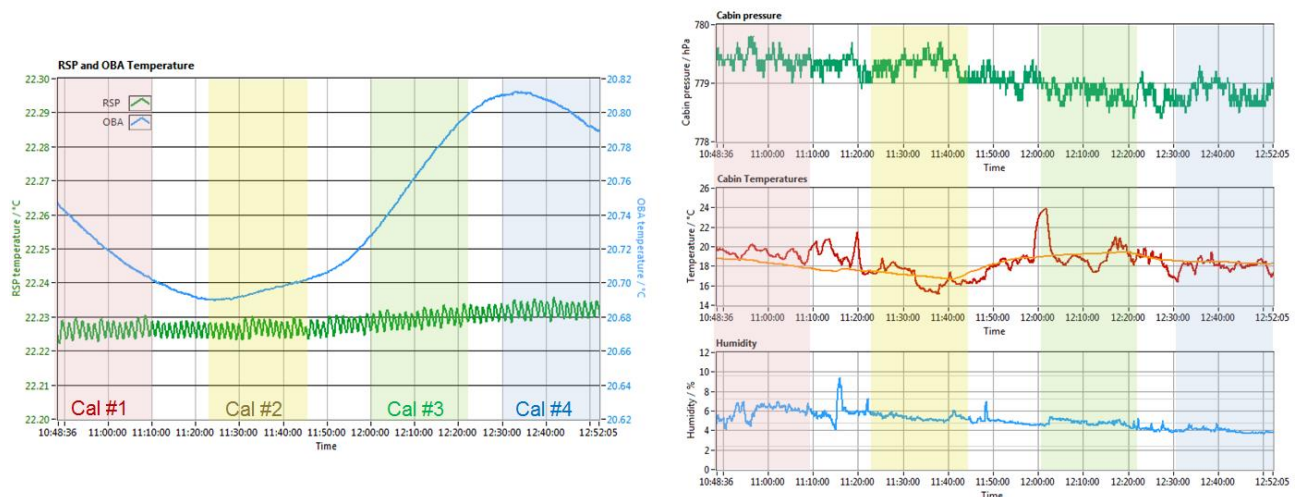
Figure 8-2: Left: Evolution of the OBA (light blue) and RSP temperature (green) in the course of the four response calibrations. Right: Cabin pressure (top), cabin temperature (middle) and humidity (bottom). The coloured shaded areas indicate the periods of the four calibrations.

8.6 Results of response calibration #1

Aside from temperature and pressure, additional housekeeping parameters are analysed for each response calibration, as they represent important quality criteria for selecting the best response calibration for the wind retrieval. Such parameters are the laser frequency stability and the pointing stability. Monitoring the UV frequency of the outgoing laser pulses by a high-precision wavemeter (HighFinesse, WS Ultimate 2) with a relative accuracy of 10^{-8} allows for the detection of e.g. incorrectly conducted frequency step commands or increased frequency instability due to aircraft vibrations induced, for example by clear air turbulence. Figure **8-3** shows the laser frequency on a pulse-to-pulse basis (purple line) over the whole frequency range of a response calibration (1600 MHz) and the pulse-to-pulse difference in black. For all four calibrations the frequency stability was on the order of 2 to 4 MHz which is a very good performance.
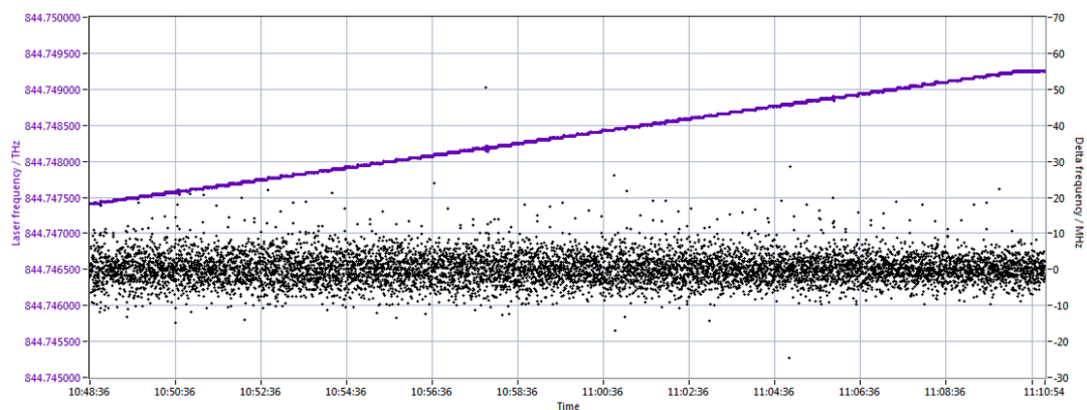
Figure 8-3: Absolute laser frequency (purple line) and pulse-to-pulse frequency difference (black dots) during the response calibration #1 performed on 29/11/2018 from 10:48 UTC to 11:10 UTC.
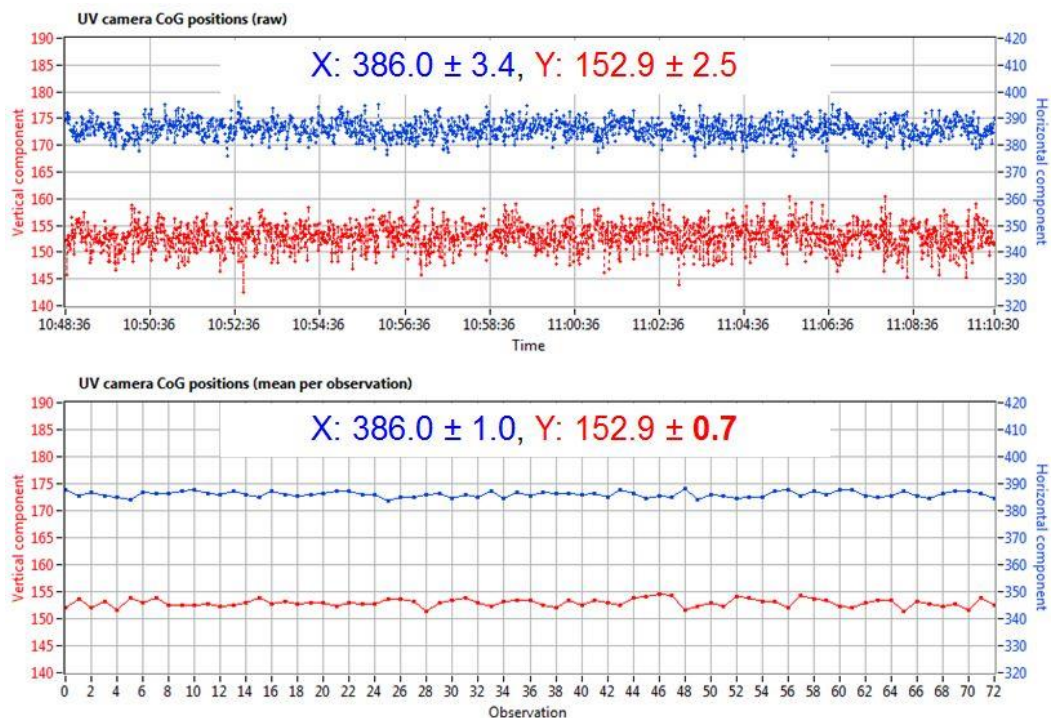
Figure 8-4: Stability of the transmit-receive co-alignment loop during the response calibration #1 performed on 29/11/2018 from 10:48 UTC to 11:10 UTC. The two panels depict the horizontal (blue) and vertical (red) component of the spot centre-of-gravity (CoG) measured with the UV camera that is integrated in the transmit-receive path co-alignment loop. The top panel shows the CoG values at the feedback sampling rate of 1s, while the bottom panel provides the data on observation level. The given values represent the mean and standard deviation for the respective components.

The pointing stability is assessed by measuring the variation in the vertical and horizontal pixel positions of the laser beam which is detected by a UV camera integrated in the front optics of the A2D, as explained in (DLR 2018a). Figure 8-4 depicts the horizontal (blue) and vertical (red) component of the spot at the feedback sampling rate of 1s (top panel) and on observation level (bottom panel). The given values represent the mean and standard deviation for the respective components. A change of one vertical pixel corresponds to a change in incidence angle of 13 µrad, and a change of one horizontal pixel corresponds to a change in incidence angle of 6.75 µrad. Thus, for calibration #1, the pointing stability was around 6 to 9 µrad both in vertical and horizontal direction, corresponding to a potential random Rayleigh wind error of 2.3 to 3.5 m/s (DLR 2012c). These fluctuations are higher than during WindVal II where the pointing stability was around 4.5 µrad (1.8 m/s).

Figure 8-5 depicts the Rayleigh and Mie raw signal intensities after DCO and background subtraction, but without range correction and bin scaling. The diagrams allow for a first rough assessment of the quality of the available response calibration. In particular, clouds and aerosol loaded regions would become visible which have to be rejected for the retrieval of the atmospheric response function in the Rayleigh channel within a dedicated quality control scheme. Also, the higher the optical thickness of a cloud, the higher is the extinction for the ground return signal. This can lead to invalid observations within the Rayleigh and Mie ground return response functions, and hence to a possibly increased random and/or systematic error in the thereby retrieved ground speeds. However, for the WindVal III campaign the mission planning team successfully managed to spot a cloud- and aerosol-free region in Italy where the A2D could perform its IRCs under almost ideal atmospheric conditions. Thus, the distributed ground return signal is visible between range gates #21 - #23 for both the Rayleigh and the Mie channel. Range gate #4 corresponds to the internal reference, i.e. the altitude of the aircraft. The measured raw atmospheric signals in the first range gates (#5 to about #8) right below are dominated by the strong near-field return (due to the R^2- range dependency) in combination with the overlap function of laser beam and telescope field of view.

In contrast to the WindVal II campaign, all four calibrations were performed over ice-free land with relatively low albedo values in the UV spectral region (~ 0.05 - 0.2). Therefore, the ground signals are considerable lower than for response calibrations over ice with high albedo values in the UV (>0.9).
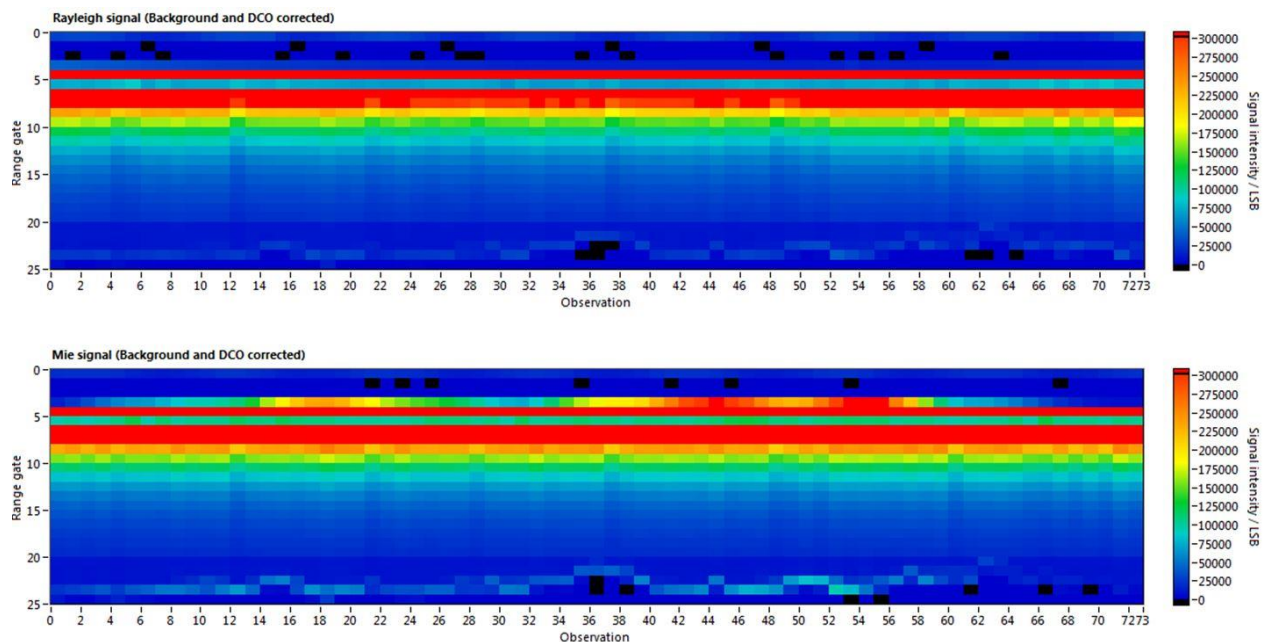
Figure 8-5: Rayleigh (top) and Mie (bottom) signal intensities on observation level measured during the response calibration #1 performed on 29/11/2018 from 10:48 UTC to 11:10 UTC. Ground signals are distributed over three different range gates (#21 to #23). Range gate (or layer) #4 corresponds to the internal reference.

The above results of calibration #1 from 29/11/2018, 10:48 UTC are exemplary for a successful and flawless IRC where the entire procedure was characterized by

- high temperature stability,
- high pressure stability,
- high pointing stability,
- high frequency stability,
- absence of missing frequency steps,
- absence of CoG outliers and
- absence of clouds.

The quality criteria presented above (spectrometer and OBA temperature, cabin pressure, laser frequency and pointing, Rayleigh and Mie raw signal intensity) can be easily checked shortly after a response calibration. Apart from that, there are additional parameters which require more extensive processing to be obtained and/or whose interpretation regarding the quality of a calibration is more subtle and not straightforward. The latter is the case for the Rayleigh spot positions and width (FWHM). All calibrations were performed at the same CoG reference position (CoG_X = 386 pixels, CoG_Y = 153 pixels) which determines the incidence angle of the backscatter return onto the receiver spectrometers and hence the image of the field stop onto the Rayleigh and Mie ACCDs. Thus, the positions and widths of the two Rayleigh spots belonging to Filter A and B were expected to be stable over the four calibrations. However, a drift in the spot positions was observed, as shown in Figure 8-6. Here, the uppermost points correspond to the internal reference which is independent of the CoG settings, as the signal is guided to the receiver separately. The spots for the atmospheric range gates below 9 km moved by about 0.05 pixel between calibration #1 and calibration #4 (2 hours). Also, a large change in the FWHM values by more than 0.3 pixel between calibration #2 and calibration #3 is evident from Figure 8-7. The change in the Rayleigh spot positions and widths in the course of the calibration flight (despite constant COG reference position) suggests a (thermo-) mechanical drift of optical components or possible influence of sub-visible cirrus below aircraft to be the root cause. The former is supported by the fact that the heating of the bottom window of the aircraft was switched-on between calibration #2 and #3. The warm air blown across the window might have heated up the turning and/or telescope mirrors located close to the window, thus altering the beam alignment.
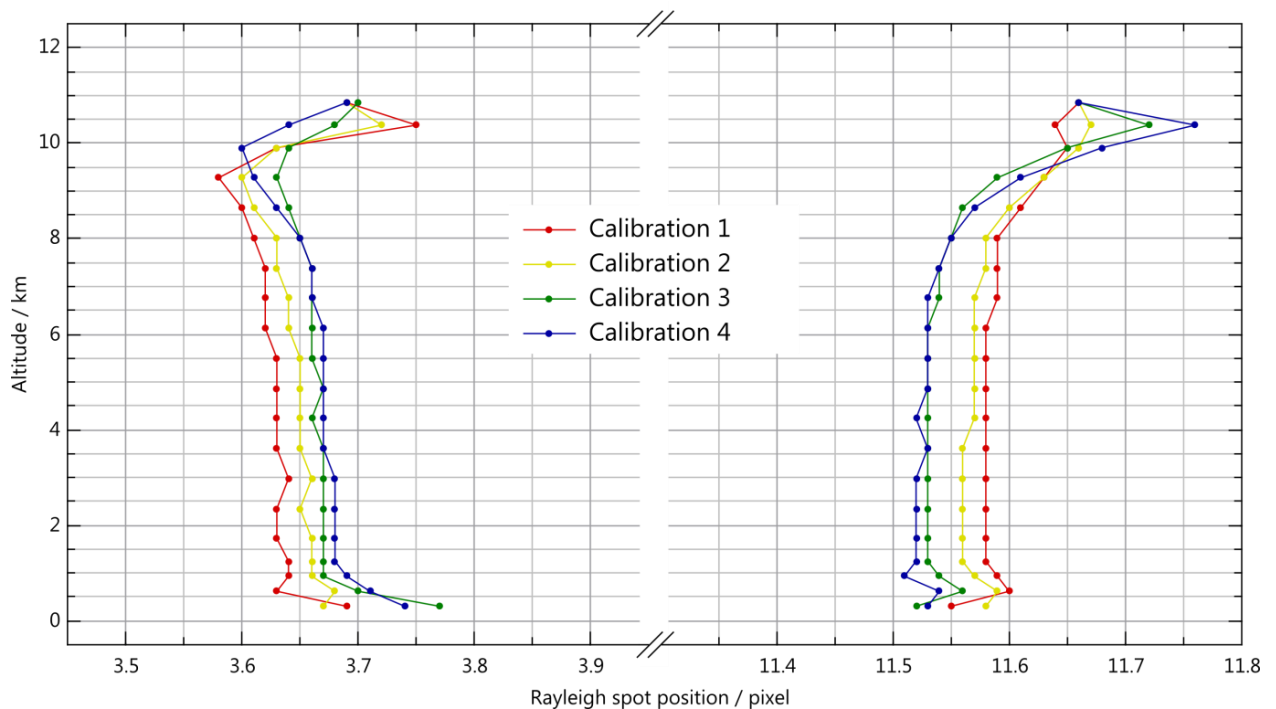
Figure 8-6: Rayleigh spot position measured during the four response calibrations (mean over all observations). The uppermost data points correspond to the internal reference.
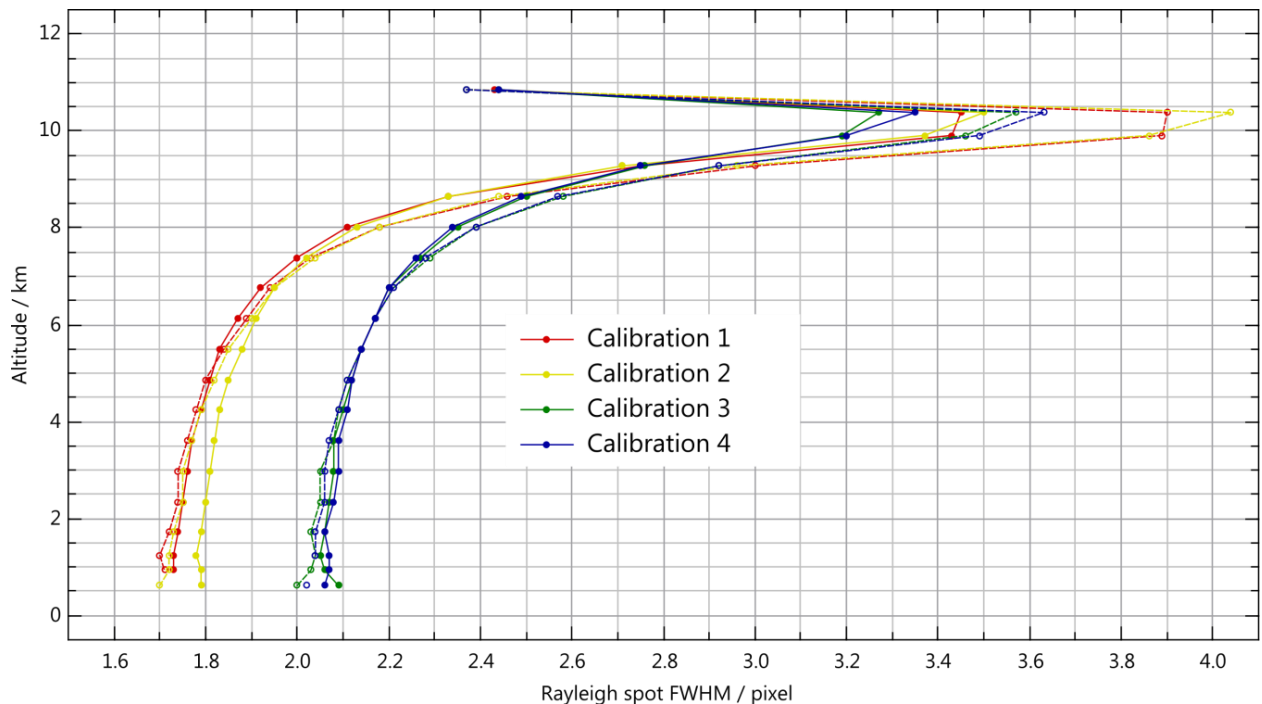
Figure 8-7: Rayleigh spot width (FWHM) measured during the four response calibrations (mean over all observations). The uppermost data points correspond to the internal reference.

The spot width is determined by the illumination of the field stop in the front optics as well as by the divergence angle of the light incident on the Rayleigh spectrometer. The FWHM for the internal reference is generally larger than for the atmospheric path due to the full (or even over-) illumination of the field stop by the divergent light emerging from the internal reference fiber. The difference in the spot width between Filter A and B can be explained with the sequential configuration of the Rayleigh spectrometer involving different paths, and hence different divergence angles of the two beams transmitted through the filters. Spot A is smaller than spot B by about 0.2 pixels, since the latter is associated to the slightly more divergent beam that is reflected from filter A before being incident on the second filter. More information on the parameters influencing the Rayleigh spot positions and width is provided in (DLR 2012c).

The impact of the Rayleigh spot positions and widths on the wind results is not straightforward, so that evaluation of the quality of a response calibration based on the spot parameters is rather difficult. Thus, no correlation was found between Rayleigh spot position, width and atmospheric responses during wind measurement mode, which could be used for correction. Nevertheless, analysis of the wind scenes conducted during WindVal III has shown, that using calibration #1 produced wind results with the highest accuracy and precision (see chapter 9), suggesting that the alignment of the A2D at the beginning of the calibration flight was the one which is most representative for the alignment during the underflights.

The Rayleigh and Mie results of response calibration #1 relevant for the wind retrieval are shown in the following two figures. Figure 8-8 depicts the Rayleigh responses in dependence on the relative laser frequency (with respect to the Rayleigh filter cross-point frequency) for the internal reference and all atmospheric range gates. The right plot illustrates the slopes and intercepts for each range gate derived from a linear fit of the respective response curve. The data points are plotted at the bin centre altitudes of the respective range gates, with the values of the internal reference given at the flight altitude. The Mie results are shown in Figure 8-9, depicting the response curves for the internal reference and the ground as well as the respective nonlinearities and residuals after applying a third-order polynomial fit to the nonlinearities. Both the Rayleigh and Mie results from calibration #1 are very consistent with those of previous campaigns. In particular, calibration coefficients entering the Rayleigh and Mie wind retrieval are a in the expected range. The same holds true for the nonlinearities and their standard deviations of the frequency range.
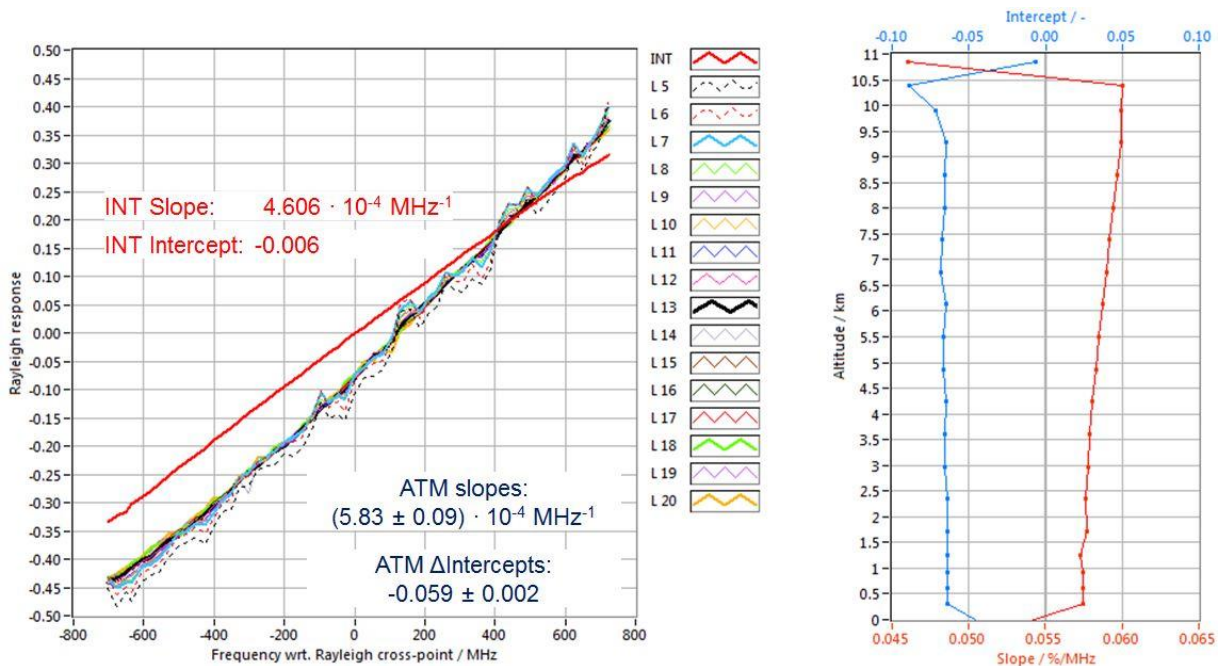
Figure 8-8: Left: Rayleigh responses in dependence on the relative laser frequency (with respect to the Rayleigh filter cross-point frequency) measured during response calibration #1 for the internal reference (red) and all atmospheric range gates. The right plot illustrates the slopes (red) and intercepts (blue) for each range gate derived from a linear fit of the respective response curve. The data points are plotted at the bin centre altitudes of the respective range gates, with the values of the internal reference given at the flight altitude.
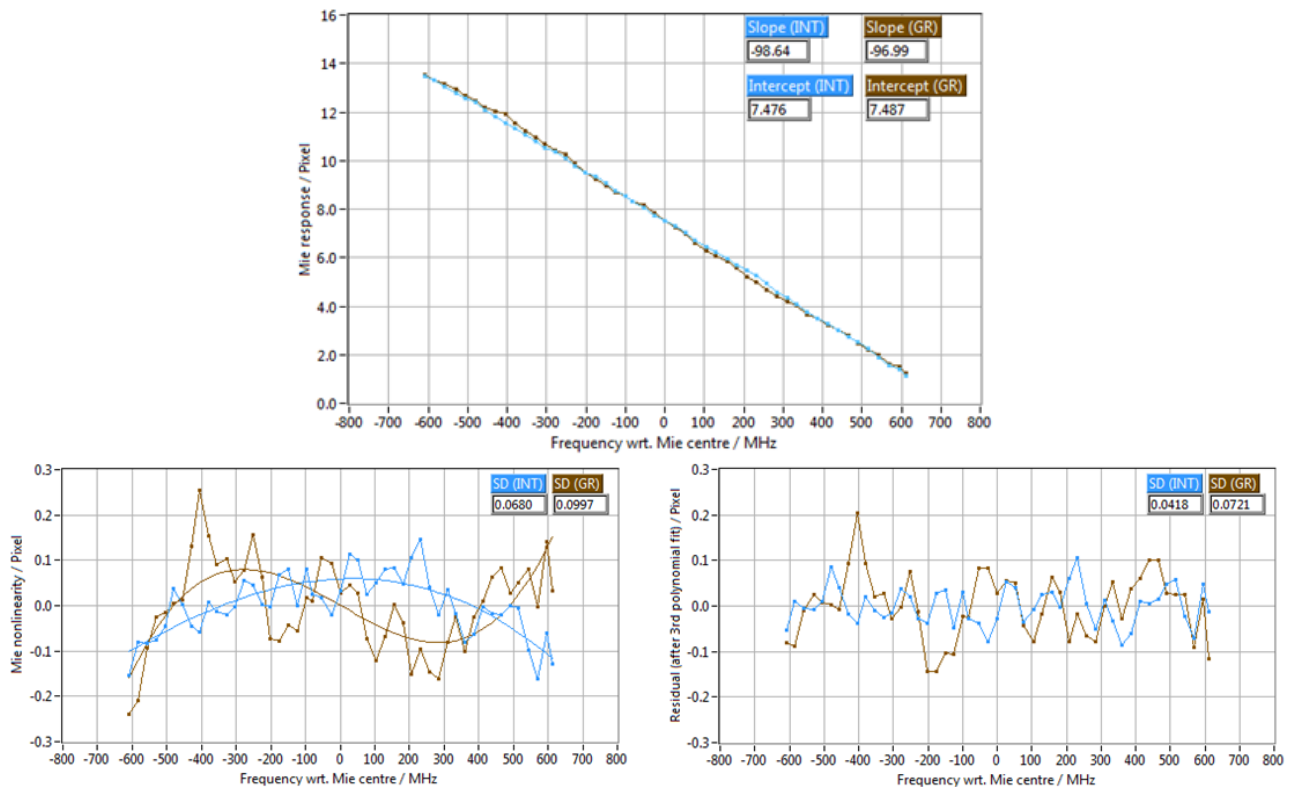
Figure 8-9: Top: Mie response curves for the internal reference (blue) and ground return (brown) derived from calibration #1. Bottom left: Mie nonlinearities for the internal reference (blue) and the ground return (brown). The respective standard deviations over the entire frequency range are given in the boxes. Bottom right: Residuals after applying a third-order polynomial fit to the nonlinearities (shown as solid lines in the left plot).

8.7 Overview of Rayleigh response calibrations

The altitude-dependent Rayleigh slopes and intercepts from all four calibrations are plotted in Figure 8-10. Here, the values for the internal reference and ground are plotted at the top and bottom, respectively. The vertical position of each data point represents the bin centre altitude of the respective range gate. For the wind retrieval, a linear interpolation is performed between the altitude-dependent coefficients deduced from the calibration in order to obtain the response function for the respective bin altitudes of the wind observation. The comparison of the slopes shows low variability both for the internal reference and over all atmospheric range gates. The different slopes are also summarized in Table 8-2. The values around $4.6 \cdot 10^{-4}$ MHz^{-1} for the internal reference and $5.8 \cdot 10^{-4}$ MHz^{-1} for the atmospheric range gates also agree well with the respective mean values from the WindVal II campaign ($4.55 \cdot 10^{-4}$ MHz^{-1}, $5.83 \cdot 10^{-4}$ MHz^{-1}) (DLR 2018a). The ground slopes are somewhat larger ($4.8 \cdot 10^{-4}$ MHz^{-1}) compared to WindVal II ($4.6 \cdot 10^{-4}$ MHz^{-1}) and show a slight drift from calibration #1 to calibration #4. They deviate from the internal reference slopes due to the atmospheric contamination, which has larger impact in case of low albedo (DLR 2018a).
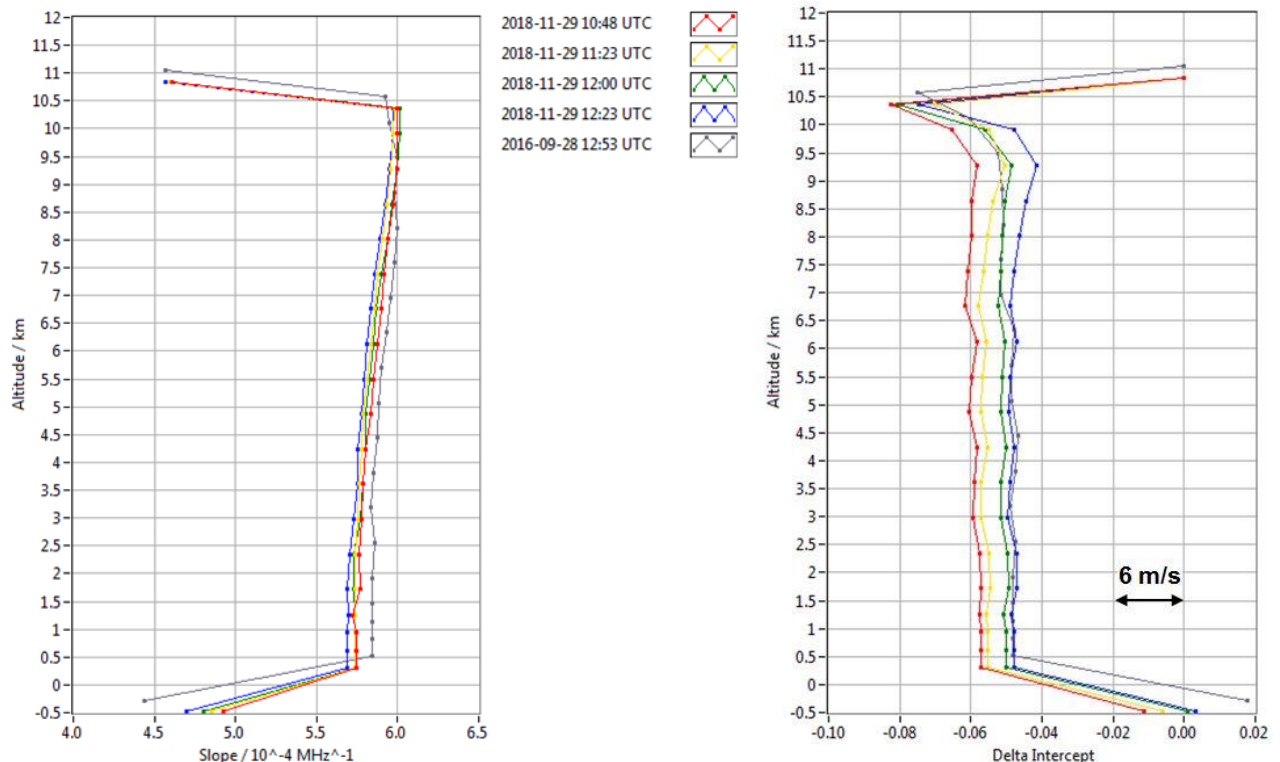
Figure 8-10: Slope (left) and Δ(intercept) (ATM – INT) values (right) determined from the linear fit of the Rayleigh response curves in dependence on the A2D range gate / altitude. The data points are colour-coded according to the four different response calibrations performed during WindVal III. The uppermost value represents the internal reference, while the lowermost point corresponds to the ground.

Regarding the Δ(intercept), i.e. the intercept values after subtraction of the internal reference intercept, a drift by more than 0.01 (3 m/s) is clearly visible from calibration #1 to calibration #4, especially in the upper range gates. This drift is in line with the observed change in the change in the Rayleigh spot positions and widths in the course of the calibration flight and most likely caused by a (thermo-)mechanical drift of optical components, as explained in the previous section. Aside from that, the atmospheric Δ(intercept) values of around -0.05 are very similar to those of the previous campaign (WindVal II: -0.049). The ground intercepts are close to that of internal reference and vary by about 0.006 which is comparable to the variations observed for the calibrations in WindVal II (0.005). These variations in the intercept correspond to wind speed variations of about 1.5 m/s.

A further parameter that should be taken into account when rating the quality of a Rayleigh response calibration is the residual error. As explained in (DLR 2017, section 8.5, DLR 2018a), it is defined as the deviation of the measured Rayleigh response from the fifth-order polynomial fitting function which is applied to account for the nonlinearities in the response curves. Calculating the standard deviation of the residual error over the frequency range of the calibration yields a measure of response variations that are not corrected during the wind retrieval, and thus introduce a random error. The obtained standard deviations per range gate are plotted in Figure 8-11. Due to the telescope overlap effect, the strongest variation, i.e. the largest standard deviation, is observed in range gates #5 to #8 close to the instrument. In the range gates underneath, the standard deviation is around 0.005 which corresponds to a random wind error of 1.5 m/s.
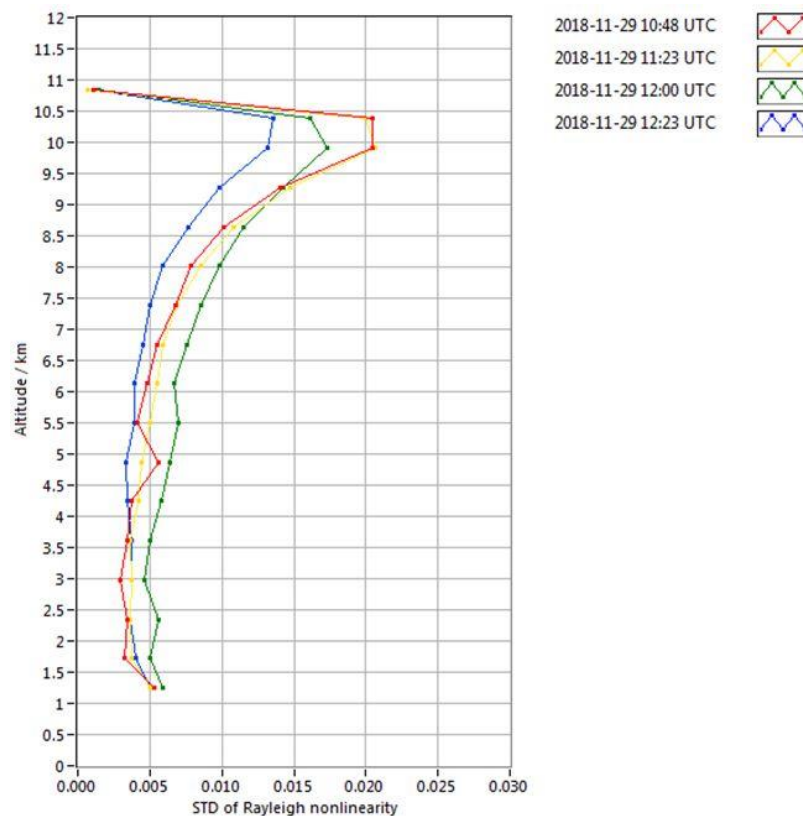
Figure 8-11: Standard deviation of the residual error in dependence on the range gate for all four calibrations performed during WindVal III (range gate #4 = internal reference).

Selection of the Rayleigh response calibration used for the wind retrieval

For choosing the best Rayleigh response calibration as the baseline for the wind retrieval, the different housekeeping parameters and Rayleigh response calibration results, as summarized in Table 8-2, were compared. Due to the high sensitivity of the Rayleigh spectrometer to variations of the incidence angle, the CoG variability is of major importance for the quality of the Rayleigh response calibrations. Here, calibration #1 showed the best performance with variations on observation level of only 1.0 pixel and 0.7 pixel for the horizontal and vertical component of the CoG, respectively (see Figure 8-4). In addition, calibration #1 is characterized by small residuals of the nonlinearities for both the internal reference and the atmospheric range gates, especially for the relevant range gates below 8 km, where only calibration #4 shows smaller values (see Figure 8 11). However, the latter calibration shows rather large CoG variations in the horizontal direction (1.4 pixel). Consequently, calibration #1 was chosen as the baseline for the Rayleigh wind retrieval. Note that, in principle, calibration parameters for the atmospheric range gates and the ground return can be taken from two different response calibrations.

Table 8-2: Overview of the Rayleigh response calibration results.

Parameter	Calibration 1	Calibration 2	Calibration 3	Calibration 4
Internal reference Slope	4.606	4.591	4.597	4.567
ATM Slope (mean ± STD from L7 to L23)	5.83 ± 0.09	5.81 ± 0.08	5.82 ± 0.09	5.78 ± 0.09
Ground Slope	4.921	4.855	4.801	4.699
Internal reference Intercept	-0.006	-0.006	-0.004	-0.003
ATM ΔIntercept (mean ± STD from L7 to L23)	-0.059 ± 0.002	-0.055 ± 0.002	-0.051 ± 0.001	-0.048 ± 0.002
Ground ΔIntercept	-0.011	-0.006	0.001	0.003
STD of residual nonlinearity (Internal reference)	0.0011 (0.4 m/s)	0.0007 (0.3 m/s)	0.0015 (0.6 m/s)	0.0013 (0.5 m/s)
STD of residual nonlinearity (ATM, mean ± STD from L7 to L23)	0.006 (1.8 m/s)	0.006 (1.8 m/s)	0.007 (2.3 m/s)	0.005 (1.5 m/s)
STD of residual nonlinearity (Ground)	0.010 (3.7 m/s)	0.007 (2.6 m/s)	0.007 (2.6 m/s)	0.007 (2.6 m/s)

8.8   Overview of Mie response calibrations

The Mie response curves for the four calibrations are depicted in Figure 8-12, while the derived calibration results are listed in Table 8-3. The figure illustrates the excellent reproducibility of the Mie responses for each frequency step. The slope values around -99 MHz/pixel for the internal reference and -97 MHz/pixel for the ground return are very similar to those of the previous campaign (-99.53 MHz/pixel, -97.63 MHz/pixel). The variations in the slope values for the internal reference and ground return are only 0.28 MHz/pixel and 0.27 MHz/pixel being a factor of two smaller than for WindVal II (0.57 MHz/pixel, 0.52 MHz/pixel). For the internal reference, this can be traced back to the implemented fiber scrambler which reduces the speckle noise of the internal reference signal incident on the Mie spectrometer. For the ground return, the lower variability is most likely due to the fact that the six calibrations from WindVal II were performed over different surfaces (4 over ice, 2 over land), resulting in a larger spread of ground slopes depending on albedo.
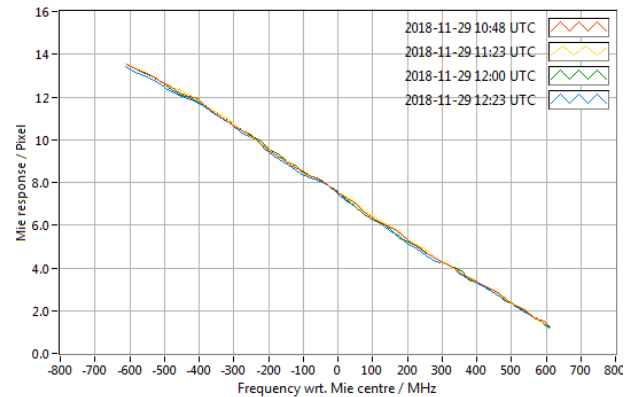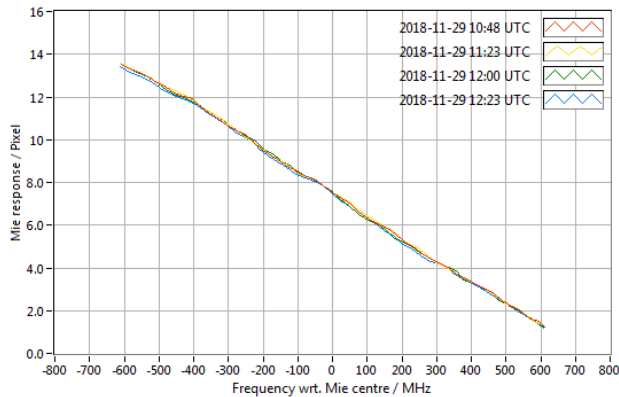
Figure 8-12: Mie response curves for the internal reference (left) and the ground return (right) derived from the four response calibrations performed during WindVal III.

Table 8-3: Overview of the Mie response calibration results.

Parameter	Calibration 1	Calibration 2	Calibration 3	Calibration 4
Slope **(Internal reference / ground)**	-98.64 MHz/pixel/ -96.99 MHz/pixel	-98.86 MHz/pixel/ -96.83 MHz/pixel	-98.69 MHz/pixel/ -96.65 MHz/pixel	-99.35 MHz/pixel/ -97.37 MHz/pixel
Intercept **(Internal reference / ground)**	7.476 pixel / 7.487 pixel	7.503 pixel / 7.502 pixel	7.479 pixel / 7.468 pixel	7.421 pixel / 7.383 pixel
STD of residual nonlinearity **(Internal reference / ground)**	0.04 pixel / 0.07 pixel	0.04 pixel / 0.07 pixel	0.04 pixel / 0.07 pixel	0.04 pixel / 0.08 pixel

The variability in the Mie intercepts of the internal reference among the calibrations of 0.03 pixels is much smaller compared to WindVal II (0.11 pixels) which is due to the considerable reduction of the speckle noise by means of the fiber scrambler. The Δ(Intercept) (INT – GR) varies by only 0.02 pixels which translates into potential wind variations of only 0.34 m/s when using a slope value of 98 MHz/pixel and the conversion factor of 5.63 MHz/(m/s). For WindVal II, the corresponding values were about 33% larger. Hence, the fiber scrambling significantly improves the reproducibility of the Mie calibrations.

Selection of the Mie response calibration used for the wind retrieval

The choice of the best Mie response calibration is driven by other criteria than for the Rayleigh channel. Since the Mie channel is much less sensitive to angular variations, the stability of the horizontal and vertical CoG components is of minor importance. Instead, the variability of the OBA temperature has a higher weight, as this parameter crucially influences the spacing of the Fizeau interferometer plates, thus affecting the measured Mie responses. The lowest variability in OBA temperature was observed for calibration #2 which is also characterized by the highest laser frequency stability. As stated above, the response calibration results are very similar for all four calibrations. Aside from the Mie slopes and intercepts, the residuals after applying a third-order polynomial to account for the Mie nonlinearities of the Mie response curve are almost identical. Hence, there are no additional arguments which favour or exclude a certain calibration. Therefore, the second response calibration was chosen for the Mie wind retrieval.

8.9   Summary of response calibrations and recommendations

The following table summarizes the relevant housekeeping parameters as well as the Rayleigh and Mie response calibration results for all four calibrations performed in the frame of the WindVal III campaign.

Table 8-4: Results of the WindVal III response calibrations: housekeeping parameters, Rayleigh and Mie calibration parameters which are relevant for the identification of the best calibration used for the wind retrieval.

Parameter	Calibration 1	Calibration 2	Calibration 3	Calibration 4
Housekeeping parameters				
Temperature variability (OBA/RSP)	48 mK / 8 mK (peak-to-peak)	12 mK / 8 mK (peak-to-peak)	70 mK / 10 mK (peak-to-peak)	20 mK / 8 mK (peak-to-peak)
Cabin pressure variability	0.8 hPa	0.7 hPa	0.6 hPa	0.6 hPa
Laser frequency variability	4.1 MHz	2.3 MHz	2.6 MHz	2.8 MHz
CoG reference position	X: 386.0 ± 1.0, Y: 152.9 ± 0.7	X: 385.8 ± 1.1, Y: 153.0 ± 0.8	X: 385.8 ± 1.3, Y: 153.1 ± 0.7	X: 386.0 ± 1.4, Y: 152.9 ± 0.7
Rayleigh results				
Slope (Internal reference / ground)	$4.606 \cdot 10^{-4}$ MHz^{-1} / $4.921 \cdot 10^{-4}$ MHz^{-1}	$4.591 \cdot 10^{-4}$ MHz^{-1} / $4.855 \cdot 10^{-4}$ MHz^{-1}	$4.597 \cdot 10^{-4}$ MHz^{-1} / $4.801 \cdot 10^{-4}$ MHz^{-1}	$4.567 \cdot 10^{-4}$ MHz^{-1} / $4.699 \cdot 10^{-4}$ MHz^{-1}
ΔIntercept ground	-0.011	-0.006	0.001	0.003
STD of residual nonlinearity (INT)	0.0011 (0.4 m/s)	0.0007 (0.3 m/s)	0.0015 (0.6 m/s)	0.0013 (0.5 m/s)
STD of residual nonlinearity (ATM)	0.006 (1.8 m/s)	0.006 (1.8 m/s)	0.007 (2.3 m/s)	0.005 (1.5 m/s)
ATM Slope (mean ± STD from L7 to L23)	$(5.83 \pm 0.09) \cdot 10^{-4}$ MHz^{-1}	$(5.81 \pm 0.08) \cdot 10^{-4}$ MHz^{-1}	$(5.82 \pm 0.09) \cdot 10^{-4}$ MHz^{-1}	$(5.78 \pm 0.09) \cdot 10^{-4}$ MHz^{-1}
ATM ΔIntercept (mean ± STD from L7 to L23)	-0.059 ± 0.002	-0.055 ± 0.002	-0.051 ± 0.001	-0.048 ± 0.002
ATM Rayleigh spot positions (A/B from L7 to L23)	(3.63 ± 0.02) pixel / (11.59 ± 0.02) pixel	(3.65 ± 0.02) pixel / (11.58 ± 0.02) pixel	(3.67 ± 0.03) pixel / (11.54 ± 0.02) pixel	(3.67 ± 0.03) pixel / (11.54 ± 0.02) pixel
ATM Rayleigh spot FWHM	(1.9 ± 0.3) pixel / (1.9 ± 0.4) pixel	(1.9 ± 0.3) pixel / (1.9 ± 0.3) pixel	(2.2 ± 0.2) pixel / (2.2 ± 0.2) pixel	(2.2 ± 0.2) pixel / (2.4 ± 0.2) pixel
Mie results				
Slope (Internal reference / ground)	-98.64 MHz/pixel/ -96.99 MHz/pixel	-98.86 MHz/pixel/ -96.83 MHz/pixel	-98.69 MHz/pixel/ -96.65 MHz/pixel	-99.35 MHz/pixel/ -97.37 MHz/pixel
Intercept (Internal reference / ground)	7.476 pixel / 7.487 pixel	7.503 pixel / 7.502 pixel	7.479 pixel / 7.468 pixel	7.421 pixel / 7.383 pixel
STD of residual nonlinearity (INT / ground)	0.04 pixel / 0.07 pixel	0.04 pixel / 0.07 pixel	0.04 pixel / 0.07 pixel	0.04 pixel / 0.08 pixel
Δ*f* (Mie center – Rayleigh crosspoint)	70 MHz	70 MHz	60 MHz	60 MHz

- Four response calibrations were carried out during one calibration flight in Northern Italy on 29 November 2018.

- All four calibrations are of high quality without cloud contamination and only minor differences in terms of laser frequency stability (3 to 4 MHz), stability of ambient pressure (0.6 to 0.8 hPa), stability of the Rayleigh spectrometer temperature (8 to 10 mK).

- However, there are differences regarding the pointing stability, especially in horizontal axis: 6.8 µrad (calibration #1) to 9.5 µrad (calibration #4).

- A drift in the Rayleigh spot positions was observed which moved by about 0.05 pixels between calibration #1 and calibration #4 (2 hours). Moreover, a large change in the FWHM values by more than 0.3 pixels between calibration #2 and calibration #3 is evident. The change in the Rayleigh spot positions and widths in the course of the calibration flight suggests a (thermo-)mechanical drift of optical components or possible influence of sub-visible cirrus below aircraft to be the root cause. The former is supported by the fact that the heating of the bottom window of the aircraft was switched-on between calibration #2 and #3. The warm air blown across the window might have heated up the turning and/or telescope mirrors located close to the window, thus altering the beam alignment.

- The drift manifest in the Rayleigh calibration Δ(intercept) values which vary from -0.011 (calibration #1) to 0.003 (calibration #4). This translates into a variation in wind speed of about 3 m/s.

- The Rayleigh response calibration results, especially the Rayleigh slopes and nonlinearities, are comparable to those obtained during the previous campaign WindVal II in 2016.

- The Rayleigh intercepts for the internal reference and ground return are very similar and vary by about 0.006 which is comparable to the variations observed for the calibrations in WindVal II (0.005). These variations in the intercept correspond to wind speed variations of about 1.5 m/s.

- Since the Rayleigh calibration results are very consistent for all calibrations apart from the Δ(intercept) values and due to the high sensitivity of the Rayleigh spectrometer to variations of the incidence angle, the CoG variability was given the highest weight for the choice of the most appropriate calibration. Regarding this parameter, calibration #1 showed the best performance with variations on observation level of only 1.0 pixel and 0.7 pixel for the horizontal and vertical component of the CoG, so that it was selected as the baseline for the Rayleigh wind retrieval.

- The Mie response calibrations were highly reproducible with small variations in the slope and Δ(intercept) values of both the internal reference and ground return. The slope variations (0.27 MHz/pixel) are smaller compared to WindVal II by a factor of two, while the Δ(intercept) variations (0.03 pixels) are even smaller by a factor of three to four. For the internal reference, this can be traced back to the implemented fiber scrambler which considerable reduces the speckle noise of the internal reference signal incident on the Mie spectrometer. For the ground return, the lower variability is most likely due to the fact that the six calibrations from WindVal II were performed over different surfaces (4 over ice, 2 over land), resulting in a larger spread of ground slopes depending on albedo.

- Due to the excellent reproducibility of the Mie response curves, the choice of the best Mie response calibration is mainly driven by the variability of the OBA temperature because this parameter crucially influences the spacing of the Fizeau interferometer plates. The lowest variability in OBA temperature was observed for calibration #2 which is also characterized by the highest laser frequency stability. Therefore, this response calibration was chosen for the Mie wind retrieval.

Recommendations for A2D and ALADIN

- The heating of the bottom window of the aircraft should always be either switched-on or switched-off during research flights in order to avoid thermos-mechanical drifts of the optical components located close to the window and, in turn, systematic wind errors.

- In addition to the requirements in terms of the RSP temperature stability (<0.01 K peak-to-peak), the OBA temperature stability should be better than 0.02 K peak-to-peak in order to avoid large variations in the Mie response calibration parameters for A2D and ALADIN.

9 A2D wind measurements

This chapter presents the results of the A2D wind measurements carried out during the WindVal III campaign in autumn 2018. After an overview of the performed wind measurement scenes and the obtained data, the Rayleigh and Mie wind results as well as their validation by statistical comparison with the 2-μm wind lidar data are exemplarily demonstrated for one selected measurement scene during the second underflight on 22 November 2018. Afterwards, additional conclusions that are drawn from the analysis of other wind measurements are outlined. Finally, the results of the statistical comparison of all flight sections are discussed, leading to a concluding summary of the findings of the campaign.

9.1 Overview of flights and wind measurements

In the framework of the WindVal III campaign, six flights were conducted including the test flight and the calibration flight. During the first Aeolus underflight on 17 November, the A2D was not operational, so that A2D wind data is only available from three other underflights plus the test flight. The acquired data from the four flights is subdivided into eleven wind scenes from which eight wind scenes were performed along the Aeolus measurement swath. An overview of these scenes, the number of usable A2D observations and the resulting wind data are presented in Table 9-1. The measurement periods range from only eight minutes (during the test flight) to more than 50 minutes, adding up to nearly five hours over the whole campaign. For each wind scene, it is indicated whether the measurements were obtained during a straight flight or curves are included in the periods. Flight sections with curves require extra analysis during the processing related to ground detection. Wind scenes along the Aeolus measurement track are indicated in bold type, where green colour indicates that the aircraft flew in the same direction as the satellite while orange colour means opposite flight direction with respect to the satellite.

The number of Rayleigh and Mie winds given in Table 9-1 corresponds to bins in the respective processed wind curtain that have passed the quality control, i.e. after sorting out invalid measurements that showed outliers in the DCO channel, saturation of single pixels on the ACCD or incorrect assignment of range-gates numbers as studied in Marksteiner (2013). The data for those wind scenes where the Falcon flew along the Aeolus measurement swath, indicated in bold printed lines in Table 9-1 are delivered as netCDF file. The respective file name is given in the last column of the table. Additional information on the data content is provided in the Annex of this report.

Table 9-1: Overview of the wind scenes and the obtained Rayleigh and Mie wind data during the WindVal III campaign in 2018. Wind scenes along the Aeolus measurement track are indicated in bold type (green – same direction as satellite, orange – opposite direction as satellite).

Flight date	Flight time (UTC)	Wind scene #	Start	End	Duration (hh:mm:ss)	Curve included?	Obs.	Meas.	Rayleigh winds	Mie winds	File name
12/11	14:12 – 17:29	1	16:34:18	16:42:43	00:08:25	Yes	28	980	236	17	-
17/11	15:14 – 19:14		*The A2D was not operational during this flight.*								
22/11	14:29 – 17:56	**2**	**15:11:37**	**15:48:13**	**00:36:36**	**Yes**	**122**	**4270**	**830**	**298**	**20181122_WIND1.nc**
		3	**16:13:07**	**16:45:31**	**00:32:24**	**Yes**	**108**	**3780**	**1604**	**115**	**20181122_WIND2.nc**
		4	**16:54:49**	**17:15:13**	**00:20:24**	**Yes**	**68**	**2380**	**446**	**220**	**20181122_WIND3.nc**
29/11	09:56 – 14:00		*Only calibrations performed during this flight.*								
03/12	15:48 – 19:31	**5**	**16:48:57**	**17:13:37**	**00:24:40**	**No**	**82**	**2870**	**1258**	**152**	**20181203_WIND1.nc**
		6	**17:22:23**	**17:48:29**	**00:26:06**	**Yes**	**87**	**3045**	**1128**	**148**	**20181203_WIND2.nc**
		7	**17:53:56**	**18:29:02**	**00:35:06**	**No**	**117**	**4095**	**1350**	**310**	**20181203_WIND3.nc**
		8	18:39:01	18:56:07	00:17:06	Yes	57	1995	413	108	-
05/12	14:56 – 18:22	**9**	**15:53:37**	**16:45:30**	**00:51:53**	**No**	**173**	**6055**	**2427**	**126**	**20181205_WIND1.nc**
		10	**16:55:33**	**17:18:58**	**00:23:25**	**No**	**78**	**2730**	**1052**	**77**	**20181205_WIND2.nc**
		11	17:25:51	17:55:51	00:30:00	Yes	100	3500	1281	169	-
Total:					**04:57:40**		**1020**	**35700**	**12025**	**1740**	

9.2 A2D wind results from the Aeolus underflight on 22 November 2018

Since the A2D was not operational during the first underflight on 17 November 2018, first collocated wind observations of the A2D and ALADIN were performed on 22 November when the Falcon flew along the satellite swath from Lecce in South Italy (40.0°N, 18.3°E) to the Austrian-Hungarian border (47.2°N, 16.5°E). Aeolus covered this track between 16:34:14 UTC and 16:36:02 UTC, while it took the Falcon more than one hour to from 16:13 UTC to 17:15 UTC to cover the distance of about 790 km. According to the weather forecast, cloud-free conditions and strong winds were expected in the southern part of the leg, while mid-level clouds and weak winds were predicted for the northern part. The geolocations of the Aeolus and A2D wind observations along the common track are indicated in Figure 9-1.
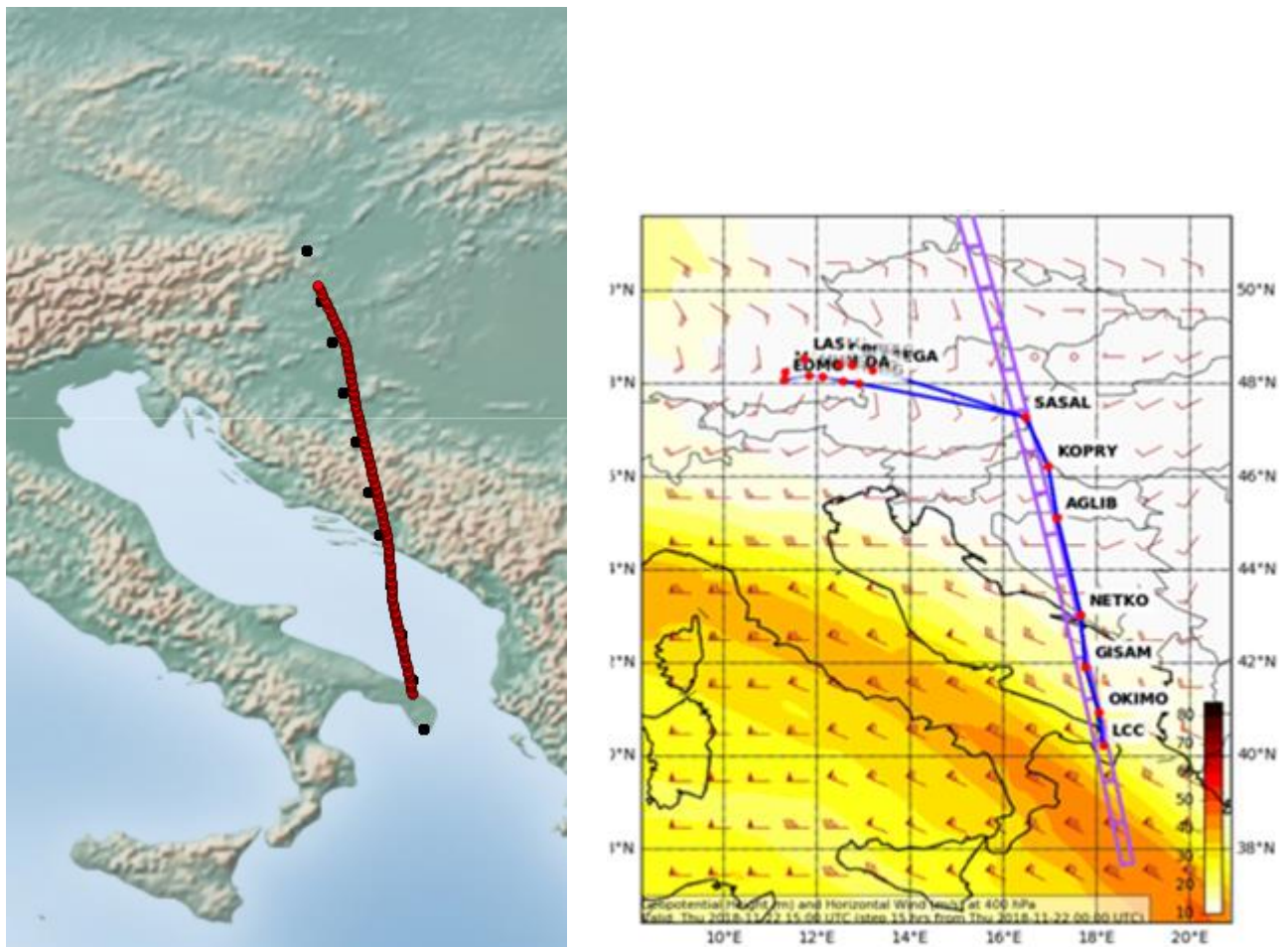
Figure 9-1: Left: map illustrating the Aeolus (black dots) and A2D wind observations (red dots) during the underflight on 22 November 2018. The dots indicate the geolocations in the middle of the respective observations. Right: Horizontal wind speed at 400 hPa on November 2018, 15:00 UTC as forecast from ECMWF model analysis together with the flight track of the Falcon 20 aircraft (blue) and the Aeolus measurement swath (violet).

During the underflight, the A2D performed two wind scenes (#3 and #4 according to Table 9-1) which were separated by a so called MOUSR (Mie Out of Useful Spectral Range) measurement. This mode aimed at the detection of the Rayleigh background signal on the Mie channel. Proper quantification of the broadband molecular return signal transmitted through the Fizeau interferometer is important for avoiding systematic errors in the determination of the fringe centroid position and, in turn, in the Mie winds. Therefore, the laser frequency was tuned away by 1.05 GHz from the Rayleigh filter cross point and Mie channel centre which defines the set frequency during the wind scenes. In this way, the laser frequency of the emitted pulses was outside of the useful spectral range of the Mie spectrometer, so that the fringe was not imaged onto the Mie ACCD and only the broadband Rayleigh signal was detected on the Mie channel. The range-dependent intensity levels per pixel were subsequently subtracted from the measured Mie raw signal.

The Rayleigh and Mie signal intensities per observation are shown in Figure 9-2. The raw signals were first corrected for the solar background and the detection chain offset (DCO) which are collected in range gates #0 and #2, respectively. Range correction (normalization to 1 km) was applied taking into account that the intensity decreases as the inverse square of the distance between the scatterer and the detector. Finally, the integration times set for each range gate were considered for normalising the signal intensities per bin to a bin size of 296 m (2.1 µs integration time). While the intensity profile for the Rayleigh channel essentially follows the vertical distribution of the atmospheric molecule density, the Mie intensity profile displays the vertical distribution of atmospheric cloud and aerosol layers along the flight track. High Rayleigh signal intensities above 10^5 a.u. can be attributed to cloud layers at different altitudes along the flight track which also manifest in increased Mie signal intensities.
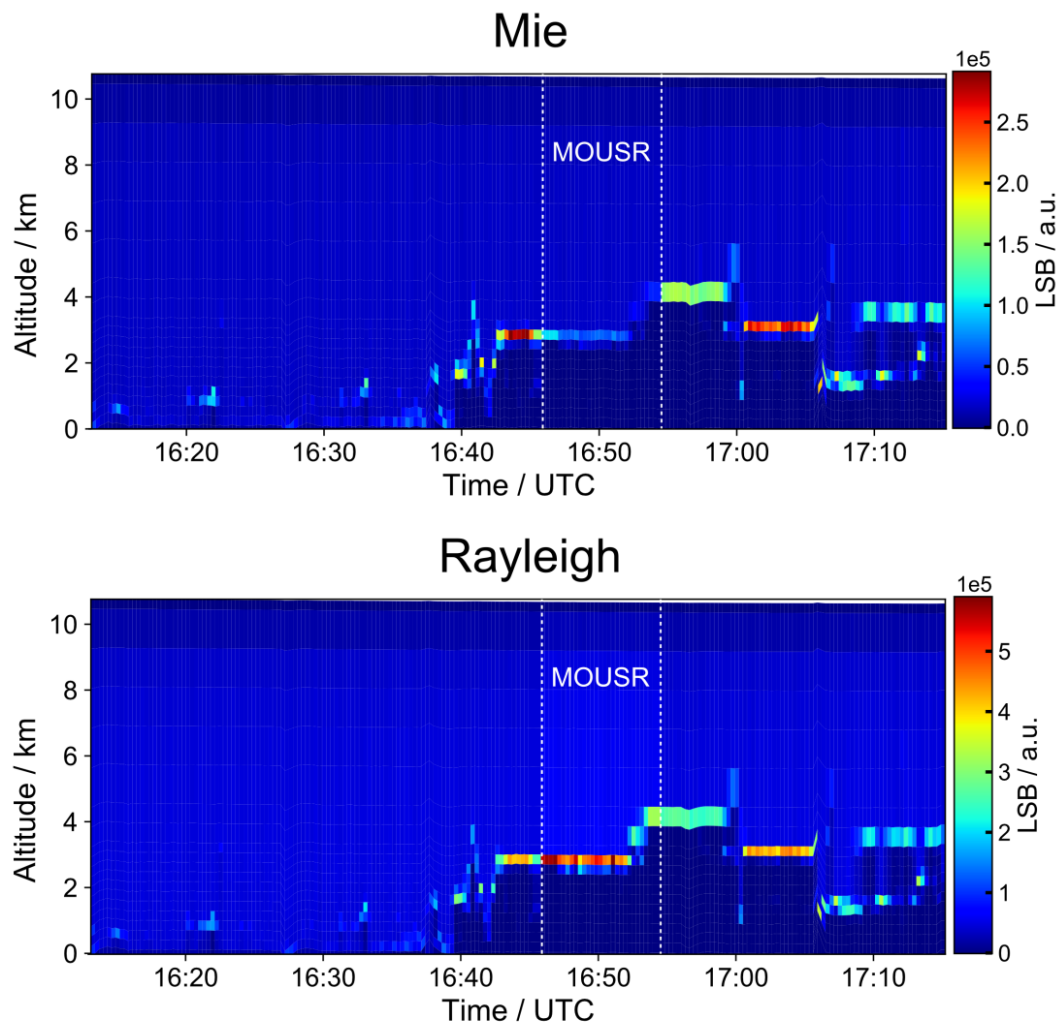
Figure 9-2: DCO- and background-corrected signal levels from the Mie (left) and the Rayleigh channel (right) measured during the underflight on 22 November 2018 between 16:14 UTC and 17:14 UTC along the Aeolus measurement track. Between 16:45 UTC and 16:54 UTC the A2D was operated in a different mode aiming at the detection of the Rayleigh background signal on the Mie channel (MOUSR).

The Rayleigh and Mie wind retrieval algorithms and implemented quality control procedures are comprehensively explained in (Marksteiner 2013), chapter 3.5, in TN 5.2 (DLR 2012b) and the Final Reports for the WindVal I (DLR 2017) and WindVal II campaigns (DLR 2018a). For the calculation of the Doppler frequency shift, and in turn the Rayleigh and Mie wind speeds, the response calibration from 29/11/2018, 10:48 UTC (calibration #1) was used for both channels. The Rayleigh nonlinearities were considered by performing a fifth-order polynomial fit of the residuals resulting from response calibration data. As already performed for the wind retrieval for the WindVal II observations, the Mie nonlinearities were taken into account as well, using a third-order polynomial fit, as explained in section 9.6 of (DLR 2017).

Figure 9-3 shows the processed HLOS Rayleigh and Mie winds plotted versus latitude (and time) and altitude for the period of the Aeolus underflight on 22 November 2018. During the first section of the flight, cloud-free conditions led to nearly complete data coverage of the Rayleigh channel from ground up to 9 km altitude. In the second half of the flight, dense mid-level clouds limited the extension of the Rayleigh wind profiles to 4 to 5 km. The data gap in between is due to the MOUSR procedure mentioned above.

In contrast to the Rayleigh channel, the Mie data coverage is rather sparse owing to the cloud cover and low aerosol load during the flight. Wind data is mainly obtained from the cloud tops along the track. Due to the high density of the clouds, the laser was strongly attenuated, thus preventing sufficient backscatter signal and valid Mie wind data over multiple range gates across the clouds. As a result, valid Mie wind data is often only obtained for one bin per profile or, in case data from a subjacent range gate passes quality control, the wind data shows a large systematic error. This is likely due to the skewness of the Mie fringe on the ACCD which influences the determination of the centroid position depending on the position the cloud within the range gates. Unfortunately, the same situation is present for the other two Aeolus underflights, so that the number of valid and good quality Mie wind data is very low compared to the Rayleigh channel.

The scarce coverage of the Mie data and the high number of outliers resulting from the Mie fringe skewness in combination with the presence of thick clouds prevents a meaningful assessment of the Mie errors, as a comparison with the 2-µm DWL and the Aeolus data would lack statistical significance. Therefore, the further analysis of the A2D wind data is restricted to the Rayleigh channel.
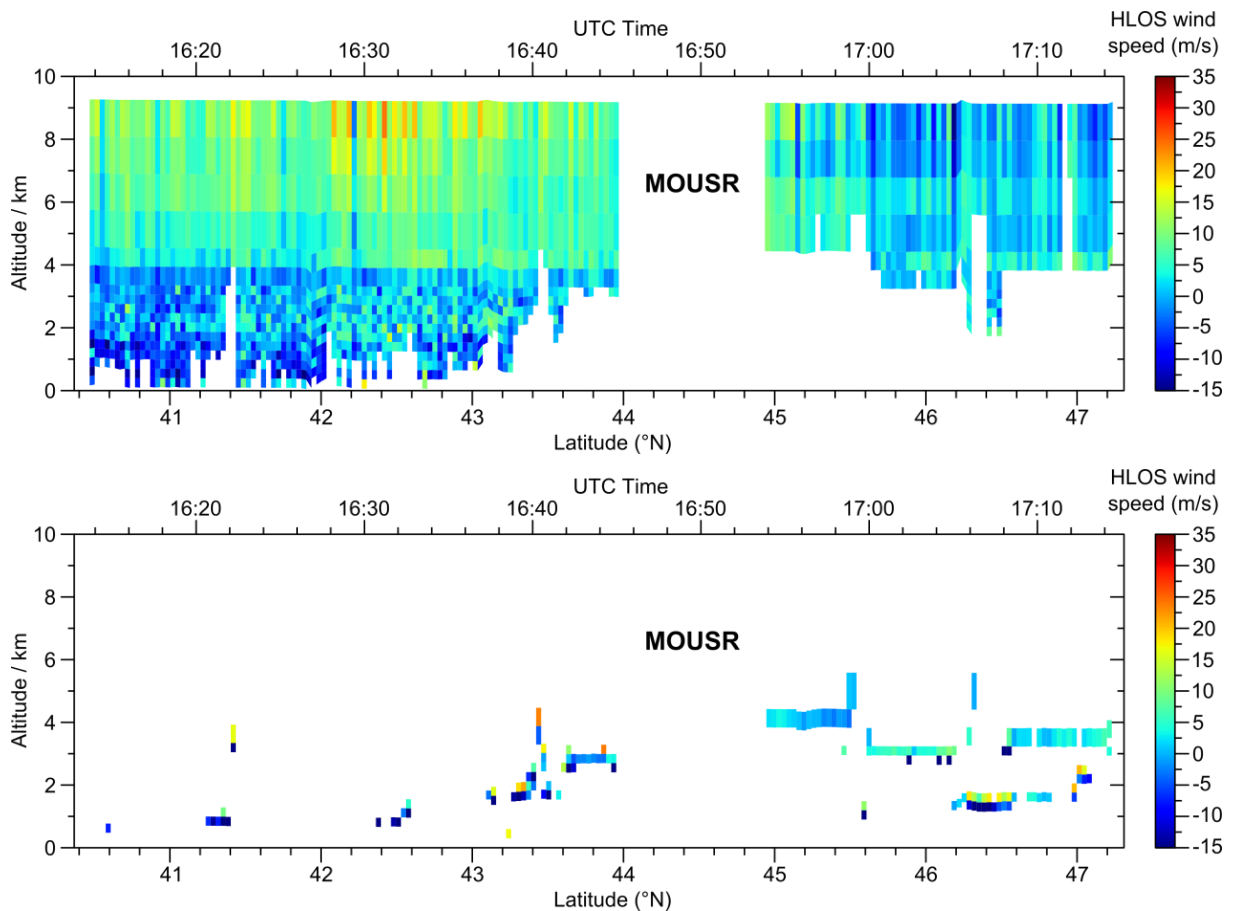
Figure 9-3: HLOS wind profiles (positive towards the instrument) measured during the underflight on 22 November 2018 between 16:14 UTC and 17:14 UTC along the Aeolus measurement track using the A2D Rayleigh (top) and Mie channel (bottom) . White colour represents missing or invalid data due to low signal, e.g. below dense clouds. The data gap between 16:45 UTC and 16:54 UTC is due to an interruption of the wind measurement during a different operation mode of the A2D instrument aiming at the detection of the Rayleigh background signals on the Mie channel (MOUSR).

9.3 Wind results from the underflights on 3 and 5 December 2018

The wind results from the two Aeolus underflights performed in France on 3 December 2018 and in Poland on 5 December 2018 are shown in Figure 9-4. The first flight was characterized by strong winds especially in Central France which were sampled in three legs along the Aeolus swath. On the two legs along the satellite direction, negative winds (away from the instrument) were measured, since the wind was blowing from west to east. Comparable wind speeds, but with opposite sign were thus observed on the leg from north to south.

The flight over Poland showed very low wind speeds along the instrument's LOS, as the wind was blowing mainly from the north. Like the flight on 22 November 2018, very high data coverage was obtained for the Rayleigh channel, while valid Mie wind data was only retrieved in a few range bins containing the top of low-level clouds. Additional information on the meteorological conditions encountered during the flights can be found in the respective flight reports.
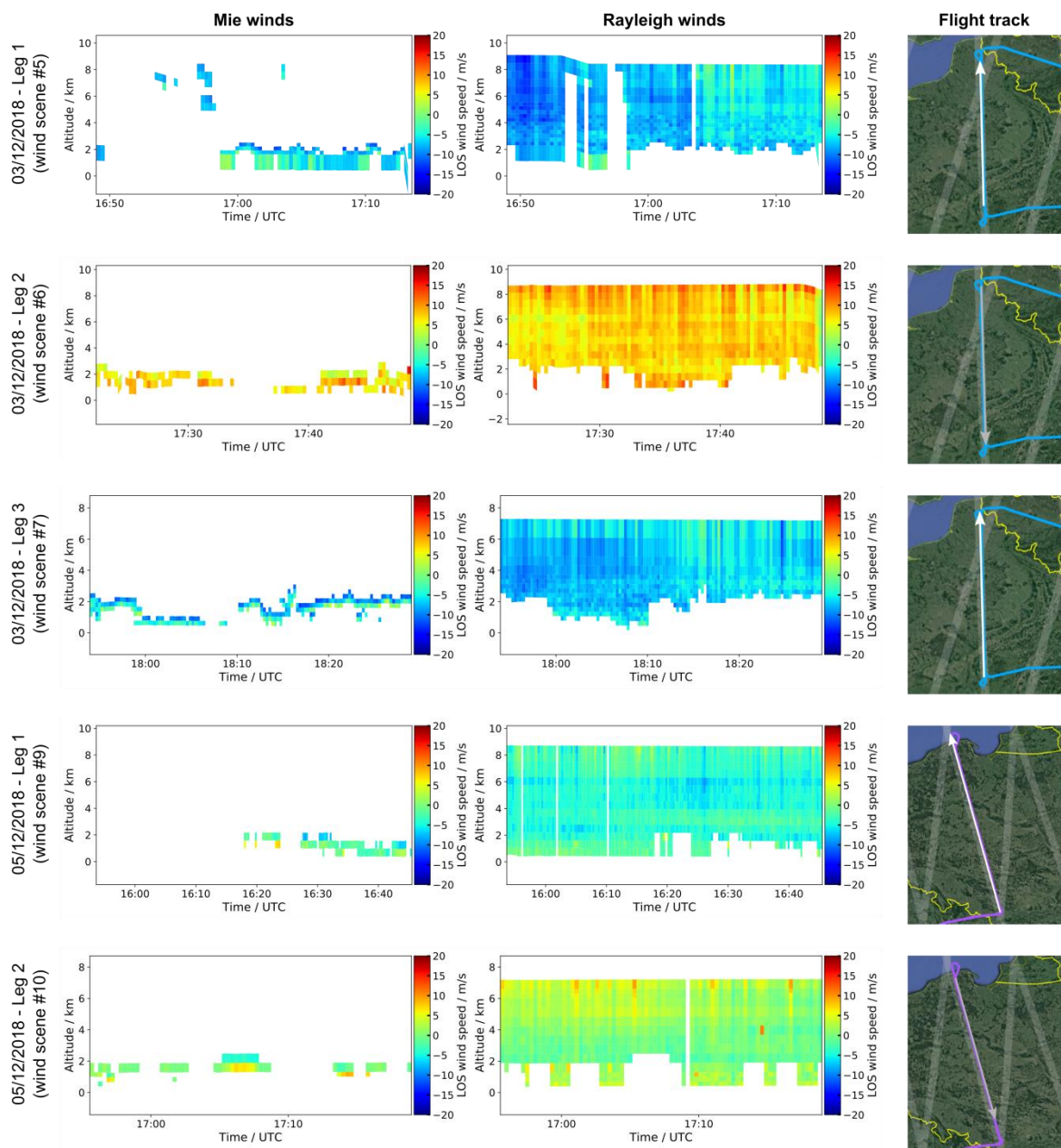
Figure 9-4: A2D LOS wind profiles measured during the underflights along the Aeolus measurement swath on 3 December and 5 December 2018 using the Mie (left) and Rayleigh channel (middle) (see data on the respective wind scenes in Table 9-1). The corresponding flight tracks are indicated by arrows in the maps on the right. White colour in the wind curtains represents missing or invalid data due to low signal, e.g. below dense clouds.

9.4 Comparison with 2-µm wind data for error assessment

Like in the previous airborne campaigns, validation of the A2D instrument performance and wind retrieval algorithms was performed by comparing the resulting wind profiles to those obtained with a well-established coherent wind lidar system emitting at 2 µm wavelength and 500 Hz repetition rate, which was operating in parallel on board the Falcon aircraft providing accuracy of the horizontal wind speed of better than 0.1 m·s^{-1} and precision of better than 1 m·s^{-1} (Weissmann et al. 2005; Chouza et al. 2016b). In contrast to the A2D, the determination of the Doppler shift by the 2-µm lidar system relies on heterodyne detection using the instruments' seed laser as local oscillator (see section 6 and Witschas et al., 2017) and thus does not rely on any calibration procedures. Moreover, the coherent wind lidar incorporates a scanner which allows retrieving the three-dimensional horizontal wind vector from a number of LOS wind measurements with a vertical resolution of 100 m. For this purpose, the instrument performs conical scans at an opening angle of 20°, while the information from 21 azimuthal positions is used for the wind vector retrieval. On each azimuthal position the signal from 500 laser pulses (1 s) is averaged to obtain one LOS profile. The time for positioning the laser at its scan starting position is around 21 s resulting in a total time of 42 s for one observation of the 2-µm wind lidar, whereas one A2D observation takes 18 s.

As elaborated in Marksteiner et al. (2011), adequate comparison of the wind profiles measured with the 2-µm and the A2D wind lidar required the projection of the three-dimensional wind vectors onto the A2D LOS axis. This was carried out for each 2-µm observation by calculating the scalar product of the measured wind vector and the mean A2D LOS unit vector under consideration of the aircraft attitude during the respective observation period. Furthermore, the different spatial and temporal resolutions of the two wind lidar instruments necessitated an adaptation of the 2-µm measurement grid to that of the A2D. This was accomplished by a weighted aerial interpolation algorithm considering the whole two-dimensional A2D wind curtain overlaid by the 2-µm grid. Hence, a single A2D bin can be covered by multiple 2-µm bins both horizontally and vertically. The overlapping regions form a new composite 2-µm bin. The contributions of the single 2-µm winds to the wind value allocated to the composite bin are weighted by the overlap of the respective 2-µm bins with the regarded A2D bin. In this way, the A2D and 2-µm wind profiles can be compared on a bin-by-bin basis.

In case that the area of an A2D range bin is not entirely covered by 2-µm bins, the 2-µm wind speed value used for comparison must be determined from the remaining contributions. To calculate a correct wind speed for the composite 2-µm bins, the wind values obtained from the valid contributions have to be scaled by the percentage of their area in the whole area of the A2D range bin. This procedure holds the risk of large discrepancies between the interpolated 2-µm wind and the compared A2D wind in case of low coverage, especially for strong wind shear on spatial scales comparable to the size of an A2D range gate. Therefore, the coverage ratio is used as a quality control parameter. For the WindVal III wind scenes, a threshold value of 25% was found to provide an optimal trade-off between comparability and quantity of the 2-µm bins, thus yielding an acceptable number of representative composite 2-µm bins used for comparison.

The statistical comparison of the Rayleigh winds with the 2-µm DWL data from all flights of the WindVal II and WindVal III campaigns is visualised in Figure 9-5. Here, the A2D winds are plotted versus the corresponding interpolated 2-µm winds, resulting in a cloud of data points that ideally lie on the dashed line representing $v_{A2D} = v_{2µm}$. The non-weighted linear fit $v_{A2D} = A \cdot v_{2µm} + B$ through the real data provides values for the slope A and intercept B that generally deviate from the ideal result $A = 1$ and $B = 0$. Bins with wind speed differences $v_{A2D} - v_{2µm}$ larger than ±10 m/s were identified as gross errors in the Rayleigh dataset and thus removed from the sample.

Although the number of compared Rayleigh winds is very similar for the two campaigns, there are much less gross errors for the WindVal III campaign (36). This is most likely explained by the fact that most WindVal III flights were planned to be conducted mainly in cloud-free conditions, minimizing the risk for heterogeneous atmospheric conditions potentially increasing the representativity of the scan-retrieved volume winds to the A2D LOS winds and also the risk for large systematic errors of the Rayleigh channel, e.g. introduced by cirrus clouds affecting the transmit-receive co-alignment feedback loop.
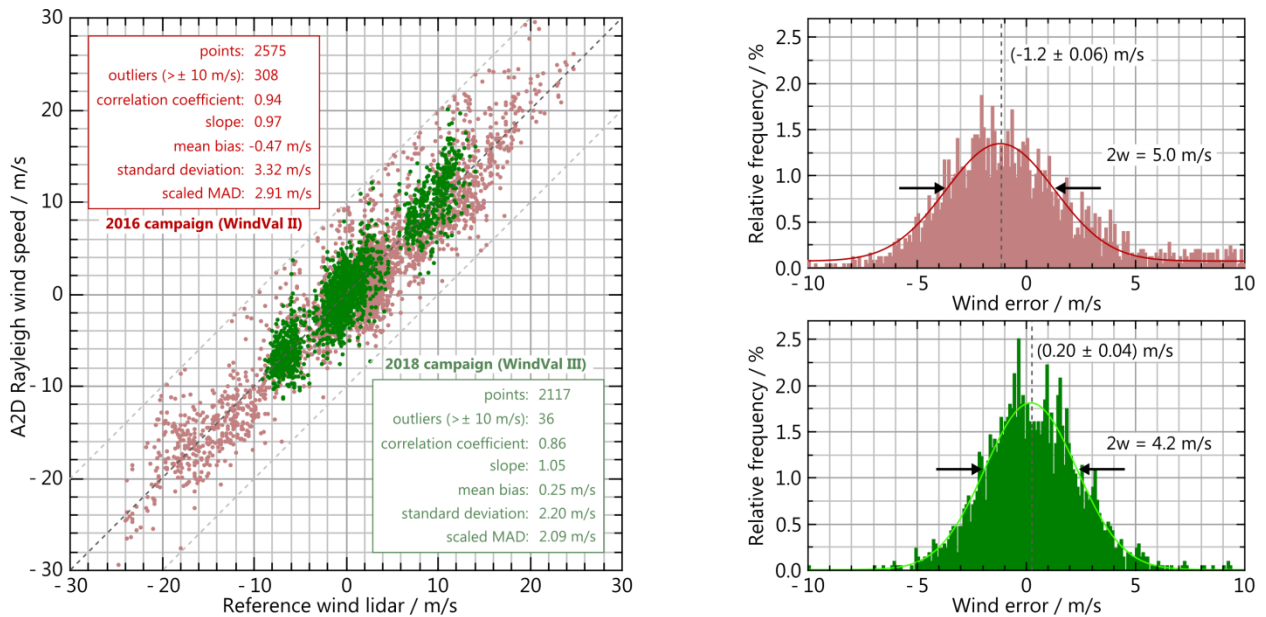
Figure 9-5: (Left) A2D LOS wind speed determined with the Rayleigh channel versus the 2-μm LOS wind speed during the WindVal II (red) and the WindVal III campaign (green). The scatterplot is obtained by adaptation of the different measurement grids of the two systems based on a weighted interpolation algorithm and a subsequent bin-to-bin comparison. The corresponding probability density functions for the wind differences (A2D – 2-μm) are shown on the right for the two campaigns. The solid lines represent Gaussian fits with the given centres and $e^{-1/2}$-widths 2w.

The statistical values derived from the scatterplot are summarized in Table 9–2 showing that the fitting parameters for both campaigns only slightly deviate from the ideal case ($A \approx 1$, $|B| < 0.5$ m·s^{-1}). It should be noted that the parameters derived from the statistical comparison are influenced by the systematic and random errors of both the A2D and the 2-μm lidar. However, since the latter provides high accuracy and precision as stated above, the total errors are dominated by the systematic and random error of the A2D. Aside from the standard deviation, the median absolute deviation (MAD) was determined as an additional parameter for evaluating the random error of the A2D wind speed measurements. It is defined as the median of the absolute variations of the measured wind speeds from the median of the wind speed differences:

$$\text{MAD} = \text{median}\big[\big|(v_{\text{A2D},i} - v_{2\mu m,i}) - \text{median}(v_{\text{A2D},i} - v_{2\mu m,i})\big|\big].$$

The MAD represents a robust measure of the variability of the measured wind speeds and is more immune to outliers compared to the standard deviation σ. If the random wind error is normally distributed, the MAD value is related to the standard deviation as σ ≈ 1.4826 · MAD. The latter quantity called *scaled MAD*.

The Rayleigh mean wind bias of 0.25 m/s is very small, confirming the good quality of the chosen response calibration. Moreover, the random error of 2.2 (STD) / 2.1 m/s (scaled MAD) is considerable smaller than for the previous campaign (3.3 m/s, 2.1 m/s) which is mainly due to the implemented fiber scrambler reducing the speckle noise of the internal reference signal.

The random error can also be approximated from probability density functions (PDFs) illustrating the frequency distribution of the wind speed differences $v_{\text{A2D}} - v_{2\mu m}$, i.e. the wind error (Figure 9-5). Since the wind error is not perfectly Gaussian-distributed for both campaigns, there is a discrepancy between the mean bias values and the centre of the Gaussian fits. For the same reason, the width of the fits is narrower than twice the standard deviations which also consider the outliers. Finally, due to the deviation from a Gaussian distribution, the scaled MAD values are smaller than σ.

The results from the individual statistical comparisons of the A2D Rayleigh data with the 2-μm wind data for each wind scene are provided in Table 9-3. The table reveals the very good performance of the Rayleigh channel with small biases <1.5 m/s for all scenes and random errors around 2 m/s except for the first wind scene on 22 November. However, only 91 Rayleigh winds entered the statistical comparison so that the accuracy and precision determined for this scene are less meaningful compared to the other wind scenes.

Table 9-2: Results of the statistical comparison between the A2D Rayleigh and the 2-µm LOS wind data obtained from all wind scenes of the WindVal II campaign in 2016 and the WindVal III campaign in 2018.

Statistical parameter	WindVal II	WindVal III
Number of compared bins	2575	2117
Number of removed bins due to gross error (>±10 m·s⁻¹)	308	36
Correlation coefficient r	0.94	0.86
Slope	0.97	1.05
Mean bias (A2D – 2-µm)	-0.47 ms^{-1}	0.25 ms^{-1}
Standard deviation	3.32 ms^{-1}	2.20 ms^{-1}
1.4826 · MAD	2.91 ms^{-1}	2.09 ms^{-1}

Table 9-3: Results of the statistical comparison between the A2D Rayleigh winds and the 2-µm winds during the WindVal III campaign. The list is limited by the availability of 2-µm data. Rayleigh response calibration #1 was used for the wind processing. Results showing good agreement between the A2D and 2-µm winds (low mean bias, small standard deviation) are highlighted in green, while large discrepancies are shown in red. The last row provides the parameters obtained from the statistical comparison of all winds.

Measurement section	N	Mean bias (m·s⁻¹)	Median (m·s⁻¹)	STD (m·s⁻¹)	1.48·MAD (m·s⁻¹)	Included Range gates	Cov. ratio (%)
22/11/2018 15:11 – 15:48	91	-0.90	-0.51	3.09	3.52	7 to 21	25
22/11/2018 16:13 – 17:15	468	1.26	1.29	1.71	1.78	7 to 21	25
03/12/2018 16:48 – 17:13	177	-0.04	-0.07	2.43	1.84	7 to 21	25
03/12/2018 17:22 – 17:48	184	0.18	0.21	2.24	2.15	7 to 21	25
03/12/2018 17:53 – 18:29	223	-0.37	-0.51	1.63	1.59	7 to 21	25
03/12/2018 18:39 – 18:56	80	0.61	0.78	2.32	2.32	7 to 21	25
05/12/2018 15:53 – 16:45	318	-1.47	-1.51	1.57	1.43	7 to 21	25
05/12/2018 16:55 – 17:18	213	0.47	0.12	2.27	1.71	7 to 21	25
05/12/2018 17:25 – 17:55	363	1.07	1.10	2.21	2.14	7 to 21	25
ALL	**2117**	**0.25**	**-0.08**	**2.20**	**2.09**		

The same statistical comparison was performed for the A2D Mie channel, resulting in the scatterplots for WindVal II and WindVal III displayed in Figure 9-6. The corresponding statistical parameters are listed in Table 9-4. The results for each individual wind scene are given in Table 9-5.
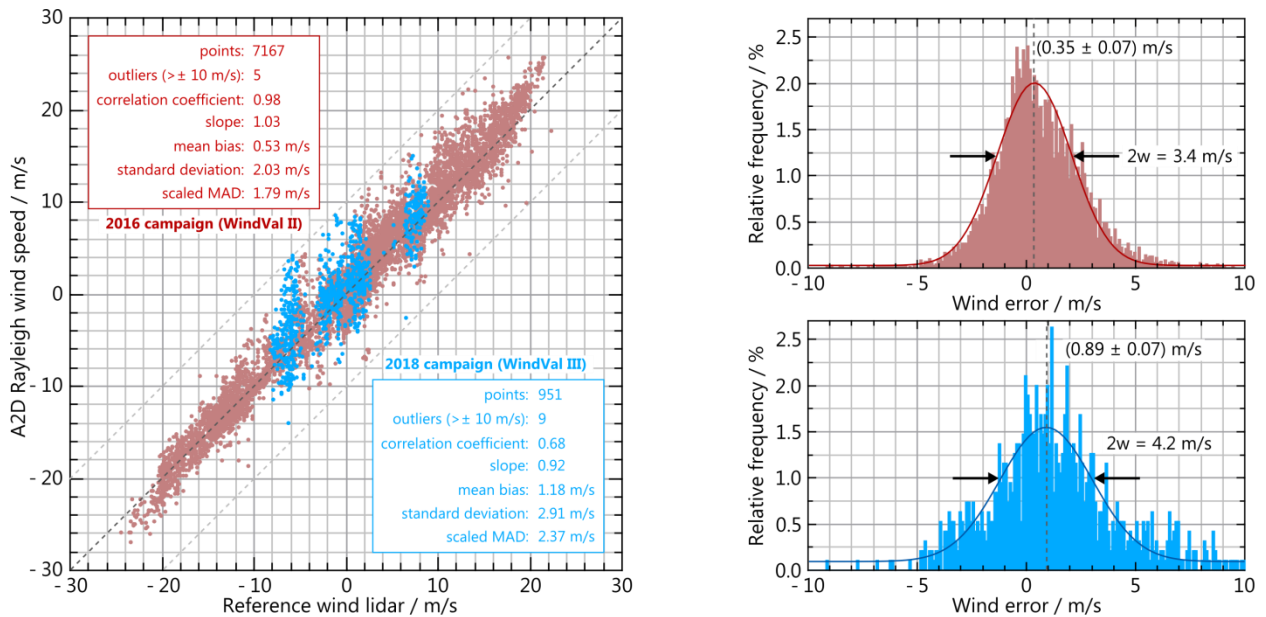
Figure 9-6: (Left) A2D LOS wind speed determined with the Mie channel versus the 2-µm LOS wind speed during the WindVal II (red) and the WindVal III campaign (blue). The scatterplot is obtained by adaptation of the different measurement grids of the two systems based on a weighted interpolation algorithm and a subsequent bin-to-bin comparison. The corresponding probability density functions for the wind differences (A2D – 2-µm) are shown on the right for the two campaigns. The solid lines represent Gaussian fits with the given centres and $e^{-1/2}$-widths 2w.

Table 9-4: Results of the statistical comparison between the A2D Mie and the 2-µm LOS wind data obtained from all wind scenes of the WindVal II campaign in 2016 and the WindVal III campaign in 2018.

Statistical parameter	WindVal II	WindVal III
Number of compared bins	7169	951
Number of removed bins due to gross error (>±10 m·s^{-1})	5	9
Correlation coefficient r	0.98	0.68
Slope	1.03	0.92
Mean bias (A2D – 2-µm)	0.53 ms^{-1}	1.18 ms^{-1}
Standard deviation	2.03 ms^{-1}	2.91 ms^{-1}
1.4826 · MAD	1.79 ms^{-1}	2.37 ms^{-1}

Table 9-5: Results of the statistical comparison between the A2D Mie winds and the 2-µm winds during the WindVal III campaign. The list is limited by the availability of 2-µm data. Mie response calibration #2 was used for the wind processing. Results showing good agreement between the A2D and 2-µm winds (low mean bias, small standard deviation) are highlighted in green, while large discrepancies are shown in red. The last row provides the parameters obtained from the statistical comparison of all winds.

Measurement section	N	Mean bias (m·s^{-1})	Median (m·s^{-1})	STD (m·s^{-1})	1.48·MAD (m·s^{-1})	Included Range gates	Cov. ratio (%)
22/11/2018 15:11 – 15:48	131	0.30	-0.29	3.06	1.73	7 to 21	25
22/11/2018 16:13 – 17:15	69	0.37	0.10	2.43	0.90	7 to 17	25
03/12/2018 16:48 – 17:13	30	2.26	2.21	1.11	0.71	7 to 21	25
03/12/2018 17:22 – 17:48	119	0.71	0.67	2.43	2.04	7 to 20	25
03/12/2018 17:53 – 18:29	252	1.75	1.72	3.60	4.01	7 to 21	25
03/12/2018 18:39 – 18:56	98	1.51	1.78	2.25	1.73	7 to 21	25
05/12/2018 15:53 – 16:45	163	1.80	1.63	2.51	1.50	7 to 20	25
05/12/2018 16:55 – 17:18	57	0.13	-0.05	2.80	1.27	7 to 18	25
05/12/2018 17:25 – 17:55	32	0.02	0.27	2.33	1.99	7 to 21	25
ALL	951	1.18	0.97	2.91	2.37		

The statistical comparison of the Mie wind data indicates are poorer performance of the Mie channel compared to the previous campaign. Apart from the larger wind bias of 1.18 m/s (WindVal II: 0.53 m/s), the random error is significantly larger (2.37 m/s compared to 1.79 m/s). Also, the overall number of valid Mie winds (951) entering the statistical comparison is much smaller than for the previous campaign (7169). This can be explained with the absence of thin cirrus clouds during the WindVal III wind scenes in contrast to WindVal II which deliver many valid Mie bins along the wind profiles over a wider wind speed range when associated with the jet stream. During WindVal III, thick low- and middle-clouds were present during all wind scenes, yielding only few valid Mie winds for the range gates containing the cloud tops. The range gates beneath often either show low Mie SNR and are thus considered invalid or exhibit large wind speed differences to the 2-µm winds. Consequently, A2D Mie winds were not further used for the comparison with Aeolus wind data.

As already discussed in the WindVal I and WindVal II Final Reports (DLR 2017, DLR 2018), a large contribution to the random error in the A2D Mie channel is also the occurrence of a heterogeneous cloud structure. In particular, the position of the top edges of optically thick clouds within one range gate has a significant influence on the wind data. According to Sun et al. (2014) who investigated the performance of Aeolus in heterogeneous atmospheric conditions using high-resolution radiosonde data, a non-uniform distribution of clouds and/or aerosols within a range bin introduces random errors in the Mie HLOS winds of several m·s^{-1} depending on the bin size and altitude.

9.5 Comparison with Aeolus wind data

The A2D Rayleigh winds were compared to the Aeolus L2B and L2C Rayleigh data for assessing the accuracy and precision of the two instruments. In contrast to the 2-μm DWL which measures the entire wind vector, the A2D also only measures one component of the horizontal wind vector along its LOS. Therefore, comparison of the obtained A2D wind data with the Aeolus winds not only requires averaging and adaptation onto the Aeolus measurement grid, as explained for the 2-μm DWL in Chapter 6, but also demands consideration of the different pointing directions of the two direct-detection wind lidar instruments. This particularly involves a conversion of the measured A2D LOS winds to comparable winds which would have been measured by the A2D if it was pointing along the same direction as Aeolus. The pointing is unambiguously determined by the respective azimuth and off-nadir angles of the two instruments. While consideration of the different off-nadir angles is straightforward, it is more complicated for the different azimuth angles. In the following, the procedure will be exemplarily shown for the second underflight on 22 November 2018 which has already been discussed in Sections 6.4.2 and 9.2.
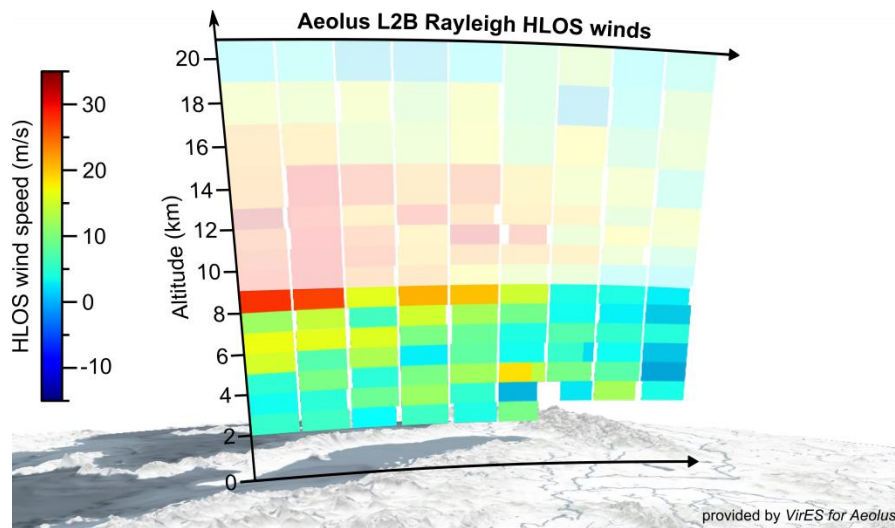

Figure 9-7: Aeolus L2B HLOS Rayleigh winds measured during the underflight on 22 November 2018 between 40.6°N and 47.2°N. Only winds with an estimated wind error of less than 6 m/s are shown. Winds at altitudes above 9 km are outside of the measurement range of the A2D and therefore shown greyed out. The figure was created based on a screenshot from the Aeolus visualization tool *VirES for Aeolus* (https://aeolus.services/).

The L2B Rayleigh winds measured by Aeolus along the common leg with the Falcon aircraft are depicted in Figure 9-7. A visual comparison with the corresponding A2D Rayleigh wind curtain in Figure 9-3 reveals large discrepancies which are due to the fact that the azimuth angles of the two instruments significantly differ from each other. This situation is illustrated in Figure 9-8 showing the flight track of the Falcon along the satellite measurement track together with the respective horizontal pointing directions of the A2D and Aeolus at a selected position on the track. While the azimuth angle of the A2D is around 68° (northeast), it is 260° (southwest) for Aeolus. As a result, the two instruments measure different components of the horizontal wind vector projected onto the respective LOS vectors.

In order to convert the A2D LOS winds, the real wind speed difference Δ which results from different azimuth angles has to be determined and added to the actual wind speed measured by the A2D:

$$v'_{A2D} = v_{A2D} + \Delta \, .$$

The determination of Δ requires an additional source of information. For this purpose, wind data from the Aeolus L2C data product which is in turn derived from ECMWF models was utilized. Knowledge of the zonal (u) and meridional (v) wind component allows calculating the wind speed difference introduced by the different azimuth angles of the A2D (φ_{A2D}) and Aeolus (φ_{Aeolus}) as follows:

$$\Delta = \left[\cos(\varphi_{A2D}) - \cos(\varphi_{Aeolus}) \right] \cdot v + \left[\sin(\varphi_{A2D}) - \sin(\varphi_{Aeolus}) \right] \cdot u \, .$$
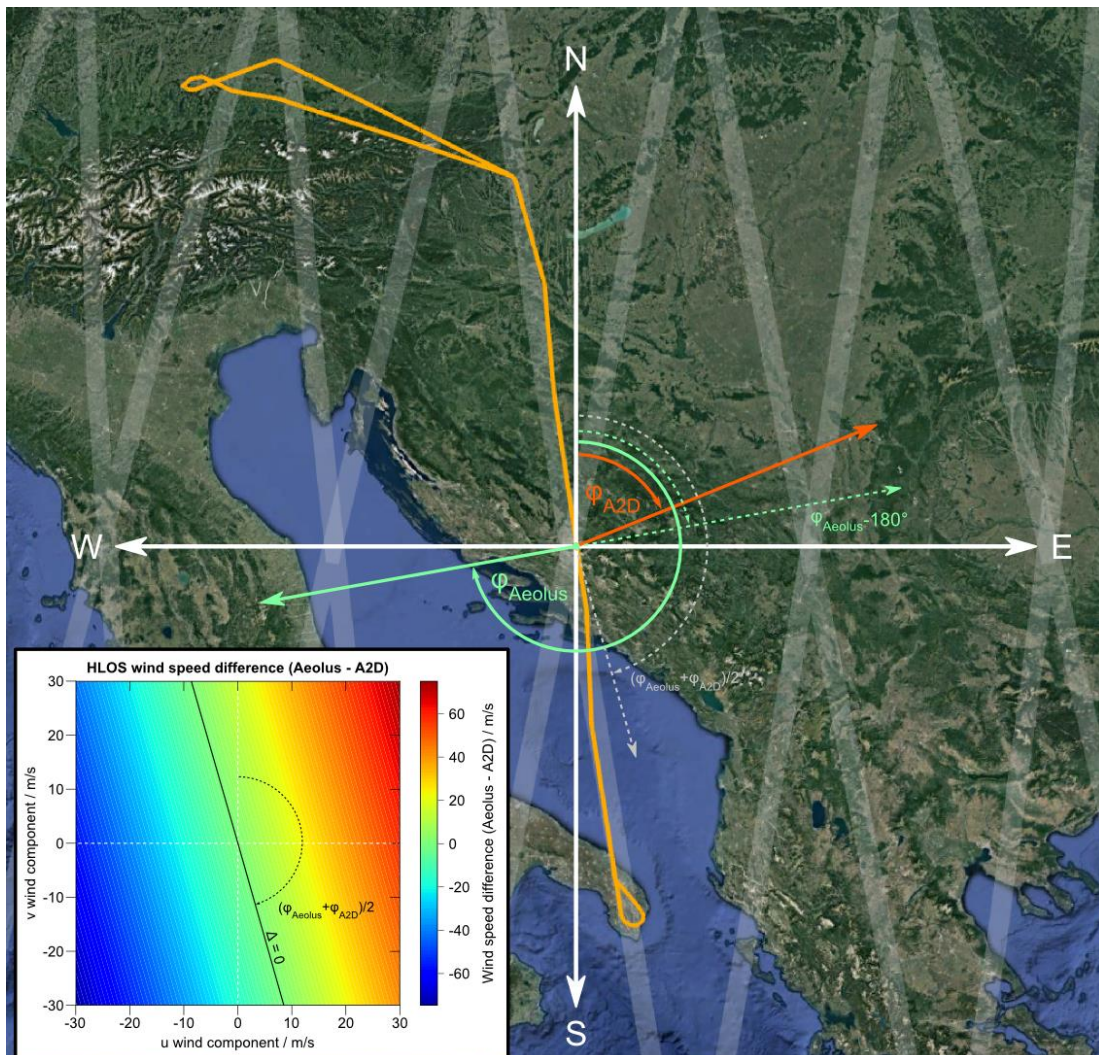
Figure 9-8: Diagram illustrating the different azimuth angles of Aeolus (green) and the A2D (orange) at the example of the underflight on 22 November 2018 indicated by the orange flight track. The inset depicts the HLOS wind speed difference in dependence on the zonal (u) and meridional (v) wind component for azimuth angles of φ_{A2D} = 68° and φ_{Aeolus} = 260°. In case the azimuth angle of the wind vector meets the condition φ_{wind} = (φ_{Aeolus}/φ_{A2D})/2, i.e. the wind direction is 164° (dashed grey arrow), the HLOS wind speed difference Δ is zero.

Using the above mentioned azimuth angles for the two instruments (φ_{A2D} = 68° and φ_{Aeolus} = 260°), the wind speed difference Δ can be as large as 50 m/s for typical zonal and meridional wind speeds, as shown in the inset of Figure 9-8. Since the Aeolus azimuth angle is generally around 260° in mid-latitudes on ascending orbits and the A2D azimuth angle is around 68° when flying on ascending satellite tracks, the plot is representative for most underflights of the WindVal III campaign. Thus, it can generally be stated, that the zonal wind component predominantly influences the wind speed difference Δ. Consequently, the azimuth correction is essential for accurate comparison of the A2D and Aeolus winds.

For taking into account the different off-nadir angles of the two instruments the A2D LOS wind speeds need to be multiplied by the factor sin(37°)/sin(20°) ≈ 1.76. As a result, one obtains A2D LOS winds along the Aeolus LOS. Finally, the Aeolus HLOS winds contained in the L2B data product need to be converted to LOS winds by multiplying a factor of sin (37°) ≈ 0.6 before comparing them to the A2D LOS winds.

The resulting wind curtains are depicted in Figure 9-9. The figure shows the Aeolus L2B Rayleigh winds; the A2D Rayleigh winds averaged onto the Aeolus measurement grid and for an off-nadir angle of 37°, but without azimuth correction; the A2D Rayleigh winds with azimuth correction and the Aeolus L2C Rayleigh winds, i.e. LOS winds based on ECMWF model data. Only Aeolus LOS winds with an estimated error below 3.6 m/s (HLOS: 6 m/s) were considered valid.
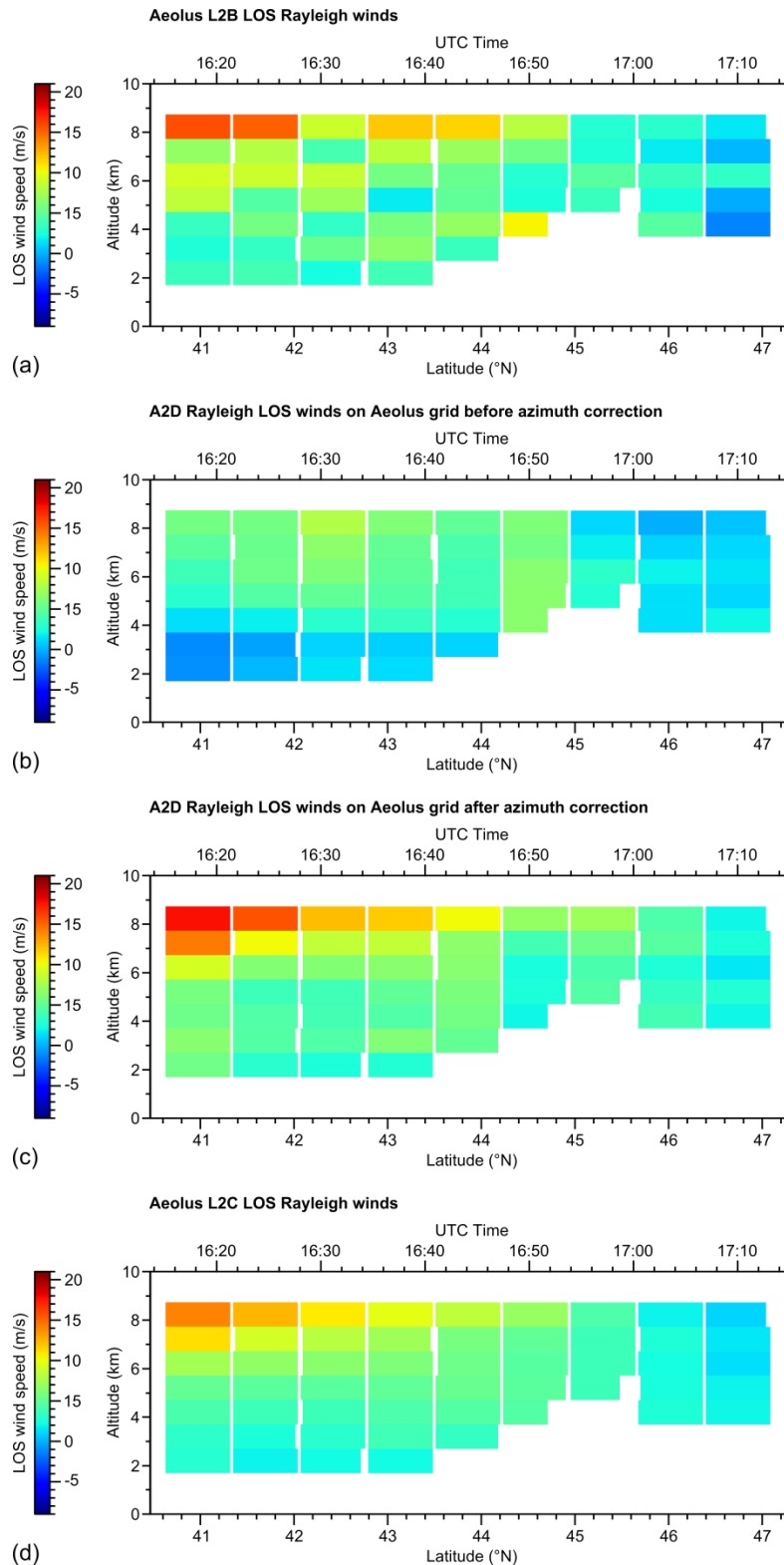
Figure 9-9: LOS wind profiles obtained during the underflight on 22 November 2018 between 40.6°N and 47.2°N: (a) Aeolus L2B Rayleigh winds, (b) A2D Rayleigh winds averaged onto the Aeolus measurement grid and for an off-nadir angle of 37°, but without azimuth correction, (c) A2D Rayleigh winds with azimuth correction and (d) Aeolus L2C Rayleigh winds, i.e. LOS winds based on ECMWF model data. White colour represents missing or invalid data of one of the two instruments, e.g. below dense clouds. Only Aeolus LOS winds with an estimated error below 3.6 m/s (HLOS: 6 m/s) were considered valid.

The adaptation of the A2D data to the Aeolus measurement grid and LOS pointing direction allowed for a statistical comparison of the wind results. The following scatterplots show the correlation of the A2D Rayleigh wind with the L2C (ECMWF model) data, the correlation of the Aeolus L2B Rayleigh wind with the L2C data and the correlation of the Aeolus L2B Rayleigh wind with the A2D data for the underflight on 22 November. Below the corresponding scatterplots containing data from all underflights are shown.

Figure 9-10: Scatterplot comparing the A2D Rayleigh LOS winds (adapted to the Aeolus LOS) with the Aeolus L2C LOS winds for the underflight on 22/11/2018. See Figure 9-9 (c) and (d) for the corresponding wind curtains. The data points are colour-coded with respect to the altitude of the respective bin used for comparison.

Figure 9-11: Scatterplot comparing the Aeolus L2B Rayleigh LOS winds with the Aeolus L2C LOS winds for the underflight on 22/11/2018. See Figure 9-9 (a) and (d) for the corresponding wind curtains. The data points are colour-coded with respect to the altitude of the respective bin used for comparison.

Figure 9-12: Scatterplot comparing the Aeolus L2B Rayleigh LOS winds with the A2D Rayleigh LOS winds (adapted to the Aeolus LOS) for the underflight on 22/11/2018. See Figure 9-9 (a) and (c) for the corresponding wind curtains. The data points are colour-coded with respect to the altitude of the respective bin used for comparison.

The comparison of the A2D winds with the model data shows good agreement for altitudes below 7 km, while a positive bias is evident for higher altitudes. This is most likely related to the incomplete telescope overlap in this region resulting in a systematic error. When comparing the data from all flights (Figure 9-13), a mean bias of -1.13 m/s is calculated with most of the underestimated winds being measured close to the ground. However, it cannot be unambiguously derived from the comparison whether the A2D exhibits an altitude-dependent systematic error or a slope error of the calibration resulting in underestimated low wind speeds at lower altitudes and overestimated high wind speeds at higher altitudes.

Comparing the L2B and the L2C wind speeds, a mean bias of 1.84 m/s and a random error of 2.18 m/s is derived. This is in fair agreement with the values obtained from the 2-µm comparison (2.5 m/s, 3.9 m/s) when converting the LOS values to HLOS values (factor of 1.66). Finally, the statistical comparison of the L2B data with the A2D winds yields a bias of 2.96 m/s and a random error of 4.11 m/s.

It has to be stated that the shown comparisons lack statistical significance, as there is only a small number of compared bins. This is mainly due to range gate setting of the A2D which had many small range gates in the lower troposphere, where Aeolus winds often exhibit large estimated wind errors. Hence, the overlap of valid wind data from the two instruments was very limited during WindVal III and can be optimized by adapting the A2D range gate setting, as shown in Figure 9-16 and by performing more flights during future campaigns.

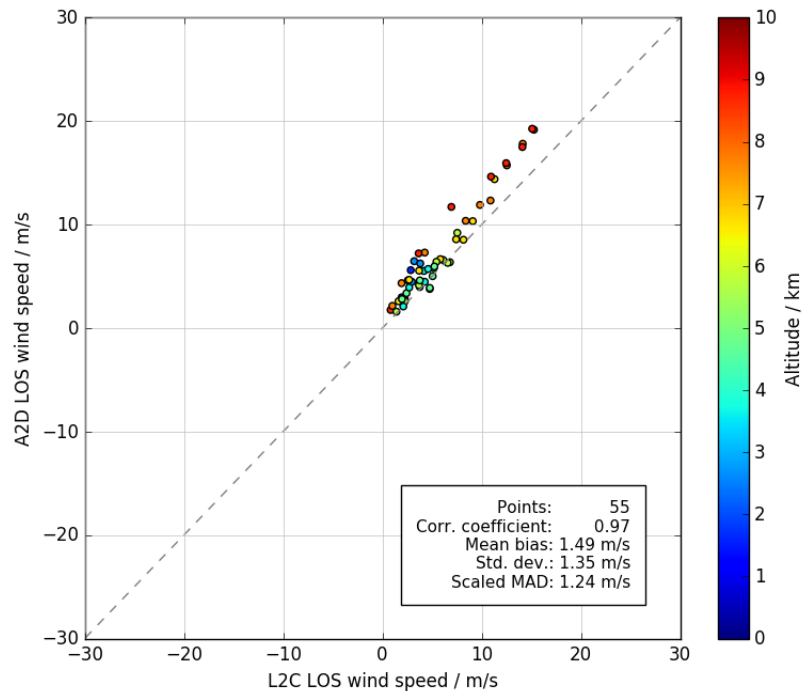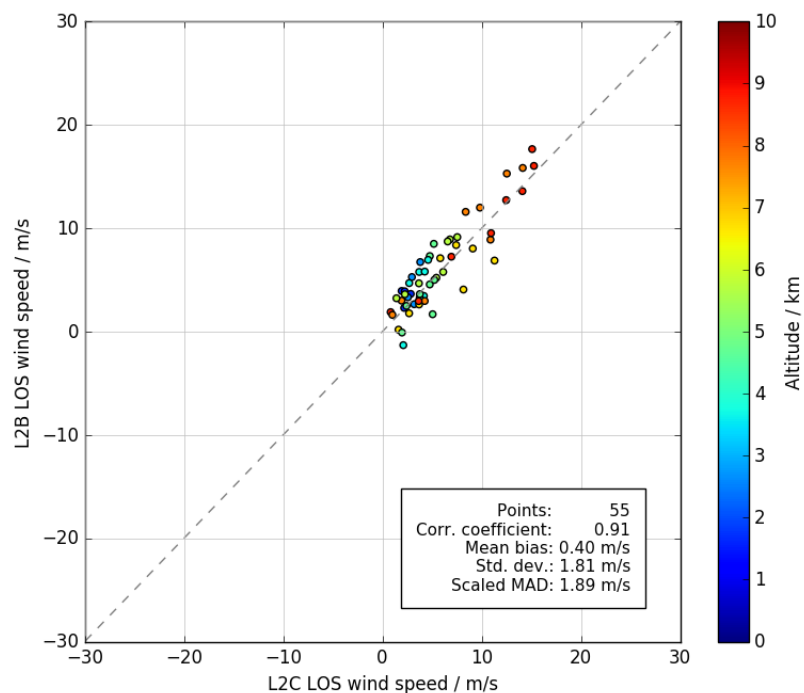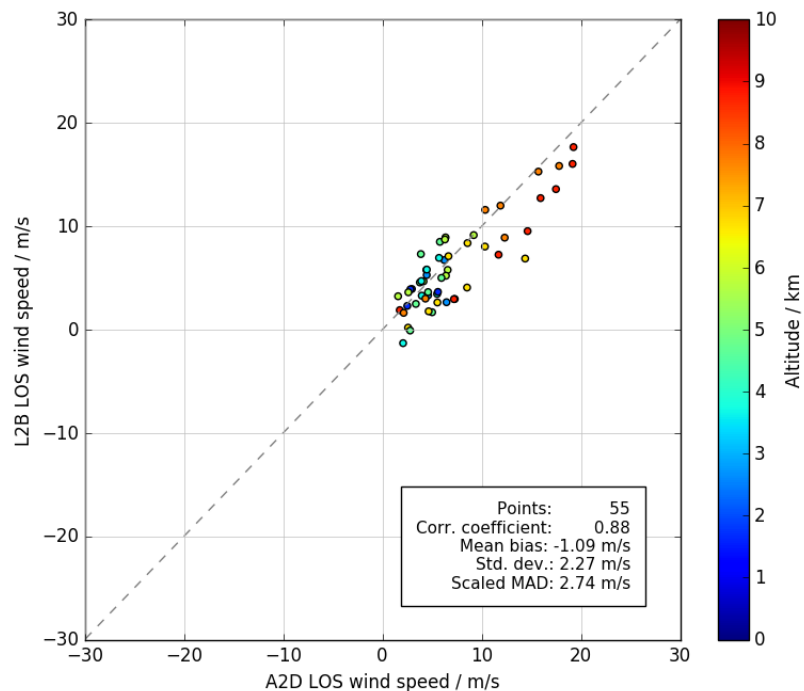**Figure 9-13: Scatterplot comparing the A2D Rayleigh LOS winds (adapted to the Aeolus LOS) with the Aeolus L2C LOS winds for all underflights of the WindVal III campaign. The data points are colour-coded with respect to the altitude of the respective bin used for comparison.+**
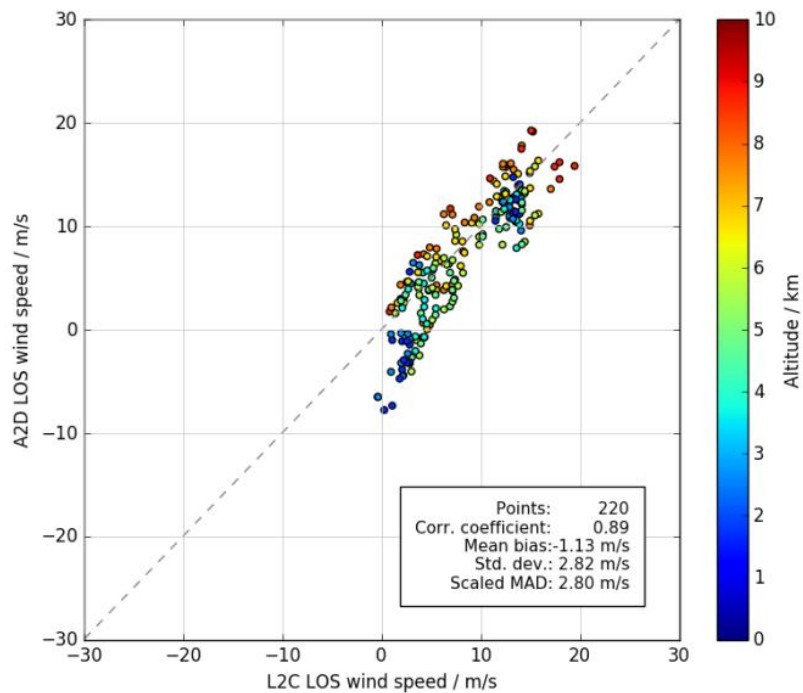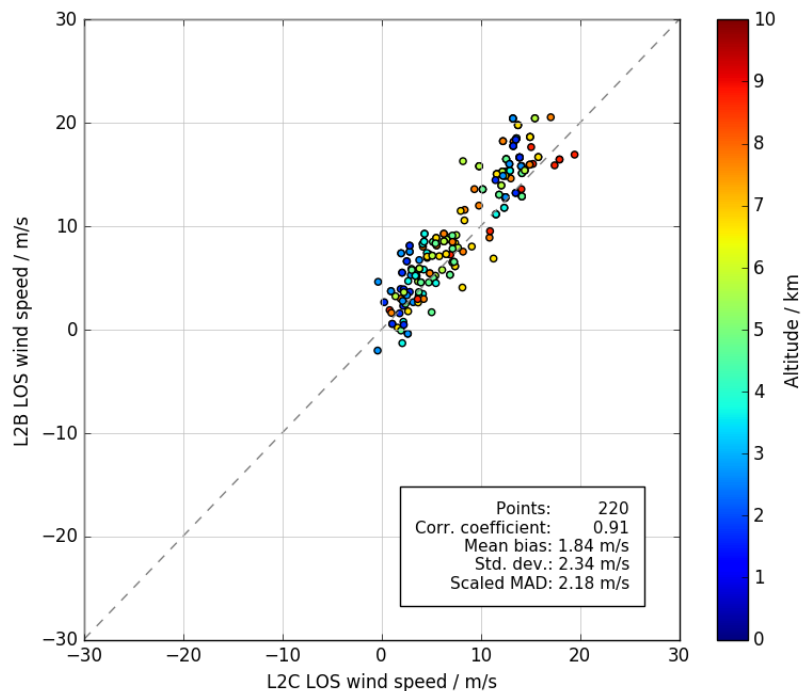

Figure 9-14: Scatterplot comparing the Aeolus L2B Rayleigh LOS winds with the Aeolus L2C LOS winds for all underflights of the WindVal III campaign. The data points are colour-coded with respect to the altitude of the respective bin used for comparison.
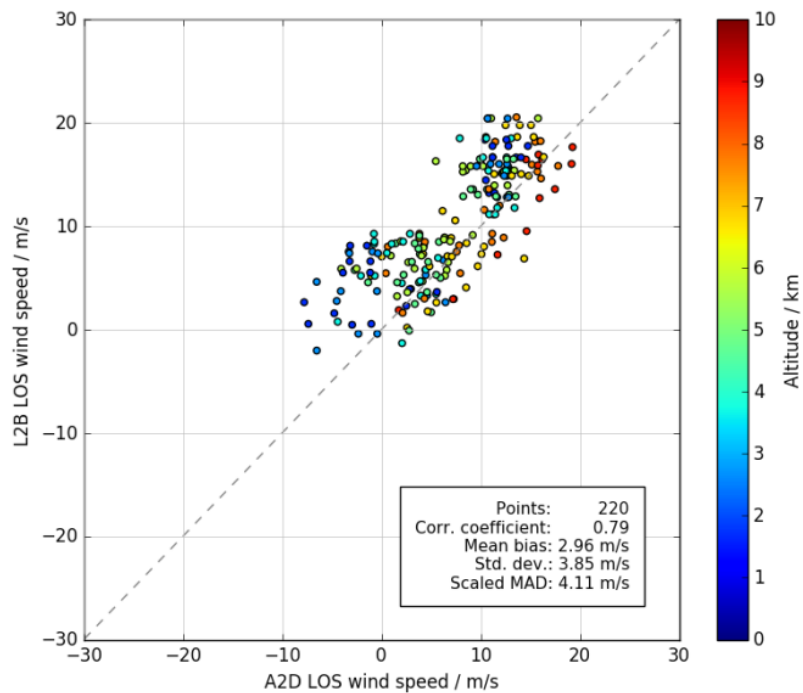
Figure 9-15: Scatterplot comparing the Aeolus L2B Rayleigh LOS winds with the A2D Rayleigh LOS winds (adapted to the LOS direction of Aeolus) for all underflights of the WindVal III campaign. The data points are colour-coded with respect to the altitude of the respective bin used for comparison.

9.6   Summary of wind measurements and recommendations

- In the frame of WindVal III six flights were conducted including the test flight and the calibration flight. During the first Aeolus underflight on 17 November, the A2D was not operational, so that A2D wind data is only available from three other underflights plus the test flight.

- The measurement periods range from only eight minutes (during the test flight) to more than 50 minutes, adding up to nearly five hours over the whole campaign.

- The duration of A2D wind measurements (five hours) relative to the overall flight duration (10.5 hours) is much longer compared to WindVal II (18 hours wind measurements during 47 flight hours). This can be traced back to the higher reliability of the A2D with shorter interruptions related to instrument malfunctions.

- Due to the preference for cloud-free conditions, the number of acquired Rayleigh winds passing the quality control (10212) is much higher than the number of valid Mie winds (1872). This is very different to the situation encountered during WindVal II where the flight planning mainly was driven by meteorological objectives of the NAWDEX community (Rayleigh 38369, Mie: 17505)

- Considering the overall wind measurement time of the campaign, 34 valid Rayleigh winds and 6 valid Mie winds were measured per minute. While the Rayleigh data output rate is similar to WindVal II (35 winds per minute), the Mie data output rate is considerable lower compared to the previous campaign (16 winds per minute). This can be explained with the absence of thin cirrus clouds during the WindVal III wind scenes in contrast to WindVal II which deliver many valid Mie bins along the wind profiles. During WindVal III, thick low- and middle-clouds were present during all wind scenes, yielding only few valid Mie winds for the range gates containing the cloud tops. The range gates beneath often either show low Mie SNR and are thus considered invalid or exhibit large wind speed differences to the 2-µm winds. Consequently, A2D Mie winds were not further used for the comparison with Aeolus wind data.

- The accuracy and precision of the processed Rayleigh and Mie wind profiles were evaluated by statistical comparison with the 2-µm wind lidar. The scaled Median Absolute Deviation (1.4826·MAD) provided a robust estimate of the standard deviation and thus random error.

- Overall accuracy and precision of the Rayleigh and Mie winds (comparison with 2-µm DWL wind data over whole campaign):

  Rayleigh: 2117 data points,   +0.25 m/s (accuracy),   2.20 m/s (precision),   2.09 m/s (1.4826 · MAD)

  Mie: 951 data points   +1.18 m/s (accuracy),   2.91 m/s (precision),   2.37 m/s (1.4826 · MAD)

- The random error of 2.20 m/s is considerable smaller than for the previous campaign (3.32 m/s) which is mainly due to the implemented fiber scrambler reducing the speckle noise of the internal reference signal.

- Although the number of Rayleigh winds compared to the 2-µm DWL is very similar to WindVal II, there are much less gross errors for the WindVal III campaign. This is most likely explained by the fact that most WindVal III flights were planned to be conducted in cloud-free conditions, minimizing the risk for heterogeneous atmospheric conditions and, in turn, the risk for large systematic errors of the Rayleigh channel, e.g. introduced by cirrus clouds affecting the transmit-receive co-alignment feedback loop.

- The statistical comparison of the Mie wind data indicates are poorer performance of the Mie channel compared to the previous campaign. Apart from the larger wind bias of 1.18 m/s (WindVal II: 0.53 m/s), the random error is significantly larger (2.37 m/s compared to 1.79 m/s). Also, the overall number of valid Mie winds (951) entering the statistical comparison is much smaller than for WindVal II (7169). This can again be explained with the very different cloud conditions encountered during the two campaigns.

- Comparison of the A2D Rayleigh wind data obtained during the underflights with the Aeolus L2B Rayleigh winds required an adaptation of the A2D LOS vector to the Aeolus LOS vector. For this purpose, wind model data from the L2C product was used to convert the A2D LOS wind speeds to those wind speeds which would have been measured in case of pointing along the Aeolus LOS (azimuth and off-nadir angle correction).

- The wind speed difference between the two pointing directions can be as large as 50 m/s depending on the meridional and zonal wind component during the wind scene. For typical azimuth angels of Aeolus on an ascending orbit (260°) and the A2D when flying along an ascending Aeolus orbit (68°), the wind speed difference between the two instruments introduced by the different azimuth angles is especially large for strong zonal components of the wind vector.

- The azimuth-corrected A2D Rayleigh winds were compared to the Aeolus L2B Rayleigh winds for the three underflights on 22 November, 3 December and 5 December. Instead of comparing HLOS wind speeds, as provided in the L2B data product, the Aeolus winds were converted to LOS winds by considering the off-nadir angle of 37°. The A2D winds (measured at an off-nadir angle of 20°) were converted to LOS winds at the Aeolus off-nadir angle. The statistical comparison yielded a positive bias of the L2B data of 2.96 m/s and a random error (scaled MAD) of 4.11 m/s.

- The comparison of the A2D winds with the model data shows good agreement for altitudes below 7 km, while a positive bias is evident for higher altitudes. This is most likely related to the incomplete telescope overlap in this region resulting in a systematic error. When comparing the data from all flights (**Figure 9-13**), a mean bias of -1.13 m/s is calculated with most of the underestimated winds being measured close to the ground. However, it cannot be unambiguously derived from the comparison whether the A2D exhibits an altitude-dependent systematic error or a slope error of the calibration resulting in underestimated low wind speeds at lower altitudes and overestimated high wind speeds at higher altitudes.

Recommendations with respect to the Cal/Val activities

- The vertical sampling strategy (RBS) for ALADIN should be optimized for the available atmospheric signal return depending on laser emit energy and alignment status. During WindVal III the ALADIN RBS was optimized for high vertical resolution in the lower troposphere where the signal return was too weak for reasonable SNR in many cases. As also the A2D RBS was optimized for maximum overlap with ALADIN vertical resolution, a significant number of A2D measurements were lost for comparison purposes because of ALADIN signals being rejected by the QC due to low SNR. Based on the available return signal the RBS should be optimized from time to time in case the laser energy or alignment degraded. An example of an optimized setting can be found in Figure 9-16.
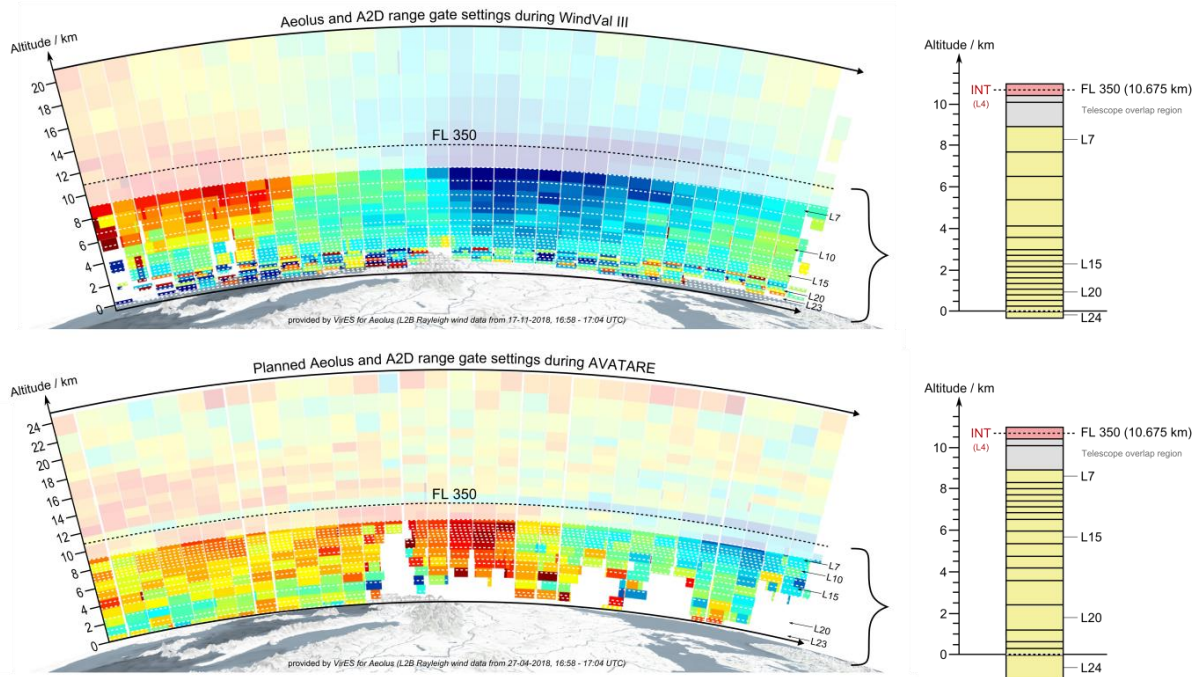
Figure 9-16: Diagram illustrating the A2D range gate setting used during the WindVal III campaign (top) and an optimized range gate setting planned to be used in forthcoming airborne validation campaigns. The left part of the figure shows exemplary Aeolus L2B Rayleigh wind curtains with indicated bin altitudes of the A2D range gates (white dashed lines) assuming a flight altitude of about 10675 m (FL 350). The corresponding vertical range gates are additionally depicted on the right. Due to the incomplete telescope overlap, the first 1.5 km below the aircraft cannot be used for wind measurements. The figure was created based on screenshots from the Aeolus data visualization tool *VirES for Aeolus (https://aeolus.services/).*

- Given the significantly lower speed of the aircraft vs. Aeolus ground track, the collocation along the overpass with the centre of the aircraft track is less important. The coarse horizontal resolution of the ALADIN data requires flying along track at least 700 km without high clouds to get enough range gates for comparison from a flight. Within the range limits of the aircraft thus short tracks should be used to shuttle forth and back to increase the data coverage, especially when using different sampling strategies on both directions. Longer comparison tracks with up to 1 h difference to the overpass time on the track ends can still provide good correlations. Strong gradients in wind speed with a wind direction preferably in the west-east plane aligned with the ALADIN and A2D LOS directions are the best cases for underflights to gain measurement principle focussed wind comparison results over a wide wind speed range with least influence from pointing direction measurement uncertainties and projection corrections. Achieving this within the limits given by ATC (flight plan due 72 h in advance) and the uncertainty in weather predictions especially for clouds combined with the given position and time of the overpass within reach on a certain day is only possible, if every reasonable chance for an underflight is planned. The downside of this approach is a high effort for flight planning and a significant amount of cancelled flights because of not good enough conditions on the actual day of flight.

- In order to obtain more valid Mie winds flights over cirrus clouds are required. However, this is likely to degrade the quality of the Rayleigh winds due to the alignment sensitivity of the Rayleigh spectrometer. It is recommended to perform underflights which are specifically dedicated to the acquisition of Rayleigh winds (cloud-free conditions) or Mie winds (cirrus clouds).

10 Summary and recommendations

This chapter summarizes the respective summary sections of each chapter of the WindVal III Final Report. The recommendations complement and partly re-emphasize the recommendations from previous campaigns (DLR 2012a, DLR 2017, DLR 2018a).

Executive Summary

The WindVal III campaign was carried out from the airport at DLR Oberpfaffenhofen in the timeframe from 5 November to 5 December 2018 including an extension of one week which could be organized on short notice during the campaign to compensate for delays and cancelled flights. Despite the limited campaign time, weather constraints, issues with the aircraft and also some with the lidar instruments, all campaign objectives for WindVal III were achieved in six performed flights with 24 flight hours total, including four Aeolus underflights with a total of 3000 km along track, a test flight and an A2D calibration flight with four performed response calibrations. It was the first airborne campaign after the launch of Aeolus on 22 August 2018 and the only campaign in the commissioning phase E1 of the mission with the flight laser FMA active after its first switch-on. Already during the campaign quick-look processing for the 2-µm DWL and the A2D could confirm the capability of ALADIN to measure reasonable winds by qualitative comparison to the collocated airborne wind lidar measurements along track. Detailed analysis resulted in random errors of 2.0 m/s for Mie winds and 3.9 m/s for Rayleigh winds (L2B HLOS) when comparing to the 2-µm reference DWL and respective biases of 2.2 m/s and 2.5 m/s. Also for the first time azimuth correction for A2D based on the model winds provided with the L2C product was developed to compare corrected A2D Rayleigh winds to the Aeolus L2B Rayleigh winds directly on the Aeolus LOS. The statistical comparison yielded a positive bias of the L2B data of 3 m/s and a random error (scaled MAD) of 4 m/s.This complements the findings of comparisons between Aeolus data and NWP weather models presented during the Aeolus Cal/Val Workshop in March 2019 and thus confirms the root-cause of the enhance bias is a not-updated calibration file that was intentionally used for data processing, together with instrumental alignment drifts, that would rather require regular calibrations.

10.1 Detailed Summary

WindVal III campaign and A2D and 2-µm DWL performance

- The WindVal III campaign: 5 Nov. – 5. Dec, 2019, 24 flight hours, 4 Aeolus underflights with 3000 km along track total, 1 test flight, 1 A2D response calibration flight, 20 flights planned, but also many cancellations due to technical issues with the aircraft, weather along track and at the airport as well as ATC limitations because of aircraft operation with permit-to-fly status.

- A2D was working as expected with only minor issues. One broken fuse in an electronic component with difficult accessibility has led to one cancelled flight and one underflight with only 2-µm DWL operated. The EOM malfunction turned out to have no detrimental influence on data quality during the performed flights.

- The 2-µm DWL performed well throughout all flights during WindVal III and provided accurate and valuable wind measurements that were used to quantitatively compare to Aeolus wind measurements. However, the performance of the 2-µm DWL was degrading during the campaign, making the lidar operation during flights quite alignment intensive. For that reason, it was decided to send the lidar system back to the manufacturer Beyond Photonics in order to investigate the root cause of the performance degradation after the campaign.

- Implementation of a fiber scrambler into the A2D considerably reduced detrimental speckle noise which represented one of the major contributors to the random wind error of the A2D. Comparison with wavemeter data showed that the frequency variations of the internal reference signal are lowered by a factor of five (Mie) and two (Rayleigh), respectively. Intensity fluctuations are decreased by 55% (Mie) and 22% (Rayleigh). In addition, the Rayleigh filter transmissions showed significantly smaller deviations from theoretical filter functions, thus allowing for a better characterization of the Rayleigh channel. Accurate knowledge of the filter parameters is crucial for simulating the behaviour of the A2D, especially the impact of pressure and temperature changes on response calibration results.

A2D algorithm enhancements, calibration and wind retrieval

- Four response calibrations were carried out during one calibration flight in Northern Italy on 29 November 2018.

- All four calibrations are of high quality without cloud contamination and only minor differences in terms of laser frequency stability (3 to 4 MHz), stability of ambient pressure (0.6 to 0.8 hPa), stability of the Rayleigh spectrometer temperature (8 to 10 mK).

- However, there are differences regarding the pointing stability, especially in horizontal axis: 6.8 µrad (calibration #1) to 9.5 µrad (calibration #4).

- A drift in the Rayleigh spot positions was observed which moved by about 0.05 pixels between calibration #1 and calibration #4 (2 hours). Moreover, a large change in the FWHM values by more than 0.3 pixels between calibration #2 and calibration #3 is evident. The change in the Rayleigh spot positions and widths in the course of the calibration flight suggests a (thermo-) mechanical drift of optical components or possible influence of sub-visible cirrus below aircraft to be the root cause. The former is supported by the fact that the heating of the bottom window of the aircraft was switched-on between calibration #2 and #3 to prevent icing. The warm air blown across the window might have also heated up the turning and/or telescope mirrors located close to the window, thus altering the beam alignment.

- The drift manifests in the Rayleigh calibration Δ(intercept) values which vary from -0.011 (calibration #1) to 0.003 (calibration #4). This translates into a variation in wind speed of about 3 m/s when applying the different calibrations.

- The Rayleigh response calibration results, especially the Rayleigh slopes and nonlinearities, are comparable to those obtained during the previous campaign WindVal II in 2016.

- The Rayleigh intercepts for the internal reference and ground return are very similar and vary by about 0.006 which is comparable to the variations observed for the calibrations in WindVal II (0.005). These variations in the intercept correspond to wind speed variations of about 1.5 m/s.

- Since the Rayleigh calibration results are very consistent for all calibrations apart from the Δ(intercept) values and due to the high sensitivity of the Rayleigh spectrometer to variations of the incidence angle, the CoG variability was given the highest weight for the choice of the most appropriate calibration. Regarding this parameter, calibration #1 showed the best performance with variations on observation level of only 1.0 pixel and 0.7 pixel for the horizontal and vertical component of the CoG, so that it was selected as the baseline for the Rayleigh wind retrieval.

- The Mie response calibrations were highly reproducible with small variations in the slope and Δ(intercept) values of both the internal reference and ground return. The slope variations (0.27 MHz/pixel) are smaller compared to WindVal II by a factor of two, while the Δ(intercept) variations (0.03 pixels) are even smaller by a factor of three to four. For the internal reference, this can be traced back to the implemented fiber scrambler which considerably reduces the speckle noise of the internal reference signal incident on the Mie spectrometer. For the ground return, the lower variability is most likely due to the fact that the six calibrations from WindVal II were performed over different surfaces (4 over ice, 2 over land), resulting in a larger spread of ground slopes depending on albedo.

- Due to the excellent reproducibility of the Mie response curves, the choice of the best Mie response calibration is mainly driven by the variability of the OBA temperature because this parameter crucially influences the spacing of the Fizeau interferometer plates. The lowest variability in OBA temperature was observed for calibration #2 which is also characterized by the highest laser frequency stability. Therefore, this response calibration was chosen for the Mie wind retrieval.

- In the frame of WindVal III six flights were conducted including the test flight and the calibration flight. During the first Aeolus underflight on 17 November, the A2D was not operational due to a broken fuse that could not easily be replaced, so that A2D wind data is only available from three other underflights plus the test flight.

- The measurement periods range from only eight minutes (during the test flight) to more than 50 minutes, adding up to nearly five hours over the whole campaign.

- The duration of A2D wind measurements (five hours) relative to the overall flight duration (10.5 hours) is longer compared to WindVal II (18 hours wind measurements during 47 flight hours). This can be traced back to the higher reliability of the A2D with shorter interruptions related to instrument malfunctions.

- Due to the preference for cloud-free conditions, the number of acquired Rayleigh winds passing the quality control (10212) is much higher than the number of valid Mie winds (1872). This is very different to the situation encountered during WindVal II where the flight planning was also driven by meteorological objectives of the NAWDEX community (Rayleigh 38369, Mie: 17505).

- Considering the overall wind measurement time of the campaign, 34 valid Rayleigh winds and 6 valid Mie winds were measured per minute. While the Rayleigh data output rate is similar to WindVal II (35 winds per minute), the Mie data output rate is considerable lower compared to the previous campaign (16 winds per minute). This can be explained with the (planned) absence of thin cirrus clouds during the WindVal III wind scenes in contrast to WindVal II which deliver many valid Mie bins along the wind profiles. During WindVal III, thick low- and middle-clouds were present during all wind scenes, yielding only few valid Mie winds for the range gates containing the cloud tops. The range gates beneath often either show low Mie SNR and are thus considered invalid or exhibit large wind speed differences to the 2-µm winds. Consequently, A2D Mie winds were not further used for the comparison with Aeolus wind data.

- The accuracy and precision of the processed A2D Rayleigh and Mie wind profiles were evaluated by statistical comparison with the 2-µm wind lidar. The scaled Median Absolute Deviation (1.4826·MAD) provided a robust estimate of the standard deviation and thus random error.

- Overall accuracy and precision of the A2D Rayleigh and Mie winds (comparison with 2-µm DWL wind data over the whole campaign):

  Rayleigh: 2117 data points, +0.25 m/s (accuracy), 2.20 m/s (precision), 2.09 m/s (1.4826 · MAD)

  Mie: 951 data points +1.18 m/s (accuracy), 2.91 m/s (precision), 2.37 m/s (1.4826 · MAD)

- The random error of 2.20 m/s is considerably smaller than for the previous campaign (3.32 m/s) which is mainly due to the implemented fiber scrambler reducing the speckle noise of the internal reference signal.

- Although the number of Rayleigh winds compared to the 2-µm DWL is very similar to WindVal II, there are much less gross errors for the WindVal III campaign. This is most likely explained by the fact that most WindVal III flights were planned to be conducted in cloud-free conditions, minimizing the risk for heterogeneous atmospheric conditions and, in turn, the risk for large systematic errors of the Rayleigh channel, e.g. introduced by cirrus clouds affecting the transmit-receive co-alignment feedback loop.

- The statistical comparison of the Mie wind data indicates are poorer performance of the Mie channel compared to the previous campaign. Apart from the larger wind bias of 1.18 m/s (WindVal II: 0.53 m/s), the random error is significantly larger (2.37 m/s compared to 1.79 m/s). However, also the overall number of valid Mie winds (951) entering the statistical comparison is much smaller than for WindVal II (7169). This can again be explained with the very different cloud conditions encountered during the two campaigns.

- Comparison of the A2D Rayleigh wind data obtained during the underflights with the Aeolus L2B Rayleigh winds required an adaptation of the A2D LOS vector to the Aeolus LOS vector. For this purpose, wind model data from the L2C product was used to convert the A2D LOS wind speeds to those wind speeds which would have been measured in case of pointing along the Aeolus LOS (azimuth and off-nadir angle correction).

- The wind speed difference between the two pointing directions can be as large as 50 m/s depending on the meridional and zonal wind component during the wind scene. For typical azimuth angels of Aeolus on an ascending orbit (260°) and the A2D when flying along an ascending Aeolus orbit (68°), the wind speed difference between the two instruments introduced by the different azimuth angles is especially large for strong zonal components of the wind vector.

- The azimuth-corrected A2D Rayleigh winds were compared to the Aeolus L2B Rayleigh winds for the three underflights on 22 November, 3 December and 5 December. Instead of comparing HLOS wind speeds, as provided in the L2B data product, the Aeolus winds were converted to LOS winds by considering the off-nadir angle of 37°. The A2D winds (measured at an off-nadir angle of 20°) were converted to

LOS winds at the Aeolus off-nadir angle. The statistical comparison yielded a positive bias of the L2B data of 2.96 m/s and a random error (scaled MAD) of 4.11 m/s.

- The comparison of the A2D winds with the model data shows good agreement for altitudes below 7 km, while a positive bias is evident for higher altitudes. This is most likely related to the incomplete telescope overlap in this region resulting in a systematic error. When comparing the data from all flights, (Figure 9-13), a mean bias of -1.13 m/s is calculated with most of the underestimated winds being measured close to the ground. However, it cannot be unambiguously derived from the comparison whether the A2D exhibits an altitude-dependent systematic error or a slope error of the calibration resulting in underestimated low wind speeds at lower altitudes and overestimated high wind speeds at higher altitudes.

10.2 Recommendations

Recommendations wrt Cal/Val data analysis and flight planning

- The vertical sampling strategy (RBS) for ALADIN should be optimized for the available atmospheric signal return depending on laser emit energy and alignment status. During WindVal III the ALADIN RBS was optimized for high vertical resolution in the lower troposphere where the signal return was too weak for reasonable SNR in many cases. As also the A2D RBS was optimized for maximum overlap with ALADIN vertical resolution, a significant number of A2D measurements were lost for comparison purposes because of ALADIN signals being rejected by the QC due to low SNR. Based on the available return signal the RBS should be optimized from time to time in case the laser energy or alignment degraded. An example of an optimized setting can be found in Figure 9-16. Based on the ALADIN performance and RBS valid Mie winds in the lower troposphere passing QC can be spars. This led to comparably few Mie winds to compare to the A2D Mie winds during WindVal III combined with the flight planning focussing on scenes without high clouds. During upcoming campaigns it will thus be checked if flying above high clouds and especially cirrus clouds for parts of some flights can be considered for flight planning. This would allow collecting more Mie winds for comparison, especially in the jet-stream area often associated with cirrus clouds, however, partly on the expense of A2D Rayleigh winds being potentially degraded by A2D alignment drifts in cases close above clouds.

- Given the significantly lower speed of the aircraft vs. Aeolus ground track, the collocation along the overpass with the centre of the aircraft track is less important. The coarse horizontal resolution of the ALADIN data requires flying along track at least 700 km without high clouds to get enough range gates for comparison from a flight. Within the range limits of the aircraft thus short tracks should be used to shuttle forth and back to increase the data coverage, especially when using different sampling strategies on both directions. Longer comparison tracks with up to 1 h difference to the overpass time on the track ends can still provide good correlations. Strong gradients in wind speed with a wind direction preferably in the west-east plane aligned with the ALADIN and A2D LOS directions are the best cases for underflights to gain measurement principle focussed wind comparison results over a wide wind speed range with least influence from pointing direction measurement uncertainties and projection corrections. Achieving this within the limits given by ATC (flight plan due 72 h in advance) and the uncertainty in weather predictions especially for clouds combined with the given position and time of the overpass within reach on a certain day is only possible, if every reasonable chance for an underflight is planned. The downside of this approach is a high effort for flight planning and a significant amount of cancelled flights because of not good enough conditions on the actual day of flight.

- The statistical comparison of 2-µm DWL and Aeolus data shows, that the random errors for Mie winds (1.93 m/s) is a factor of two smaller than the one for Rayleigh winds (3.93 m/s). This is likely due to the larger signal levels of Mie returns. On the other hand, the occurrence of Mie winds (# 98) is almost a factor of three less than for Rayleigh winds (# 288). → It is recommended to process Mie winds for a lower horizontal averaging period, or rather on measurement level in order to increase the number of available Mie winds. The random error suggests that this is suitable.

- It is demonstrated that due to the temporal and spatial constraints of planning a satellite underflight, the flight planning cannot additionally consider aerosol load and relative humidity in order to increase the 2-µm DWL vertical data coverage → It is recommended to plan the flight legs below the satellite in different flight levels in order to spread the 2-µm data points over different altitudes. The change in flight level

should be as flexible as possible. In case the quick look during flight shows that such a flight level change is not needed, the aircraft should fly as high as possible, also in order to support A2D operation.

- The horizontal and vertical resolution of Aeolus data is much lower than the one of the 2-µm DWL. Thus, first tests were performed in order to modify the accumulation data algorithm. In particular, power spectra of single LOS measurements are averaged vertically and horizontally in order to increase the signal to noise ratio and thus to enhance the data coverage for comparison to Aeolus data. → It is recommended that future Cal/Val flights and campaigns data is used to investigate the possibility of such a retrieval modification and if it is worth to do so.

Recommendations for A2D operation

- The heating with warm air flow of the bottom window of the aircraft should always be either switched-on or switched-off during research flights in order to avoid thermos-mechanical drifts of the optical components located close to the window and, in turn, systematic wind errors.

- In addition to the requirements in terms of the RSP temperature stability (<0.01 K peak-to-peak), the OBA temperature stability should be better than 0.02 K peak-to-peak during response calibrations in order to avoid large variations in the Mie response calibration parameters for A2D and ALADIN.

11   References

Chouza, F., Reitebuch, O., Jähn, M., Rahm, S., Weinzierl, B. (2016a): Vertical wind retrieved by airborne lidar and analysis of island induced gravity waves in combination with numerical models and in situ particle measurements, Atmos. Chem. Phys., 16, 4675–4692.

Chouza, F., Reitebuch, O., Benedetti, A., Weinzierl, B. (2016b): Saharan dust long-range transport across the Atlantic studied by an airborne Doppler wind lidar and the MACC model, Atmos. Chem. Phys., 16, 11581–11600, doi:10.5194/acp-16-11581-2016.

DLR: Reitebuch, O., Paffrath, U., Nikolaus, I. (2010): TN 5.1 ADM-Aeolus Ground Campaigns Results, V 1.1, 26/02/2010, 309 pages.

DLR: Reitebuch, O. et al. (2012a): Final Report ADM-Aeolus Airborne Campaigns Results, V 1.0, 15/06/2012, 34 pages.

DLR: Reitebuch, O., Marksteiner, U., Lemmerz, C. (2012b): TN 5.2 ADM-Aeolus Airborne Campaigns Results, V 3.0, 24/02/2012, 202 pages.

DLR: Reitebuch, O., Marksteiner, U., Lemmerz, C. (2012c): TN 5.3 A2D Rayleigh spectrometer alignment sensitivity, V 2.0, 12/01/2012, 48 pages.

DLR: Witschas, B., Marksteiner, U., Reitebuch, O., Lemmerz, C., Lux, O. (2016): Analysis of enhanced noise in A2D observations, V 2.0, 11/07/2016, 110 pages.

DLR: Reitebuch, O. et al. (2017): Final Report Joint DLR-ESA-NASA Wind Validation for Aeolus, V 1.1, 27/07/2017, 146 pages + Annex 39 pages.

DLR: Reitebuch, O. et al. (2018a): Final Report Wind Validation II for Aeolus, V1.1, 26/06/2018, 203 pages + Annex 70 pages.

DLR: Lemmerz, C. et al. (2018b): WindVal III Campaign Implementation Plan, V 1.1, 15/11/2018, 24 pages.

DLR: Lemmerz, C., Lux, O., Rahm, S., Reitebuch, O., Witschas, B., Geiss, A. (2019): WindVal III: Data Acquisition Report (DAR) Wind Validation III for Aeolus. V1.0, 22/03/2019, 24 pages + appendix.

ESA: Schüttemeyer, D. (2016): Statement of Work on "Technical Assistance for the Deployment of the ALADIN Airborne Demonstrator (A2D) lidar during WINDVAL II". EOP-SM/3000/DS-ds from 29/06/2016, Contract No. ESA 4000114053/15/NL/FF/gp.

ESA: Fehr, T. (2018): Statement of Work on "Technical Assistance for the Deployment of the ALADIN Airborne Demonstrator (A2D) lidar during WINDVAL III". ESA-EOPSM-AEOL-SOW-3319, issue 1, revision 1, 17/05/2018.

Lux, O., Lemmerz, C., Weiler, F., Marksteiner, U., Witschas, B., Rahm, S., Schäfler, A., and Reitebuch, O. (2018): Airborne wind lidar observations over the North Atlantic in 2016 for the pre-launch validation of the satellite mission Aeolus, Atmos. Meas. Tech., 11, 3297–3322.

Marksteiner, U. (2013): Airborne Wind-Lidar Observations for the Validation of the ADM-Aeolus Mission. Ph. D Thesis at Technical University Munich, DLR FB 2013-25, 176 pages.

Marksteiner, U., Lemmerz, C., Lux, O., Rahm, S., Schäfler, A., Witschas, B., and Reitebuch, O. (2018): Calibrations and Wind Observations of an Airborne Direct Detection Wind Lidar Supporting ESA's Aeolus Mission, Remote Sens., 10, 2056.

Paffrath, U., Lemmerz, C., Reitebuch, O., Witschas, B., Nikolaus, I., Freudenthaler, V. (2009): The airborne demonstrator for the direct-detection Doppler wind lidar ALADIN on ADM-Aeolus: II. Simulations and Rayleigh receiver radiometric performance. J. Atmos. Ocean. Tech., 26, 2516-2530.

Reitebuch, O., Lemmerz, C., Nagel, E., Paffrath, U., Durand, Y., Endemann, M., Fabre, F., Chaloupy, M. (2009): The airborne demonstrator for the direct-detection Doppler wind lidar ALADIN on ADM-Aeolus: I. Instrument design and comparison to satellite instrument. J. Atmos. Ocean. Tech., 26, 2501-2515.

Sun, X. J., Zhang, R. W., Marseille, G. J., Stoffelen, A., Donovan, D., Liu, L., Zhao, J. (2014): The performance of Aeolus in heterogeneous atmospheric conditions using high-resolution radiosonde data, Atmos. Meas. Tech., 7, 2695–2717.

Weissmann, M., Busen, R., Dörnbrack, A., Rahm, S., Reitebuch, O. (2005): Targeted Observations with an Airborne Wind Lidar. J. Atmos. Ocean. Tech., 22, 1706-1719.

Witschas, B., Rahm, S., Dörnbrack, A., Wagner, J., Rapp, M. (2017). Airborne Wind Lidar measurements of vertical and horizontal winds for the investigation of orographically induced gravity waves. Journal of Atmospheric and Oceanic Technology, 34, 1371-1386.

12 Annex – Description of the A2D netCDF files

The wind scenes measured with the A2D in the frame of the WindVal III campaign are summarized in Table 9-1 which also includes the file names of the respective netCDF files containing the data of the eight scenes along the Aeolus measurement swath. The content and structure of the eight files is explained in Table 12-1. The parameters are given as float64 values, where the times, geolocation coordinates and instrument angles (in an Earth-fixed coordinate system) are provided in one-dimensional arrays per observation, whereas the bin altitudes and LOS wind speeds are provided in two-dimensional arrays per observation and per layer for the Rayleigh and Mie channel.

Table 12-1: Structure and content of the A2D Rayleigh and Mie data in netCDF file format. All parameters are given as float64 values.

Block	Parameter	Unit	Comments
Dimensions	layer		Number of range gates (= layers) including background (layer 0), DCO (layer 2), Internal reference (layer 4) and atmospheric layers (layers 5...24)
	obs		Number of observations
Data variables	start_time	s	UTC time at start of observation in seconds since 01-01-2000
	stop_time	s	UTC time at end of observation in seconds since 01-01-2000
	start_longitude	°E	Longitude of intersection of laser footprint with DEM at start of observation
	start_latitude	°N	Latitude of intersection of laser footprint with DEM at start of observation
	stop_longitude	°E	Longitude of intersection of laser footprint with DEM at end of observation
	stop_latitude	°N	Latitude of intersection of laser footprint with DEM at end of observation
	rayleigh_bin_bottom_altitude	m	Bottom altitude of Rayleigh layer per layer and obs.
	rayleigh_bin_top_altitude	m	Top altitude of Rayleigh layer per layer and obs.
	rayleigh_los_wind	m/s	Rayleigh LOS wind speed per layer and obs.
	mie_bin_bottom_altitude	m	Top altitude of Mie layer per layer and obs.
	mie_bin_top_altitude	m	Top altitude of Mie layer per layer and obs.
	mie_los_wind	m/s	Mie LOS wind speed per layer and obs.
	azimuth_angle	°	Azimuth angle of the instrument in an Earth-fixed coordinate system starting from North (clockwise positive) per obs.
	off_nadir_angle	°	Off-nadir angle (= 90° - elevation angle) of the LOS vector in an Earth-fixed coordinate system per obs.
Attributes	description		Date of the wind scene, e.g. "20190517b"
	_NCProperties		File version, e.g. "version=2,netcdf=4.6.3,hdf5=1.10.5"
	history		Date and time of creation of the file